

UNIVERSITY OF ALBERTA

MICROFLUIDIC DEVICES FOR LABEL FREE PROTEIN MICROARRAYS

BY

ERIC FLAIM 

A THESIS SUBMITTED TO THE FACULTY OF GRADUATE STUDIES AND RESEARCH
IN PARTIAL FULFILLMENT OF THE REQUIREMENTS FOR THE DEGREE OF

DOCTOR OF PHILOSOPHY

DEPARTMENT OF CHEMISTRY

EDMONTON, ALBERTA

FALL 2008



Library and
Archives Canada

Published Heritage
Branch

395 Wellington Street
Ottawa ON K1A 0N4
Canada

Bibliothèque et
Archives Canada

Direction du
Patrimoine de l'édition

395, rue Wellington
Ottawa ON K1A 0N4
Canada

Your file *Votre référence*

ISBN: 978-0-494-46316-1

Our file *Notre référence*

ISBN: 978-0-494-46316-1

NOTICE:

The author has granted a non-exclusive license allowing Library and Archives Canada to reproduce, publish, archive, preserve, conserve, communicate to the public by telecommunication or on the Internet, loan, distribute and sell theses worldwide, for commercial or non-commercial purposes, in microform, paper, electronic and/or any other formats.

The author retains copyright ownership and moral rights in this thesis. Neither the thesis nor substantial extracts from it may be printed or otherwise reproduced without the author's permission.

AVIS:

L'auteur a accordé une licence non exclusive permettant à la Bibliothèque et Archives Canada de reproduire, publier, archiver, sauvegarder, conserver, transmettre au public par télécommunication ou par l'Internet, prêter, distribuer et vendre des thèses partout dans le monde, à des fins commerciales ou autres, sur support microforme, papier, électronique et/ou autres formats.

L'auteur conserve la propriété du droit d'auteur et des droits moraux qui protègent cette thèse. Ni la thèse ni des extraits substantiels de celle-ci ne doivent être imprimés ou autrement reproduits sans son autorisation.

In compliance with the Canadian Privacy Act some supporting forms may have been removed from this thesis.

Conformément à la loi canadienne sur la protection de la vie privée, quelques formulaires secondaires ont été enlevés de cette thèse.

While these forms may be included in the document page count, their removal does not represent any loss of content from the thesis.

Bien que ces formulaires aient inclus dans la pagination, il n'y aura aucun contenu manquant.

■+■
Canada

Dedicated to my parents,
Thomas and Lucia Flaim.

Consider this a gift for all you have sacrificed for me.
If I have achieved anything it is because of your unflinching love and support.

ABSTRACT

Microfluidic devices for biochemical microarrays are fabricated and tested. They are designed and used for the purpose of label free protein assays within a Surface Plasmon Resonance (SPR) detection system. These microfluidic devices consist of microchannels and spotting regions, defined in PDMS, aligned to gold patterned SPR slides. Solution flow through the microchannel devices is achieved using vacuum. As solutions are flowed through and incubated in the microchannels, immobilization occurs at the gold sensing regions of the SPR slides. The dimensions of the gold sensing regions are optimized for coupling with the dimensions of the microchannel and the optical sensing system of the SPR instrument. The gold deposition is achieved in a thermal evaporator using a novel lithographically produced PDMS shadow mask. These masks can be used to produce metal deposited patterns in the 10^{-6} m range. Considerations for the design of the microchannel manifold included; ease of fabrication, assembly and use, minimization of the number of inlets and outlets, channel design to minimize possible air bubble trapping, ensuring no cross-spot contamination and maintaining equal resistance to flow between microchannels. Physisorption of human blood serum proteins; albumin, fibrinogen, IgA, IgM and IgG were investigated against functionalized C_{11} thiol thin films. Use of the microfluidic spotting device as a flow cell is also demonstrated through in situ covalent protein immobilization and protein assay testing. Initial work is also presented in developing an IgE immunoassay utilizing SPR label free detection.

ACKNOWLEDGMENTS

I would like to thank my supervisor Professor Jed Harrison for providing me with many opportunities and experiences, both professionally and personally, throughout my time in his group. Also, I would like to thank Professor Mark McDermott for all his helpful discussions over the years. I especially would like to thank Abedaw Jemere, Dolores Martinez, Josh Wasylycia and Kowlasar Misir for providing support both inside and outside the lab.

Many aspects of what is presented here could not have been done without the efforts of the staff at the University of Alberta Nanofabrication Facility and the Department of Chemistry Machine Shop and Electronics Shop. Special thanks need to be given to Dr. Ken Westra, Dieter Starke, Ed Feschuk, Al Chilton and Kim Nguyen-Do.

Special thanks need to be given to my wonderful family for their constant love and support. My parents, Thomas and Lucia Flaim, have sacrificed in many ways to afford me every opportunity and always encouraged me to aim as high as I possibly wanted and always told me that if I wanted to achieve something, I could do it, if I just put my heart into it. To them I owe everything, and in return I can only give my deepest heartfelt thanks. In addition, while we may be separated by geography and professions, my brother and sister, Roger and Nadia have always served as examples of inspiration, to which I constantly try to aspire.

These acknowledgments would not be complete without my loving thanks to Malgosia Ejsmont. A love such as yours, has made all the ups of this work that much sweeter and all the lows much more bearable. Your never ending optimism and words of encouragement always provided me with extra strength, motivation and love. Words can not express my gratitude, nor can I imagine ways of repaying you, except to say, I love you with all my heart.

TABLE OF CONTENTS

LIST OF FIGURES	4
LIST OF TABLES	7
LIST OF ABBREVIATIONS	8
LIST OF EQUATIONS	10
LIST OF SYMBOLS	11
CHAPTER 1: INTRODUCTION	13
1.1 INTRODUCTION	14
1.2 SURFACE PLASMON RESONANCE	16
1.3 MICROFLUIDICS IN SPR	19
1.4 THIOL SELF ASSEMBLED MONOLAYERS	22
1.5 PLASMA PROTEINS	24
1.6 PROTEIN ADSORPTION	29
1.7 IMMUNOASSAYS	31
1.8 SCOPE OF THE THESIS	33
1.9 REFERENCES	34
CHAPTER 2: MICROFLUIDIC SPR SENSOR: DESIGN AND FABRICATION	38
2.1 INTRODUCTION	39
2.2 CHIP DESIGN	40
2.2.1 SI MASTER PROCESSING	42
2.2.1.1 MASK DIMENSIONS	42
2.2.2 PDMS PROCESSING	49
2.2.2.1 MICROCHANNEL MANIFOLDS	50
2.2.2.2 MICROSPOT ARRAYS	51

2.2.3 SPR SLIDE FABRICATION	56
2.2.4 DEVICE ASSEMBLY	57
2.3 EVALUATION	59
2.3.1 SPOT-TO-SPOT CONTAMINATION	60
2.3.2 RESISTANCE TO FLOW	63
2.4 NEW DESIGNS	68
2.5 96 SPOT MICROFLUIDIC SPR ARRAY	72
2.5.1 FABRICATION	75
2.5.2 EVALUATION	77
2.5.3 IMPROVEMENTS	78
2.6 CONCLUSIONS	79
2.7 REFERENCES	80
CHAPTER 3: SPR PLASMA PROTEIN ADSORPTION STUDIES	83
3.1 INTRODUCTION	84
3.2 EXPERIMENTAL	86
3.2.1 REAGENTS AND SOLUTIONS	87
3.2.2 INSTRUMENTATION	88
3.2.3 PROCEDURE	89
3.3 RESULTS	93
3.3.1 HUMAN PLASMA PROTEIN ISOTHERMS	93
3.3.2 THIOL REFRACTIVE INDEX CHANGES	102
3.4 CONCLUSIONS	107
3.5 REFERENCES	108

CHAPTER 4: MICROFLUIDIC DEVICES FOR PROTEIN MICROARRAYS	113
4.1 INTRODUCTION	114
4.2 EXPERIMENTAL	116
4.2.1 REAGENTS AND SOLUTIONS	117
4.2.2 CHIP DESIGN AND FABRICATION	118
4.2.3 SPR IMAGING	119
4.2.4 PROCEDURES	122
4.3 RESULTS	124
4.4 IGE ASSAY DEVELOPMENT	139
4.5 CONCLUSIONS	144
4.5 REFERENCES	145
CHAPTER 5: CONCLUSIONS AND FUTURE WORK	148
5.1 INTRODUCTION	149
5.2 CONCLUSIONS	149
5.3 ON-GOING WORK	150
5.3.1 CHIP DESIGN	150
5.3.2 PROTEIN ADSORPTION STUDIES	153
5.4 REFERENCES	155

LIST OF FIGURES

CHAPTER ONE	INTRODUCTION
Figure 1.1: Schematic of surface plasmon resonance phenomena	17
Figure 1.2: Illustration of characteristic SPR curves	19
Figure 1.3: Surface patterning utilizing parallel microfluidic channels	21
Figure 1.4: Alkyl thiol packing on a gold surface	24
Figure 1.5: The structure of three isotypes of immunoglobulins	25
Figure 1.5 continued: Structure of human albumin and fibrinogen	26
Figure 1.6: Protein adsorbing at a solid liquid interface	31
Figure 1.7: Labeled detection in immunoassays	32
CHAPTER TWO	MICROFLUIDIC SPR SENSOR: DESIGN AND FABRICATION
Figure 2.1: Design layouts considered for microfluidic spotter	41
Figure 2.2: CAD chip outlines used as masks for photolithography	43
Figure 2.3: Printed transparency mask	44
Figure 2.4: Process flow for SU-8 2050 negative photoresist	46
Figure 2.5: 100 μm thick SU-8 2050 coated Si wafer	48
Figure 2.6: Silanization of a silicon surface	50
Figure 2.7: Various sized Au spot SPR images	52
Figure 2.8: PDMS shadow mask fabrication procedure	54
Figure 2.9: Fabricated 100 μm thick PDMS shadow mask	56
Figure 2.10: Homebuilt alignment microscope	58
Figure 2.11: Au patterned sensor with a PDMS microchannel manifold	59
Figure 2.12: SPR images of Au patterned arrays	60

Figure 2.13: Images from video of solution flow through micro-channels	61
Figure 2.14: Image from of flow through redesigned PDMS micro-channels	62
Figure 2.15: Complete layout of the microfluidic channel manifold	63
Figure 2.16: PSpice flow simulation	66
Figure 2.17: Dye solution flowing through set of micro-channels	67
Figure 2.18: New design of microfluidic spotter to alleviate unequal flow	70
Figure 2.19: Four channel PDMS flow cell	72
Figure 2.20: CAD layout for the full 96 spot microfluidic device	74
Figure 2.21: Completed 96 spot microfluidic SPR sensor device	76
Figure 2.22: SPR difference image for protein surface binding	78
CHAPTER THREE	
SPR PLASMA PROTEIN ADSORPTION STUDIES	
Figure 3.1: Schematic diagram SPR holder assembly	89
Figure 3.2: Aligned 24 Au spot SPR slide and PDMS microfluidic manifold	90
Figure 3.3: Determination of binding by use of difference images	92
Figure 3.4: Human IgA, IgM, IgG and serum albumin isotherm plots	94
Figure 3.5: Surface adsorption plot of Human fibrinogen	95
Figure 3.6: SPR image response for –OH, –CH ₃ , –COOH and –NH ₂ surface	103
Figure 3.7: SPR curve for –OH, –CH ₃ , –COOH and –NH ₂ surface	104
Figure 3.8: Refractometry plot of –OH, –CH ₃ , –COOH and –NH ₂ alkyl thiols	106
CHAPTER FOUR	
MICROFLUIDIC DEVICES FOR PROTEIN MICROARRAYS	
Figure 4.1: A schematic representation of a SPR imaging instrument	120
Figure 4.2: EDC/NHS reaction scheme	122
Figure 4.3: Aligned SPR slides and PDMS microfluidic manifold	125

Figure 4.4: Reaction profile for EDC/NHS covalent amine coupling	127
Figure 4.5: Reaction profile for anti human IgG	129
Figure 4.6: Cross reactivity time series profile for anti h IgG and anti s IgG	133
Figure 4.7: Representation of combined spotting and microfluidic flow cell	134
Figure 4.8: Anti h IgG isotherm formed from using microfluidic flow cell	135
Figure 4.9: Cross reactivity isotherms formed from using microfluidic flow cell	138
Figure 4.10: Microfluidic flow cell SPR difference image	140
Figure 4.11: Reaction profile for 50 $\mu\text{g mL}^{-1}$ hIgE	141
Figure 4.12: Humand IgE calibration curve generated using the Biacore 3000	142
Figure 4.13: Sensograms of 1:25 human plasma on various surfaces	143
Figure 4.14: NSA for increasing human plasma concentrations	144
CHAPTER FIVE	CONCLUSIONS AND FUTURE WORK
Figure 5.1: Outline for forming tubing adapters to PDMS	151
Figure 5.2: Possible alternate designs	152

LIST OF TABLES

CHAPTER TWO	MICROFLUIDIC SPR SENSOR: DESIGN AND FABRICATION	
Table 2.1:	Comparison of SU-8 processing parameters	47
Table 2.2:	Determined SU-8 processing parameters	49
Table 2.3:	Calculation of diffusion distance	61
Table 2.4:	Channel flow rates	63
Table 2.5:	Calculated flow resistances	64
Table 2.6:	Calculated flow resistances	64
CHAPTER THREE	SPR PLASMA PROTEIN ADSORPTION STUDIES	
Table 3.1:	Langmuir isotherm fitting parameters for IgA	94
Table 3.2:	Langmuir isotherm fitting parameters for IgM	94
Table 3.3:	Langmuir isotherm fitting parameters for HSA	94
Table 3.4:	Langmuir isotherm fitting parameters for IgG	94
CHAPTER FOUR	MICROFLUIDIC DEVICES FOR PROTEIN MICROARRAYS	
Table 4.1:	Langmuir isotherm fitting parameters for Anti h IgG binding	135
Table 4.2:	Langmuir isotherm fitting parameters for cross reactivity binding	138

LIST OF ABBREVIATIONS

SPR	Surface Plasmon Resonance
DNA	Deoxyribonucleic acid
RNA	Ribonucleic acid
FTIR	Fourier transform infrared
ELISA	Enzyme linked immunosorbent assay
TIR	Total internal reflection
CCD	Charge-couple device
μ TAS	Micro total analysis systems
PDMS	Polydimethylsiloxane
LB	Langmuir-Blodgett
SAM	Self assembled monolayer
IRAS	Infrared reflection adsorption spectroscopy
XRD	X-ray diffraction
-NH ₂	11-mercaptoundecylamine
-COOH	11-mercaptoundecanoic acid
-CH ₃	11-undecanethiol
-OH	11-mercapto-1-undecanol
h	Human
s	Sheep
b	Bovine
Ig	Immunoglobulin
IgG	Immunoglobulin G

IgA	Immunoglobulin A
S-IgA	Secretory immunoglobulin A
SC	Secretory component
IgM	Immunoglobulin M
IgE	Immunoglobulin E
HSA	Human serum albumin
BSA	Bovine serum albumin
HF	Human fibrinogen
ADP	Adenosine diphosphate
rpm	Revolutions per minute
HEPA	High efficiency particulate air
PEB	Post exposure bake
LMW	Low molecular weight
L	Length
W	Width
D	Depth
CAD	Computer assisted design
PBS	Phosphate buffered saline
RAST	Radioallergosorbent test
HBS	HEPES buffered saline
EDC	1-ethyl-3-[3-dimethylaminopropyl]carbodiimide hydrochloride
NHS	N-hydroxysuccinimide
RIU	Relative intensity units

NSA Non-specific adsorption

LIST OF EQUATIONS

- 1.1** Incident light wavevector equation
- 1.2** Surface plasmon wavevector equation
- 1.3** Determination of difference images
- 2.1** UV lithography exposure time determination
- 2.2** Longitudinal diffusion calculation
- 2.3** Resistance to flow calculation
- 3.1** Langmuir isotherm

LIST OF SYMBOLS

θ_i	Incident Angle
θ	Fractional surface coverage
%R	Reflected light intensity as a percent of maximum
$\Delta\%R$	Change in percent reflectivity
I_p	Intensity of p-polarized light
I_s	Intensity of s-polarized light
k_{sp}	Plasmon wavevector
k_i	Incident light wavevector
n	Refractive index
K_{ads}	Adsorption coefficient
[C]	Solution concentration
D	Diffusion coefficient
R	Resistance
η	Viscosity
Å	10^{-10}
n	10^{-9}
μ	10^{-6}
m	10^{-3}
c	10^{-2}
k	10^3
g	Grams
m	Meter

mol	Mole
M	Molar
Pa	Pascal
cal	Calorie
Da	Dalton (atomic mass unit)
Ca	Calcium
I ¹³¹	Iodine 131
Si	Silicon
s	Second
min	Minute
°C	Degrees celsius
UV	Ultra violet
λ	Wavelength
t	Time
L	Liter
Au	Gold
Cr	Chromium
H ₂ SO ₄	Sulfuric acid
H ₂ O ₂	Hydrogen peroxide
N ₂	Nitrogen
O ₂	Oxygen
Al	Aluminum
pI	Isoelectric point

CHAPTER 1	INTRODUCTION
1.1 INTRODUCTION	14
1.2 SURFACE PLASMON RESONANCE	16
1.3 MICROFLUIDICS IN SPR	19
1.4 THIOL SELF ASSEMBLED MONOLAYERS	22
1.5 PLASMA PROTEINS	24
1.6 PROTEIN ADSORPTION	29
1.7 IMMUNOASSAYS	31
1.8 SCOPE OF THE THESIS.....	33
1.9 REFERENCES	34

1.1 INTRODUCTION

Surface plasmon resonance (SPR) has emerged as a unique detection method utilized extensively in research and clinical laboratories for bioanalytical measurements. SPR is based on the refractive index change measured on a solid/liquid interface during surface binding events. It has quickly been utilized as a label free detection method for biomolecular binding events including investigations of polypeptides,¹ polymer films,² immunoassays,³ drugs,⁴ allergens⁵ and viruses.⁶ The early use of SPR for biosensing can be traced back to the early 1980s and the work of Liedberg et al.^{7,8}

Label free methods of detection are extremely useful for monitoring biomolecule binding events. DNA labeling requires a relatively facile procedure due to the homogenous nature of its structure and its ability to intercalate dyes for non-covalent labeling, while protein labeling can be difficult. The heterogeneous nature of protein structures can lead to cumbersome labeling protocols, multiple labels per target, possible interference with binding sites or possible perturbation of protein activity. Thus, the development of label free detection methods for protein interactions has received much attention. Examples include; ellipsometry, FTIR, quartz crystal microbalance, and mass spectroscopy. However, SPR is capable of performing in situ, real time, high throughput analysis all within a novel instrumental design (Chapter 4.2.3). Furthermore, SPR instrumentation has developed to include imaging systems capable of detecting arrayed analytes for simultaneous monitoring of multiple bimolecular interactions.

Immunosensors based on the principle of solid-phase immunoassays and antigen antibody binding are one of the most popular techniques for biosensing. This results from the specific “lock and key” binding that can be achieved from various types of biomolecular analytes, such as proteins and nucleic acids. The most extensively used protocol for immunosensors is enzyme linked immunosorbent assay (ELISA). This method is used for the detection of a vast array of clinically important analytes such as disease biomarkers, hormones, lipoproteins, antibodies, viruses, bacteria and microbes in biological samples. ELISA relies on labeled reagents for the detection of binding between a surfaced immobilized target and its complementary probe. While analysis throughput up to 1536 wells is routine, difficulties involving sample handling, long analysis times and high consumption of expensive sample and reagents exists. These

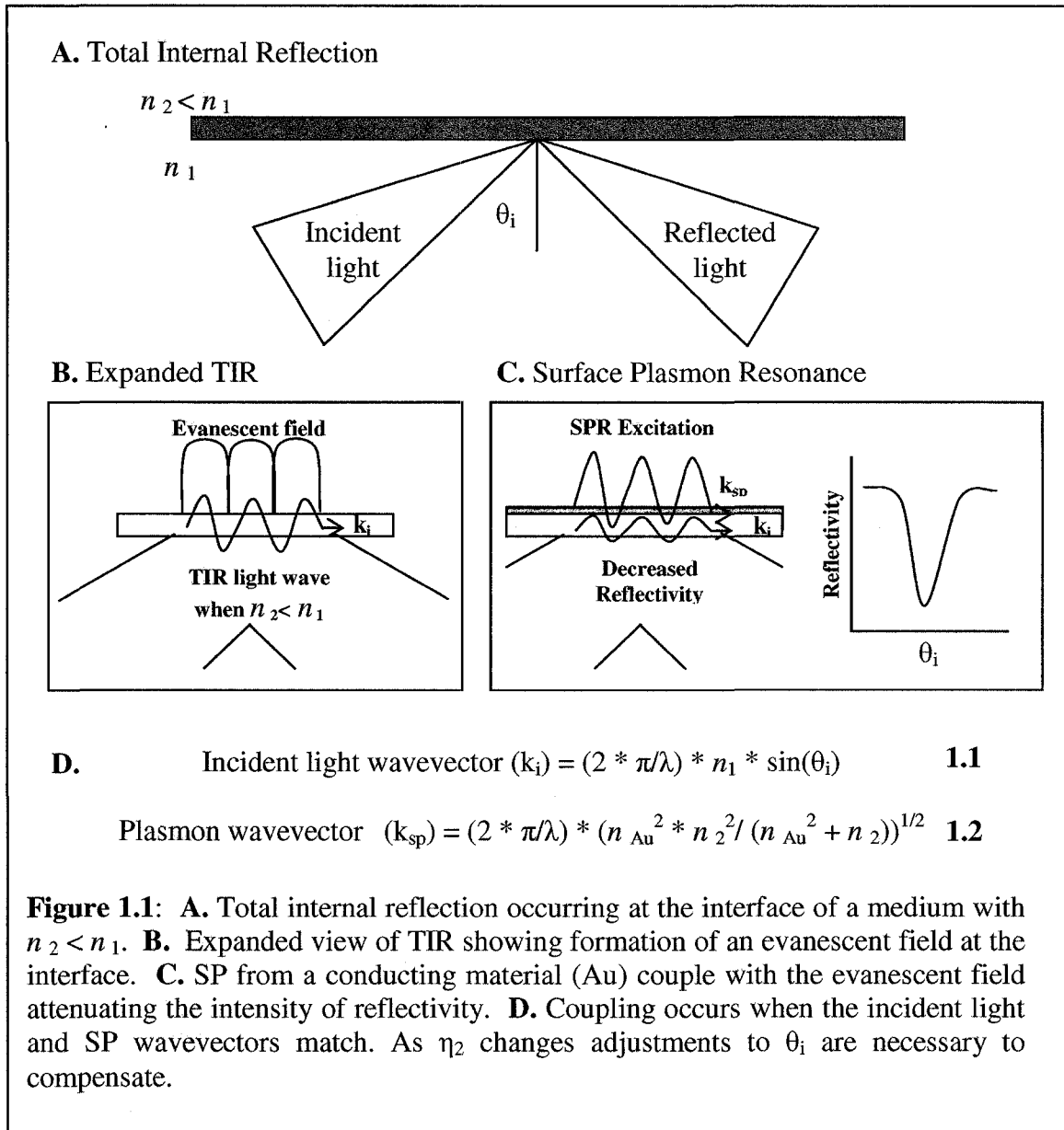
compromises may be acceptable in order to achieve throughput of samples in the thousands, as effectively showed by Schrieber et al.⁹ However, for lower density sample arrays in clinical diagnostics, bedside or point of care devices and investigations of relatively few analytes in research labs, the difficulties of ELISA can be burdensome. Also, ELISA can require expensive specialized equipment for implementation, which may not be cost effective for low density array analysis. To alleviate these difficulties and associated high cost of entry into this type of bioanalytical measurements, research has focused on the use of microfluidics as a platform for immunoassays.

Immunoassays based on microfluidic designs result in reduced sample and reagent consumption, as well as providing a path for miniaturized integrated functionalities such as flow control, mixing and detection. Combining these can potentially lead to lower cost of analysis. Furthermore, the high surface to volume ratio of microfluidics devices enhance solution mass transport to the surface, resulting in decreased analysis time. Delamarch et al.¹⁰ reported on the successful implementation of ELISA measurements in a microfluidics platform, resulting in less consumption of reagents and faster incubation times. Since these initial results, more sophisticated, fully integrated microfluidics platforms have emerged for ELISA measurements.¹¹

Considering the benefits associated with microfluidic systems for immunoassays, applications utilizing SPR detection have moved towards incorporating microfluidics.^{12, 13} In this way, benefits of a label free detection method are incorporated with the benefits of miniaturization. SPR based immunosensors utilizing microfluidics would be uniquely positioned, for bedside monitoring, point of care systems and research laboratory analysis. These types of applications would benefit from this combined analysis method, offering rapid, straightforward, and potentially low cost. Kurita et al.,¹⁴ reported the development of a SPR system using microfluidics for detection of a cardiac biomarker. This system resulted in comparable sensitivity for detection of clinically relevant samples, within a straightforward and portable instrument, compared to labeled detection methods utilizing fluorescence and radioisotope detection. While this example was specific for a particular biomarker, it illustrates the great potential for combined SPR microfluidic devices. Yet, there still exists the need for further designing and development of microfluidic devices for implementation with SPR detection.

1.2 SURFACE PLASMON RESONANCE

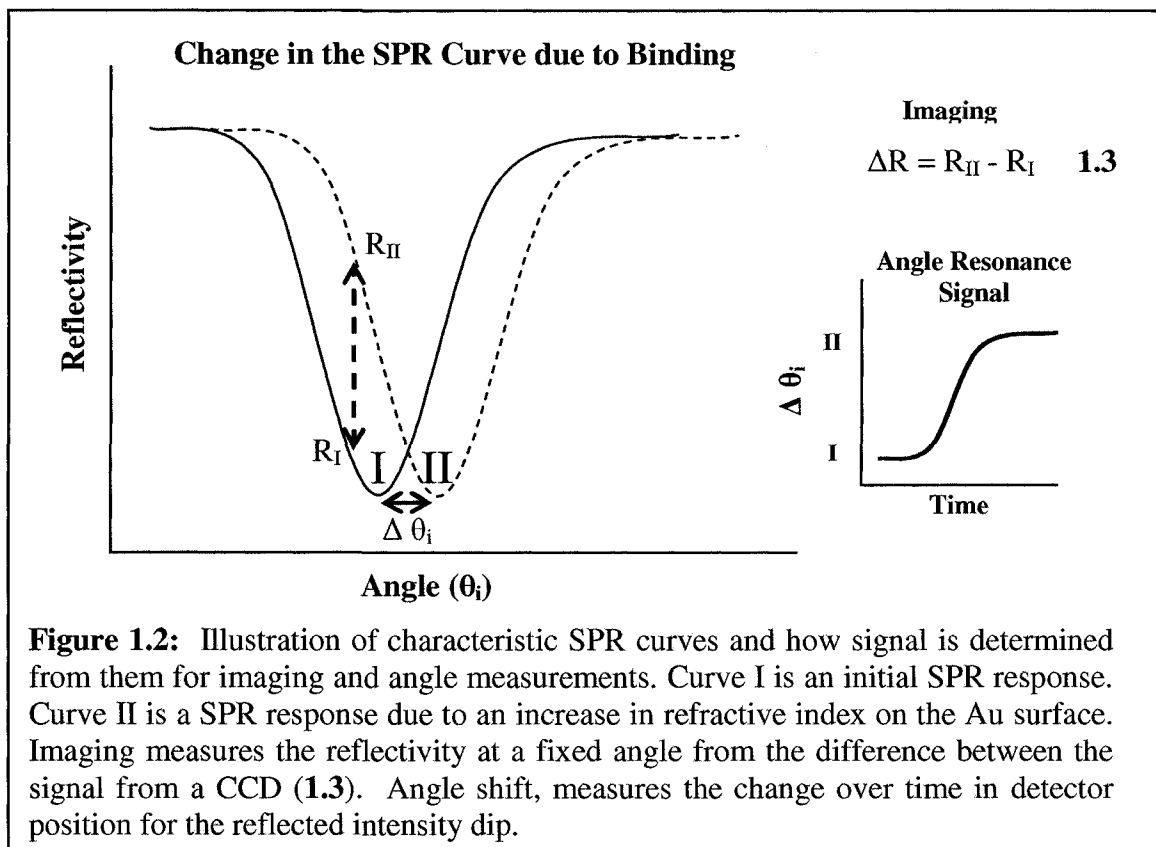
Surface plasmon resonance (SPR) is an intriguing surface sensitive phenomenon used to characterize molecular thin films on the surface of a conducting material, often gold. It was first reported by Wood in 1902.¹⁵ SPR relies on the phenomenon of total internal reflection (TIR) which occurs when light travels from a medium of high index of refraction and reflects completely at the boundary of a medium with a lower index of refraction. TIR only occurs above a critical angle that is defined by the ratio of the two index of refraction values forming the medium boundary. While the incoming light is fully reflected under conditions of TIR, the electromagnetic field of the reflected photons extends beyond the reflecting surface, forming an evanescent wave. If the boundary interface of the two differing mediums is coated with a layer of conducting material, such as gold, the evanescent wave can interact with the surface plasmon waves propagating within the gold layer. Surface plasmon is the term used to describe the natural fluctuations of the free valence surface electrons in a metallic solid. Since the plasmon waves are bound to the metal surface, interaction with the incident light evanescent wave is only with the component of the incident light that is parallel to the conductor surface (p-polarized). At a certain angle of incidence (θ_i) and wavelength of light (λ) there is a wave vector and energy match between the evanescent wave and surface plasmons. This match results in a resonant adsorption and surface plasmon excitation that causes a characteristic drop in the intensity of the reflected light. This excitation of the surface plasmons by reflected photons is termed Surface Plasmon Resonance. Changes in the refractive index adjacent to the gold surface, through which the surface plasmon wave penetrates, causes a mismatch of the evanescent wave and surface plasmons. This mismatch can be compensated for by changing the angle of incidence of the TIR required to create anew the SPR phenomenon. Figure 1.1 graphically illustrates the SPR phenomenon.



The fields associated with surface plasmons extend into the media adjacent to the interface and exponentially decay away with a maximum decay length of approximately 200 nm. Within this 200 nm region, the optical fields are sensitive to changes in the index of refraction caused by changes in the thickness of the molecular layer on the gold surface. Since the thickness of the molecular thin film is determined by the number and size of the attached molecules, SPR can be used to monitor molecular binding in the absence of labels. This is extremely valuable in studies of protein interactions, where molecular labels are often difficult to attach and labeling protocols may result in altering the characteristics or activity of the protein. Both increases and decreases in layer

thickness at the Au surface are readily detectable by SPR, thus binding and dissociation events may be measured.

SPR measurements can be made using two methods: 1. angle shift and 2. imaging. In both cases incident light reflectivity is measured as a function of incident angle, this is known as an SPR curve. At a particular angle, the reflected intensity is attenuated as a result of coupling with surface plasmons. The angle at which the minimum reflected intensity occurs is known as the SPR angle. This is the angle at which coupling with surface plasmons is maximized. The position and shape of the SPR curve are sensitive to changes in the local surface index of refraction, which is affected by any changes in the thickness or index of refraction of adsorbed films on the gold surface. For angle shift measurements, changes in the local refractive index are measured as a change in the angle associated with maintaining the minimum of the SPR curve. In this way the angle is scanned. For SPR imaging measurements the angle is maintained, and changes in the adsorbed surface film are measured as differences in intensity of reflected light at a constant angle. This method lends itself to ready implementation in an array format, where reflected light intensities can be measured spatially with a CCD sensor. Thus, an initial and final reflectivity image may be taken, and when subtracted from each other, result in a difference image showing areas of binding. Figure 1.2 illustrates the angle shift and imaging SPR measurement methods.



1.3 MICROFLUIDICS IN SPR

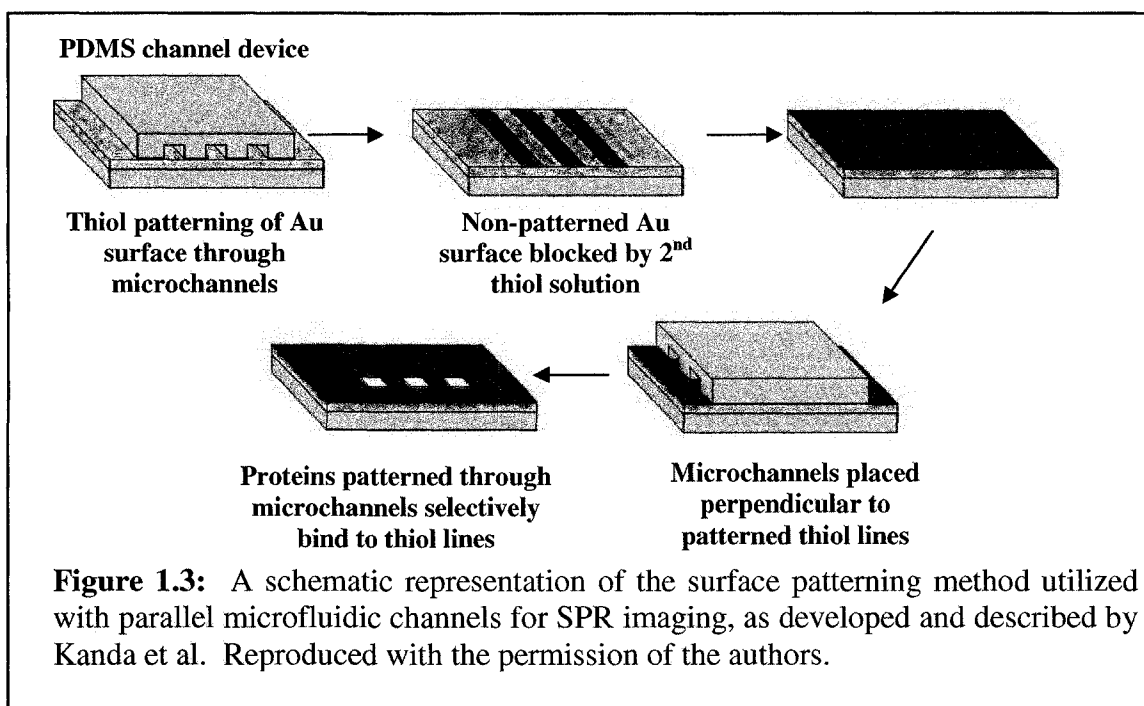
Microfluidics is the concept of fluid flow through miniaturized channels and has been an active area of research since the early 1990s. One of the first papers in this field dealt with a detailed analysis of the benefits possible through the miniaturization of chemical analysis systems to the micrometer scale.¹⁶ This work by Manz et al. describe the possibility of rapid analysis times, lower sample and reagent consumption, increased throughput and the ability to multiplex numerous analyses within one testing system. Derived from the idea of miniaturization and increased multiplexing is the Micro Total Analysis System (μ TAS) in which all aspects of sample handling, and detection would be possible in a miniaturized system.

From this initial analysis, microfluidic devices have been utilized in a variety of bio-analytical applications such as genetic analysis,¹⁷ clinical analysis¹⁸ and immunoassays.¹⁹ Considering the relative simplicity of SPR detection methods and the advantages of microfluidics for solution transportation and manipulation, combining

these two complementary approaches could possibly lead to great benefits for a wide variety of applications such as medical research and diagnostics, drug discovery and bio-analytical sensors.

Much of the work involved in combining microfluidic devices and SPR detection has focused on single channel sensors^{20, 21} used for incubating patterned sensor surfaces with analyte solutions. Patterning of the sensor surface with target biomolecules was initially achieved predominately by incubation of the sensor slide in a bulk solution of sample. This allowed for only one surface immobilized sample to be investigated at a time. These types of experiments were conducted with SPR spectroscopy methods monitoring the angle shift of the surface after binding. With the introduction of SPR imaging allowing for detection of arrayed samples, surface patterning of the sensor for increased sample density was achieved by the use of robotic pin printing or manual pepping methods. These methods allowed for a higher density of surface immobilized targets to be probed within one incubation experiment. While successful, these methods are labor intensive, requiring multiple steps and specialized procedures, with limited solution flexibility. Also, both methods of immobilization require extensive treatment of the surface in order to avoid spreading of sample droplets.²²

To alleviate some of these drawbacks, these types of experimental protocols were further expanded to patterning the sensor surface using parallel microfluidic channels, a method adapted from work utilizing microfluidics for fluorescence detection.^{10, 23} Utilizing microfluidics for surface patterning allowed for reduced reagent consumption, fewer patterning steps for minimizing non-specific adsorption and the creation of discrete regions of immobilization and detection. Figure 1.3 outlines the general experimental protocol used in this type of microfluidic patterning method, as presented in work by Kanda et al.¹²



In an attempt to ease array fabrication and increase sample density, SPR imaging sensors have moved towards using metal patterned sensor surfaces.²⁴ This allows for localization of the SPR phenomenon to specific areas of the sensor, reducing bulk background signal and easing detection. Immobilization to these patterned metal areas is achieved by again utilizing manual pepping or robotic pin printing. As previously discussed, these methods are effective at patterning the sensor surface with multiple targets, they still result in single sample incubation using a single port flow cell. While spot patterning of samples is convenient for array fabrication, drawbacks include rapid drying of droplet solutions and a necessity to pretreat the sensor surface to avoid spreading of sample droplets to neighboring Au spots.²⁴ A combined approach of metal patterning of the sensor surface with microfluidics, for both sample immobilization and as a multi channel flow cell for incubation with multiple probe analytes, could be advantageous, drawing from the benefits of both approaches. The most recent published work by Luo et al.¹³ in this field illustrates a similar approach.

The most successful implementation of microfluidics with SPR detection have been achieved by Biacore Inc. (Uppsala, Sweden). They provide systems with four integrated microfluidic channels for immobilization and detection. These systems are

widely used in bio-molecular and biochemistry research and have also been investigated for use in biomarker detection.²⁵ While successful, these systems are expensive, limited in their customizability and require specialized manufacturer accessories. Another drawback of the Biacore systems is their lack of an imaging component, thus not allowing for array format measurements. At the time of writing, Biacore had just released a new instrument capable of single exposure incubations over a 400 spot array of immobilized analytes.

1.4 THIOL SELF ASSEMBLED MONOLAYERS

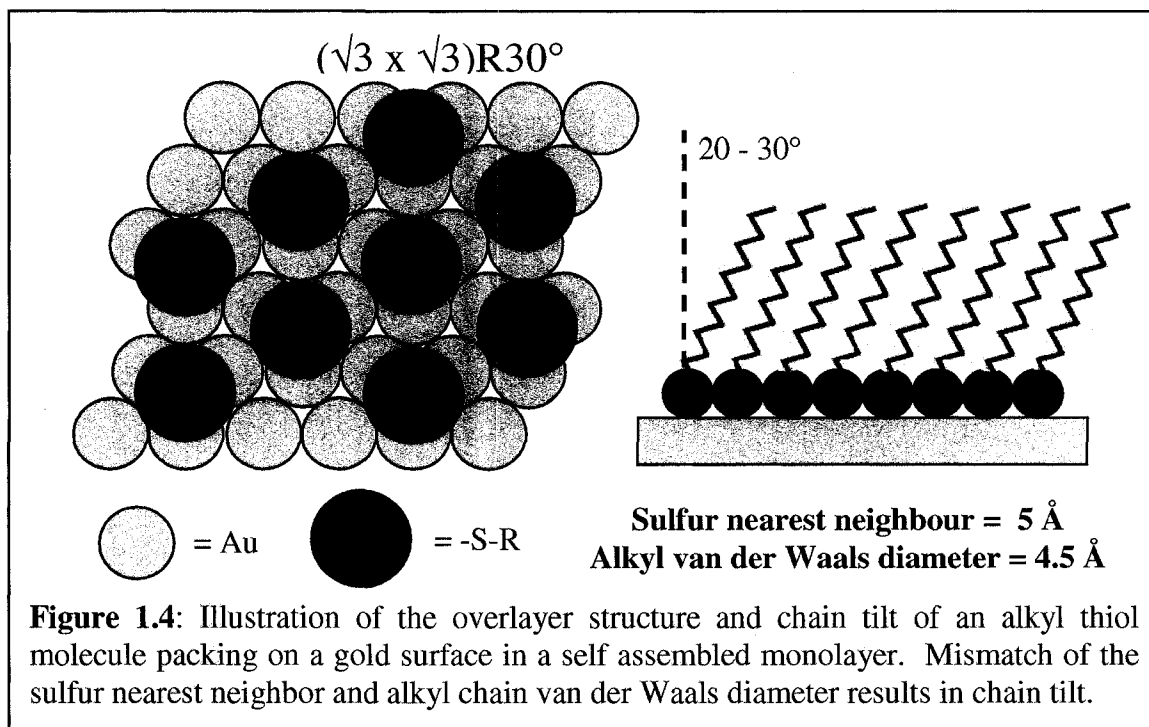
A significant amount of work has occurred in the area of thin film development for the purpose of achieving selective partitioning films for chemical and biochemical sensors and chromatographic systems.²⁶ The ability of organic molecules to organize into monolayer films through self assembly provides a route capable of well defined composition, thickness and chemical and physical properties. Early assembled thin films were formed by the Langmuir-Blodgett (LB) technique.^{27, 28} Here organic monolayers are formed first on the surface of an air-water interface for deposition onto a solid surface through the immersion of a substrate support. Typically the deposited film consists of an amphiphilic molecule, with a hydrophobic tail and hydrophilic head. The amphiphilic nature of the molecule is important to ensure a strong anisotropic interaction of the molecule with water thus favoring crystallization into a monolayer at the air-water interface. Subsequent immersions allow for the formation of multilayered films and control of the film thickness.

Drawbacks of LB films have limited their overall usefulness and versatility. These drawbacks include; film defects over large areas, instability of the films at high temperatures, lack of grain boundaries, amorphous structures, inhomogeneities due to substrate defects and noncovalent bonding interactions with the surface. An alternative for thin film monolayer formation on surfaces is self assembled monolayers (SAMs). Here, a substrate is covered by a solution containing the molecule of interest, which can spontaneously bind to the substrate surface forming a monolayer coating. This method provides a facile way of preparing surfaces with well defined thickness and permits the control of chemical and physical properties.

The most widely used SAM chemistry involves the chemisorption of organosulfur compounds to gold surfaces. This was first reported by Nuzzo and Allara who demonstrated the monolayer formation of alkyl disulfides.²⁹ This work was quickly followed by monolayer formation with thiol compounds.³⁰ The self assembly process is driven by the sulfur gold affinity which has a binding energy of 40-45 kcal mol⁻¹.³¹ For an alkyl chain with a thiol head group there is the spontaneous forming of a Au-S bond anchoring the alkyl chain to the substrate surface. As surface sites are occupied by sulfur groups a close packed monolayer forms, resulting in the alkyl tails packing together due to van der Waals forces. The mechanism of monolayer formation is thought to initially proceed with rapid formation of islands that over time then merge into a completely crystalline surface.

Studies utilizing infrared reflection adsorption spectroscopy (IRAS) and X-ray diffraction (XRD) have shown that thiol monolayers formed on Au(111) surfaces consist of densely packed alkyl chains which are pinned to the gold surface via the sulfur molecule in a ($\sqrt{3} \times \sqrt{3}$)R30° overlayer structure.³² The n-alkyl chains orient themselves in a ~ 20 - 30° angle relative to the surface normal due to a mismatch between the nearest neighbour distance on the surface (~ 5Å) and the alkyl chain van der Waals diameter (~ 4.5Å). This tilt allows for greater van der Waals interactions between the chains. The result is a structurally stable, ordered and crystalline monolayer. Alkyl chain length of thiol compounds used to form monolayers has also been studied. Porter et al.³⁰ reported that longer chain lengths (n > 9 carbon units) formed well ordered, densely packed crystalline monolayers. Shorter alkyl thiol chains resulted in lower packing densities and a more fluid like monolayer. Figure 1.4 illustrates the packing of the thiol chains that result in the SAM layer.

By forming ordered, crystalline monolayer surfaces on gold through SAMs it now becomes possible to systematically tune surface properties by changing the alkyl thiol end group. Common functional end groups that have been studied and reported on in the literature include, -NH₂, -COOH, -OH, -CH₃, and -OCH₂CH₂-X (polyethylene oxide). These end groups allow for tuning of surface chemistry based on charge and hydrophobicity.



1.5 PLASMA PROTEINS

Human blood is a specialized fluid continuously circulating throughout the body. It is composed of three types of blood cells (red, white and platelets) which are suspended in plasma, the liquid component of blood that is composed of approximately 90% water. The main constituent of the remaining 10% of plasma are proteins, with trace amounts of dissolved glucose, minerals, hormones and various waste byproducts, carbon dioxide, urea and lactic acid. Immunoglobulin G, A, M, albumin and fibrinogen comprise greater than 99% of the proteins in human plasma. Because of their relative abundance in human plasma these proteins were chosen for subsequent experiments involving protein adsorption studies. Thus, a brief discussion is given regarding their structure, function and properties. Figure 1.5 shows illustrations of these five proteins.

Immunoglobulins (Ig) are a class of glycoproteins known as antibodies. Functionally, antibodies are characterized by their ability to bind to antigens (complementary binding partners). Structurally, antibodies are characterized by their unique Y shape comprising of two heavy chain and two light chain polypeptides. Furthermore, based on their structures, the number of Y like units and type of heavy

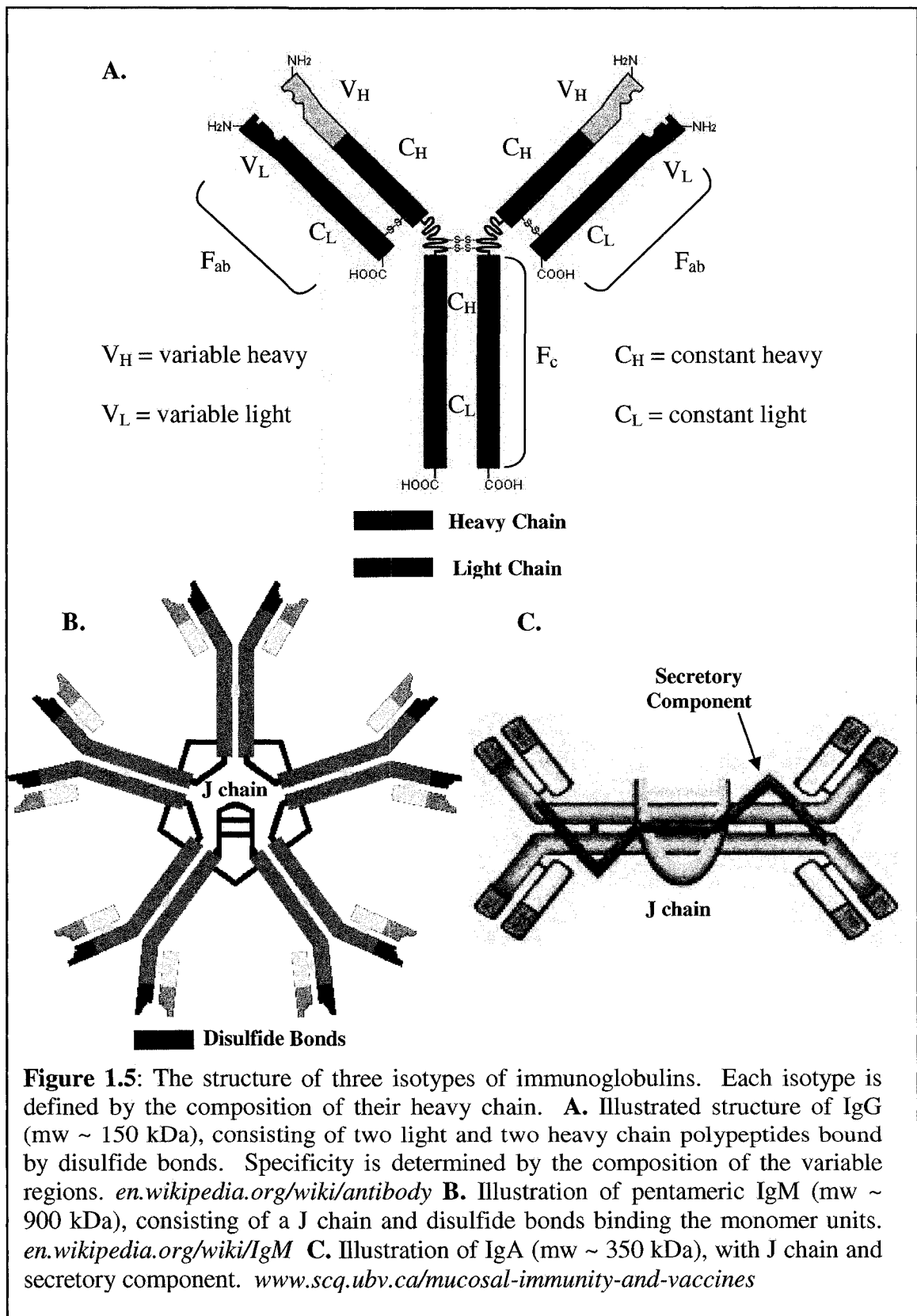


Figure 1.5: The structure of three isotypes of immunoglobulins. Each isotype is defined by the composition of their heavy chain. **A.** Illustrated structure of IgG (mw ~ 150 kDa), consisting of two light and two heavy chain polypeptides bound by disulfide bonds. Specificity is determined by the composition of the variable regions. en.wikipedia.org/wiki/antibody **B.** Illustration of pentameric IgM (mw ~ 900 kDa), consisting of a J chain and disulfide bonds binding the monomer units. en.wikipedia.org/wiki/IgM **C.** Illustration of IgA (mw ~ 350 kDa), with J chain and secretory component. www.scq.ubv.ca/mucosal-immunity-and-vaccines

D.



E.

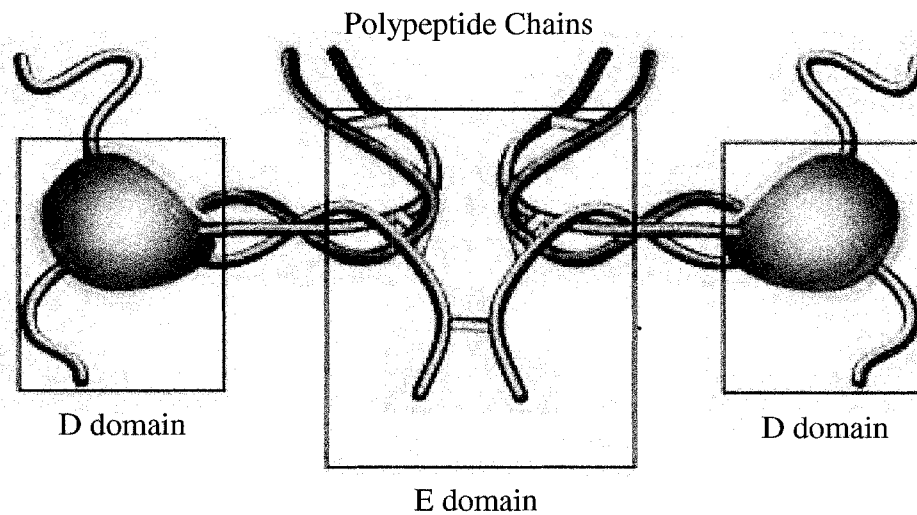


Figure 1.5 continued: **D.** Structure of albumin (mw ~ 67 kDa), a single polypeptide consisting mainly of α helices. en.wikipedia.org/wiki/human_serum_albumin **E.** Structure of fibrinogen (mw ~ 310 kDa), a dimer of 3 polypeptide chains with multiple domains. Fibrinogen is a large protein with a length of ~47 nm and a thickness of ~4 - 6 nm. www.sigmaldrich.com

chain, antibodies can be divided into five isotypes, IgA, IgD, IgE, IgG and IgM. In blood plasma IgA, IgG and IgM isotypes can be found in mg ml^{-1} concentrations. IgD and IgE are low abundant proteins found in plasma in the ng ml^{-1} concentration range. While IgD is important as a signal mediator and IgE is the primary antibody in the immune response of allergies, due to their low abundance, focus in this work was preferentially paid to IgA, IgG and IgM.

Many important structural features of immunoglobulins are shared among the different isotypes. For this reason, IgG antibodies, the most abundant antibody isotype in plasma, accounting for approximately 75% of total Igs, will be considered generally for all isotypes, with differences discussed separately.

IgG antibodies consist of three domains. Two of these domains have identical forms and constitute the arms of the Y. Each arm contains a site that may bind an antigen, thus making IgG, and each Y structural unit bivalent. These domain sites are known as Fab (fragment that antigen binds). The third domain constitutes the base of the Y structure and binds to various cell receptors and is known as Fc (fragment that crystallizes). These structural domains are formed from two heavy and two light chain polypeptides. Heavy and light chain polypeptides contain constant and variable regions. The constant regions are identical in all antibodies of the same isotype with the variable regions of both heavy and light chains combining to form one antigen binding site. There are five types of heavy chain polypeptides that result in the five isotypes, α , ϵ , δ , γ , μ . The differences in the heavy chain polypeptides, found primarily in the Fc domains, allow these proteins to function in different types of immune responses. The IgG structure is stabilized by four intermolecular disulfide bonds and has a molecular mass of ~ 150 kDa.

The different classes of antibodies can also vary in the number of Y like units that join to form a complete protein. IgM antibodies are composed of five Y structural units and form a pentamer linked together through disulfide bonds. Its structure contains an additional unit known as a J chain, a 15 kD polypeptide. It is the largest antibody in the human body with a molecular mass of ~ 900 kDa. IgA antibodies can also exist as polymeric structures of two or three IgA monomers. Polymeric IgA is found in human secretions and is known as secretory IgA. It consists of two additional structural units, a

J chain and a secretory component, a 70 kDa polypeptide that is added to IgA when it passes through epithelial cells. This secretory component is used to transport IgA protein through the cells and remains attached to the IgA molecule upon secretion. These three antibodies were chosen for study because they represented a variety of structures and chemistries within a single protein class.

The most abundant protein in human plasma is albumin. It is a monomeric protein with a molecular mass of ~ 67 kDa. Therefore, it is the smallest of the abundant blood plasma proteins. Its main function is as a transporter of species which may have low solubility in the aqueous environment of the blood, such as, hormones, fatty acids and drugs. Albumin possesses a heart shaped structure that contains mostly α helix. At physiological pH albumin possesses an overall -18 negative charge. Albumin is of interest because it is often used to passivate surfaces in protocols wanting to limit non-specific adsorption of proteins. Because it exists in high concentrations, it can also influence adsorption behavior of other proteins through competitive binding or the Vroman effect.³³

Another biologically critical protein is fibrinogen. It is the central protein in thrombosis, the blood clotting process that prevents excessive bleeding through a wound. These clots initially form when the enzyme thrombin converts fibrinogen to fibrin. These fibrin monomers polymerize to form a mesh like structure where platelet cells can adhere due to their fibrin surface receptors. Further platelet adhesion is stimulated by the release of Ca^{2+} and adenosine diphosphate (ADP) by surface bound platelets. With increased platelet aggregation, a stable clot is formed limiting bleeding. To achieve this type of behavior, the structure of fibrinogen is quite diverse. It is a 340 kDa dimeric glycoprotein that contains three different polypeptide chains (α , β , and γ) linked together by disulfide bonds. Attached to each γ chain is an oligosaccharide group. Within this diverse structure, there have been four major domains identified with varying hydrophobicities. The D and E domains are more hydrophobic, while both the C and M domains (located on the α chain) are both hydrophilic with the M domain exhibiting greater hydrophilicity. The resulting overall chemical behaviour at physiological pH is domains D and E are negatively charged and C and M are positively charged, with the overall charge of fibrinogen being -10. This variety of chemical properties, large size and distribution of charge allow fibrinogen to adsorb to a variety of surfaces.³⁴

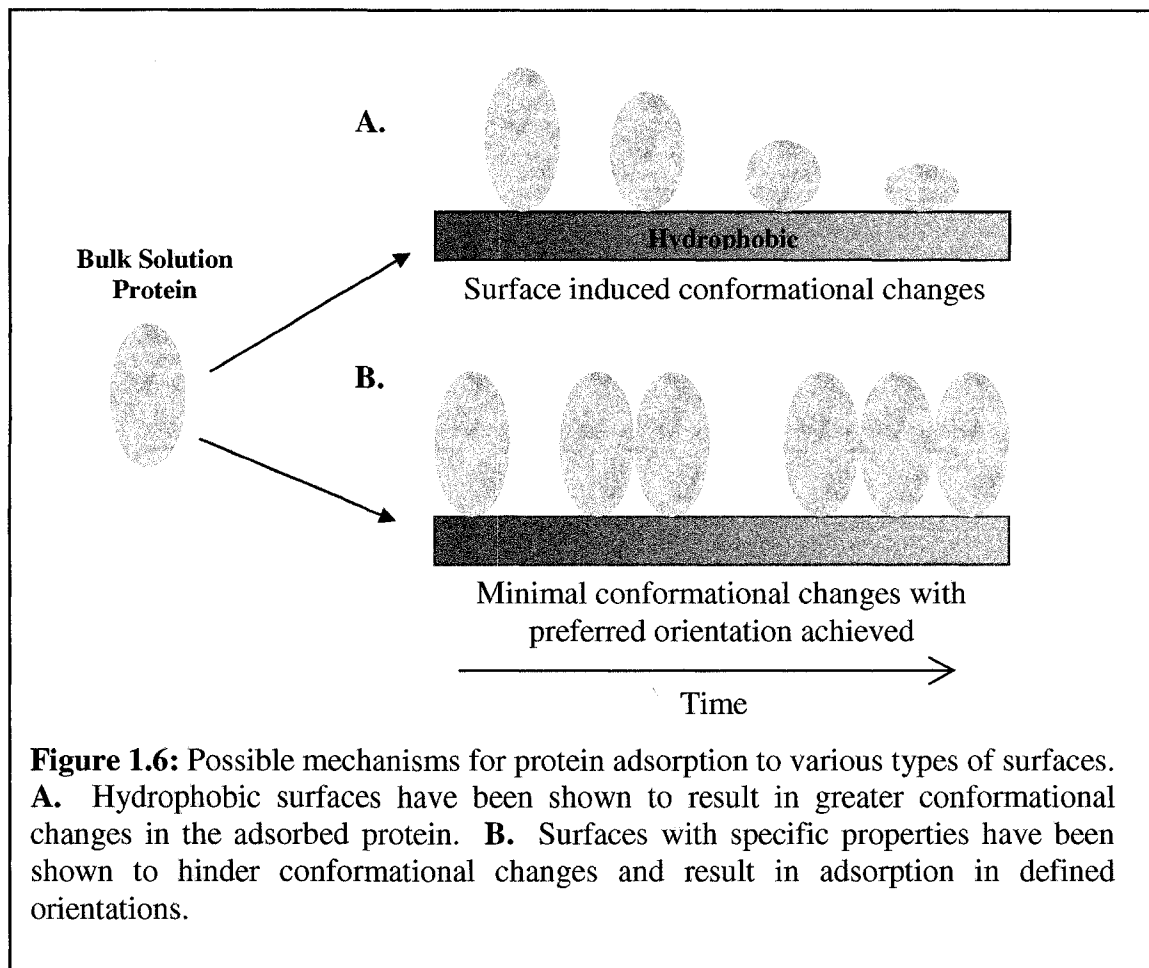
IgE is the least abundant of the immunoglobulin isotypes in human plasma, typically found in the $< 50 \text{ ng mL}^{-1}$ concentration range in healthy individuals. It has a bivalent, monomer structure similar to IgG, however, with an epsilon heavy chain. As a unit of the immune system it is part of the human body response to allergens. Allergens are foreign substances to the body that can cause extreme physiological reactions, such as eczema, hives and anaphylaxes. IgE has also been reported to have a role in the immune systems response to parasitic worms.^{35,36} When an individual possesses an allergy sensitivity they are said to be atopic and their IgE levels can measure in the mg mL^{-1} range. The mechanism of allergy response is based on the binding of IgE to Fc receptors on mast cells and basophiles called FcεRI.³⁷ Binding and aggregation of IgE on mast cells and basophiles causes degranulation of these cells and release of inflammatory mediators, such as histamines. It is not yet fully understood why allergy responses can vary from a mild runny nose to extreme anaphylaxes.

1.6 PROTEIN ADSORPTION

Proteins are biochemical molecules that perform specific functions within living systems. The functional properties of proteins depend upon their 3 dimensional structures which arise from their specific linear sequence of amino acids. There are 20 amino acids which are distinguished from each other through their varying side chains. These amino acids are joined together through peptide bonds in long chains forming polypeptides. This long chain of polypeptides is referred to as a protein's primary structure. As a result of interactions between the varying side chains of the polypeptide amino acids localized regular secondary structures, alpha (α) helices and beta (β) sheets form. Packing of secondary elements into compact globular units called domains leads to a proteins tertiary structure. This overall 3 dimensional shape is determined by the formation of disulfide bridges and non-covalent interactions (hydrogen bonding, electrostatic and van der Waals) that result in the sequestration of hydrophobic amino acids in the protein core and hydrophilic amino acids on the protein surface. Disruption in a protein's 3 dimensional structure, known as denaturation, leads to loss of activity. Denaturation can occur when the protein is exposed to external stress, such as, heating, increased ionic strength, exposure to organic solvents, large changes in pH or adsorption

to surfaces. These stresses can cause polypeptide chain unfolding and loss of secondary and tertiary conformation by disrupting the non-covalent interactions of the amino acids.

Due to the complex surface chemistry of proteins, a wide range of surface activities are possible, dependent on protein size, charge and structure. Larger proteins may interact to a greater degree with interfaces due to an increased number of contact points. Surface regions of various hydrophobicities and charges on the protein may exhibit preferential binding to interfaces of similar properties or opposite charges. Protein structural instability, determined by the lack of disulfide bonds, may result in proteins that unfold more readily on interfaces, increasing their area and interaction with the surface. This complexity leads to the ability of proteins to adsorb to a wide variety of surfaces. Understanding the process involved in the adsorption of proteins to surfaces is important in a number of different applications such as biosensors, chromatographic separations and materials biocompatibility. Along with the surface of adsorbing proteins the chemical properties of the surface interface also plays a key role in determining the characteristics of adsorption and the resulting adsorbed film. As a protein from the bulk solution phase approaches a surface interface it interacts with the surface through intermolecular forces. This interaction leads to attachment of the protein to the surface and relaxation of the adsorbed protein to achieve an optimal surface configuration. This relaxation can be driven by noncovalent interactions or entropic factors caused by surface induced conformational changes.³⁸ Due to these relaxation mechanisms the adsorbed protein film may undergo spreading of the protein molecules, structural rearrangements and conformational changes. As an example, it has been reported that hydrophobic surfaces induce greater conformational changes by increasing the hydrophobic interactions of inner amino acid groups.³⁹ Also, amine surfaces have been shown to hinder conformation changes and emphasize specific active molecular orientations.⁴⁰ Figure 1.6 illustrates how proteins may interact with various types of surfaces starting from a bulk solution adjacent to the surface interface to a final adsorbed film. These observations show a need for methods to systematically investigate the affect of surfaces and proteins on adsorption to solid interfaces.

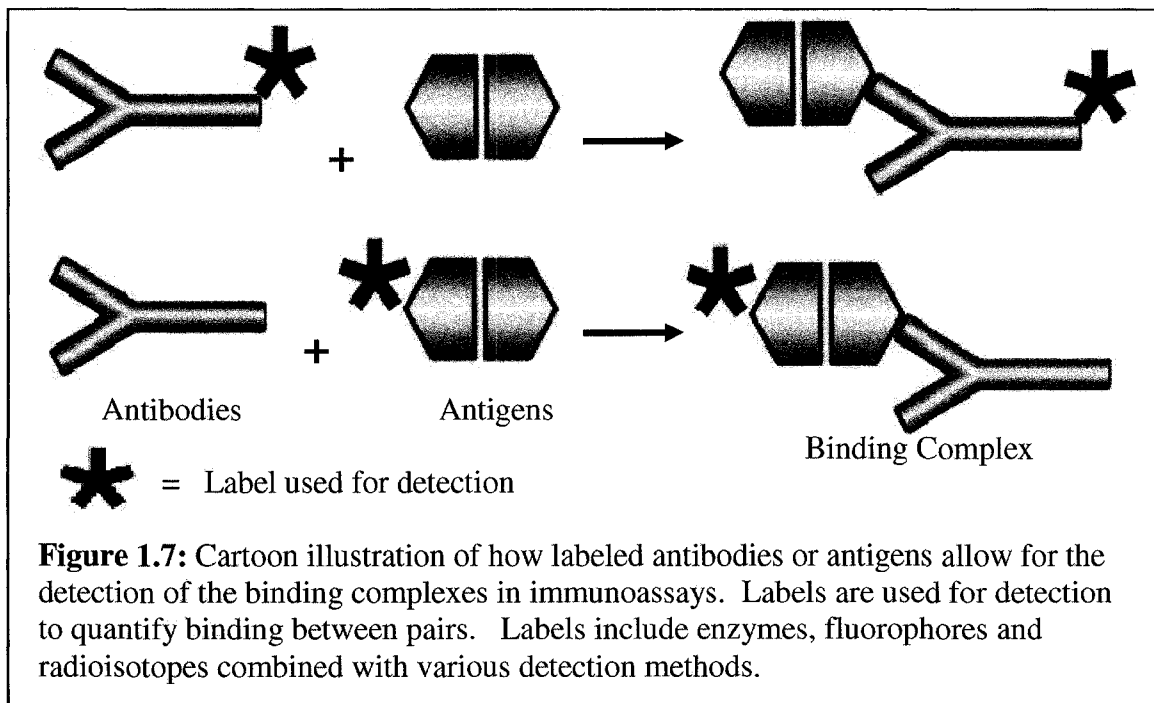


1.7 IMMUNOASSAYS

Immunoassays are tests that use antibody-antigen complexes to measure the presence of a specific analyte in a sample. Antibodies are proteins produced by the body that possess high specificity to foreign substances. These are part of the body's immune response mechanism. An exception to this, are autoimmune diseases, in which the body produces antibodies to normal naturally occurring bodily substances. By detecting the presence of specific antigens through their binding to known antibodies, diagnostic testing of healthy and disease states can be achieved. This experimental approach was first developed by Yalow and Berson in 1959 for the detection of the hormone insulin.⁴¹ Since this pioneering work, immunoassays have become one of the most important scientific and diagnostic tools utilized, with assays being developed for a wide variety of

analytes. As a result of this techniques rapid importance and its application Dr. Yalow received the Nobel Prize in Medicine in 1977 for his work.

The key factor in immunoassays is the detection of the antibody-antigen complex. This is achieved using labels, attached to one of the assay components that can be subsequently detected. During the early work of immunoassays, the most widely used label was radioactive iodine, I^{131} , which can be detected by scintillation counters. Due to the technical and safety disadvantages of radioisotopes, new labels based on chemiluminescence and fluorescence were developed,⁴² for which detection is achieved through measuring the intensity of emitted light. Figure 1.7 is a schematic representation of a typical binding immunoassay.



An extension of this work is that of protein arrays,⁴³ in which an array of proteins can be screened for biochemical activity against a range of analytes such as DNA, RNA, other proteins and ligands in a similar manner as immunoassays. While these methods are successful, there are drawbacks associated with the need for labeling to achieve detection. Two methods of labeling can be implemented, covalent attachment of the label to the analyte and non-covalent binding. Covalent labeling methods are time consuming often requiring special equipment and skills. They can also be hampered by

incomplete labeling, multiple labeling and the potential of labels interfering with the inherent activity of the protein. While non-covalent binding between labels and proteins has been demonstrated,⁴⁴ this does not provide a suitably generic protocol due to the variable reactivity and selectivity of these labels towards widely diverse proteins. Also, detection of labels often requires expensive specialized equipment focused on high throughput analysis. While cost effective, due to the large number of detected analytes, the need for this type of instrumentation for the investigation of limited subsets, or individual, proteins and antibodies may be burdensome. Thus, a straightforward, lower cost detection method would be advantageous.

Considering the number of potential proteins and antibodies that can be investigated, eliminating the necessity of labeling, while allowing for a more cost effective detection method, can potentially increase the ease of implementation of new protein and antibody tests. Recently, the label free detection method of SPR has been successfully proven for detection of immunoassays¹² and in single component clinical diagnostic tests of a cardiac bio marker.¹⁴ The work presented here is a further continuation of the use of SPR for label free detection of multi component immunoassays.

1.8 SCOPE OF THE THESIS

The work presented herein is divided into two sections: 1. device design and fabrication, and 2. applications of devices conceived. Here is a brief overview of topics to be discussed in the subsequent chapters.

Various designs and fabrication process flows are investigated and tested in Chapter 2 for the fabrication of polymer based microfluidic devices for SPR imaging measurements. With regards to device fabrication, a thick photoresist, SU-8 2050, was used as a template for casting polymer devices. Upon beginning this work SU-8 2050 was a non-standard resist in the University of Alberta Nanofabrication facility. Details of the optimum standard operating procedure developed for processing thick SU-8 photoresist will be discussed. Also presented, will be the operating procedures for processing thin films of polydimethylsiloxane (PDMS) used as a masking layer for metal deposition onto the SPR sensor substrates. Over the course of this work various designs

and design elements were introduced, augmented or removed to achieve a more straightforward process flow and device as possible. Various iterations will be discussed, that ultimately lead to the two main designs used in subsequent chapters. Further details regarding PDMS processing, mask design and flow testing of fabricated devices will also be presented.

Upon design and fabrication of proof-of-concept devices, an initial application was necessary for evaluating the potential of these microfluidic designs for SPR imaging. Chapter 3 presents investigations into the use of these devices for monitoring the simultaneous adsorption behavior of human plasma proteins to various surface chemistries. This work demonstrated the possibility of a facile experimental procedure, based on a microfluidic device and SPR imaging, for studying adsorption behavior of a variety of proteins to a variety of surfaces.

To further investigate the usefulness of the designed microfluidic devices, and to extend their experimental capabilities for SPR imaging, immunoassay experiments were undertaken. Chapter 4 examines human immunoglobulin assays performed using two different device designs, as well as an experimental procedure for an assay protocol utilizing both designs.

Through the work presented on the proof of concept microfluidic devices fabricated and experimentally tested, experience and knowledge of their performance was gained. Chapter 5 deals with applying this experimental experience to possible future modifications to the device design for increased usability and functionality. Also, proposals are made for possible future experiments that may further extend the experimental capacity of this microfluidic-SPR imaging platform.

1.9 REFERENCES

- (1) Woodbury, R. G.; Wendin, C.; Clendenning, J.; Melendez, J.; Elkind, J.; Bartholomew, D.; Brown, S.; Furlong, C. E. *Biosensors & Bioelectronics* **1998**, *13*, 1117-1126.
- (2) Green, R. J.; Davies, J.; Davies, M. C.; Roberts, C. J.; Tendler, S. J. B. *Biomaterials* **1997**, *18*, 405-413.
- (3) Hutchinson, A. M. *Analytical Biochemistry* **1994**, *220*, 303-307.

- (4) Kalab, T. *Chemicke Listy* **1995**, 89, 363-376.
- (5) Pierson, L.; Allauzen, S.; Blumenthal, M.; Rosenberg, A. *Journal of Immunological Methods* **1998**, 211, 97-109.
- (6) Schofield, D. J.; Dimmock, N. J. *Journal of Virological Methods* **1996**, 62, 33-42.
- (7) Liedberg, B.; Nylander, C.; Lunström, I. *Sensors and Actuators* **1983**, 4, 299-304.
- (8) Nylander, C.; Liedberg, B.; Lind, T. *Sensors and Actuators* **1982**, 3, 79-88.
- (9) MacBeath, G.; Schreiber, S. L. *Science* **2000**, 289, 1760-1763.
- (10) Delamarche, E.; Bernard, A.; Schmid, H.; Michel, B.; Biebuyck, H. *Science* **1997**, 276, 779-781.
- (11) Wang, C.-H.; Lee, G.-B. *Biosensors and Bioelectronics* **2005**, 21, 419-425.
- (12) Kanda, V.; Kariuki, J. K.; Harrison, D. J.; McDermott, M. T. *Analytical Chemistry* **2004**, 76, 7257-7262.
- (13) Luo, Y.; Yu, F.; Zare, R. N. *Lab on a Chip* **2008**, 8, 694-700.
- (14) Kurita, R.; Yokota, Y.; Sato, Y.; Mizutani, F.; Niwa, O. *Analytical Chemistry* **2006**, 78, 5525-5531.
- (15) Wood, R. W. *Proceedings of the Physical Society of London* **1902**, 18, 269-275.
- (16) Manz, A.; Graber, N.; Widmer, H. M. *Sensors and Actuators B: Chemical* **1990**, 1, 244-248.
- (17) Woolley, A. T.; Sensabaugh, G. F.; Mathies, R. A. *Analytical Chemistry* **1997**, 69, 2181-2186.
- (18) Deng, Y. Z.; Henion, J.; Li, J. J.; Thibault, P.; Wang, C.; Harrison, D. J. *Analytical Chemistry* **2001**, 73, 639-646.
- (19) Cheng, S. B.; Skinner, C. D.; Taylor, J.; Attiya, S.; Lee, W. E.; Picelli, G.; Harrison, D. J. *Analytical Chemistry* **2001**, 73, 1472-1479.

- (20) Oh, B. K.; Chun, B. S.; Park, K. W.; Lee, W. C.; Lee, W. H.; Choi, J. W. *Materials Science & Engineering C-Biomimetic and Supramolecular Systems* **2004**, *24*, 65-69.
- (21) Leonard, P.; Hearty, S.; Quinn, J.; O'Kennedy, R. *Biosensors & Bioelectronics* **2004**, *19*, 1331-1335.
- (22) Shumaker-Parry, J. S.; Zareie, M. H.; Aebersold, R.; Campbell, C. T. *Analytical Chemistry* **2004**, *76*, 918-929.
- (23) Rowe, C. A.; Scruggs, S. B.; Feldstein, M. J.; Golden, J. P.; Ligler, F. S. *Analytical Chemistry* **1999**, *71*, 433-439.
- (24) Wark, A. W.; Lee, H. J.; Corn, R. M. *Analytical Chemistry* **2005**, *77*, 3904-3907.
- (25) Yang, C. Y.; Brooks, E.; Li, Y.; Denny, P.; Ho, C. M.; Qi, F. X.; Shi, W. Y.; Wolinsky, L.; Wu, B.; Wong, D. T. W.; Montemagno, C. D. *Lab on a Chip* **2005**, *5*, 1017-1023.
- (26) Pesek, J. J., Matyska, M. T., Abuelafiya, R. R., Ed. *Chemically Modified Surfaces*; Royal Society of Chemistry: London, 1996.
- (27) Peterson, I. R. *Journal of Physics D-Applied Physics* **1990**, *23*, 379-395.
- (28) Ulman, A. *An Introduction to Ultrathin Organic Films: From Langmuir-Blodgett to Self-Assembly*; Academic Press: Boston, 1991.
- (29) Allara, D. L.; Nuzzo, R. G. *Journal of Electron Spectroscopy and Related Phenomena* **1983**, *30*, 11-11.
- (30) Porter, M. D.; Bright, T. B.; Allara, D. L.; Chidsey, C. E. D. *Journal of the American Chemical Society* **1987**, *109*, 3559-3568.
- (31) Dubois, L. H.; Zegarski, B. R.; Nuzzo, R. G. *Journal of the American Chemical Society* **1990**, *112*, 570-579.
- (32) Chidsey, C. E. D.; Liu, G. Y.; Rowntree, P.; Scoles, G. *Journal of Chemical Physics* **1989**, *91*, 4421-4423.
- (33) Vroman, L.; Adams, A. L. *Surface Science* **1969**, *16*, 438.

- (34) Feng, L., Andrade, J. D. In *Proteins at Interfaces II: Fundamentals and Applications* Horbett, T. A., Brash, J. L., Ed.; American Chemical Society: Washington, DC., 1995, pp 66 - 79.
- (35) Fitzsimmons, C.; McBeath, R.; Joseph, S.; Jones, F.; Walter, K.; Hoffmann, K.; Kariuki, H.; Mwatha, J.; Kimani, G.; Kabatereine, N.; Vennervald, B.; Ouma, J.; Dunne, D. *Int. Arch. Allergy Immunol.* **2007**, *142*, 40–50.
- (36) Watanabe, N.; Bruschi, F.; Korenaga, M. *Trends Parasitol.* **2005**, *21*, 175–8.
- (37) Kinet, J. P.; *Annu. Rev. Immunol.* **1999**, *17*, 931-72.
- (38) Norde, W. *Macromol. Symp.* **1996**, *103*, 5 - 18.
- (39) Brash, J. L., Horbett, T. A. In *Proteins at Interfaces II: Fundamentals and Applications* Horbett, T. A., Brash, J. L., Ed.; American Chemical Society: Washington, DC., 1995, pp 1.
- (40) Chen, S. F.; Liu, L. Y.; Zhou, J.; Jiang, S. Y. *Langmuir* **2003**, *19*, 2859-2864.
- (41) Yalow, R. S.; Berson, S. A. *Nature* **1959**, *184*, 1648-1649.
- (42) Schroeder, H. R.; Vogelhut, P. O.; Carrico, R. J.; Boguslaski, R. C.; Buckler, R. T. *Analytical Chemistry* **1976**, *48*, 1933-1937.
- (43) Zhu, H.; Snyder, M. *Current Opinion in Chemical Biology* **2001**, *5*, 40-45.
- (44) Jin, L. J.; Giordano, B. C.; Landers, J. P. *Analytical Chemistry* **2001**, *73*, 4994-4999. (35)

2.1 INTRODUCTION	39
2.2 CHIP DESIGN	40
2.2.1 Si MASTER PROCESSING	42
2.2.1.1 MASK DIMENSIONS	42
2.2.2 PDMS PROCESSING	49
2.2.2.1 MICROCHANNEL MANIFOLDS	50
2.2.2.2 MICROSPOT ARRAYS	51
2.2.3 SPR SLIDE FABRICATION	56
2.2.4 DEVICE ASSEMBLY	57
2.3 EVALUATION	59
2.3.1 SPOT-TO-SPOT CONTAMINATION	60
2.3.2 RESISTANCE TO FLOW	63
2.4 NEW DESIGNS	68
2.5 96 SPOT MICROFLUIDIC SPR ARRAY	72
2.5.1 FABRICATION	75
2.5.2 EVALUATION	77
2.5.3 IMPROVEMENTS	78
2.6 CONCLUSIONS	79
2.7 REFERENCES	80

2.1 INTRODUCTION

Surface Plasmon Resonance (SPR) imaging has emerged as an extremely versatile technique allowing for the multiplexed microarray analysis of various bioaffinity interactions (e.g., DNA, RNA, peptide, protein, carbohydrate).¹⁻⁷ In a SPR imaging experiment the change in reflectivity from a metal thin film due to changes in the local refractive index near the surface is used to monitor the adsorption of biomolecules from solution. The collected SPR imaging difference image can be quantitatively analyzed for the amount of adsorption without the need of any labeling agents, such as fluorophores, isotopes or nanoparticles.

Since the first reporting and development of SPR imaging⁸ there has been a progression in the immobilization methods and techniques used. Single analysis was readily achievable on fully-gold coated sensors. However, to take advantage of the multi-analysis capabilities of SPR imaging, UV photopatterning⁹ and linear microfluidic channels cast in PDMS¹⁰ were employed to aid in creating areas of high and low biomolecule specificity. These methods included patterning with Langmuir-Blodgett films and the use of various self assembled monolayers (SAMs) of ω -substituted alkanethiols. With UV photopatterning, deposition of solution to the surface was achieved by robotic or manual micro spotting, whereas adsorption to the surface using microfluidic channels results in deposition that occurs from the bulk solution rather than micro droplets.

Further developments resulted in a SPR imaging, sensor chip with patterned areas of gold.¹¹ These sensors offer high contrast areas for detection as the bulk sensor background gives zero signal since it is only in the presence of gold that the surface can manifest the Surface Plasmon Resonance (SPR) effect. While high detection contrast is important, these devices still require robotic pin printing or manual pipetting, usually with cumbersome protocols involving humidity and temperature control. Also, due to the close proximity of the spots used to achieve an optimal spot density, various surface chemistry modifications of the underlying glass must be used to confine the droplet within the gold area and avoid droplet spreading. These extra protocol steps and limitations ultimately hinder the experimentalist in terms of time and the combinations of solutions that may be used to avoid spot-to-spot contamination (e.g., aqueous or organic).

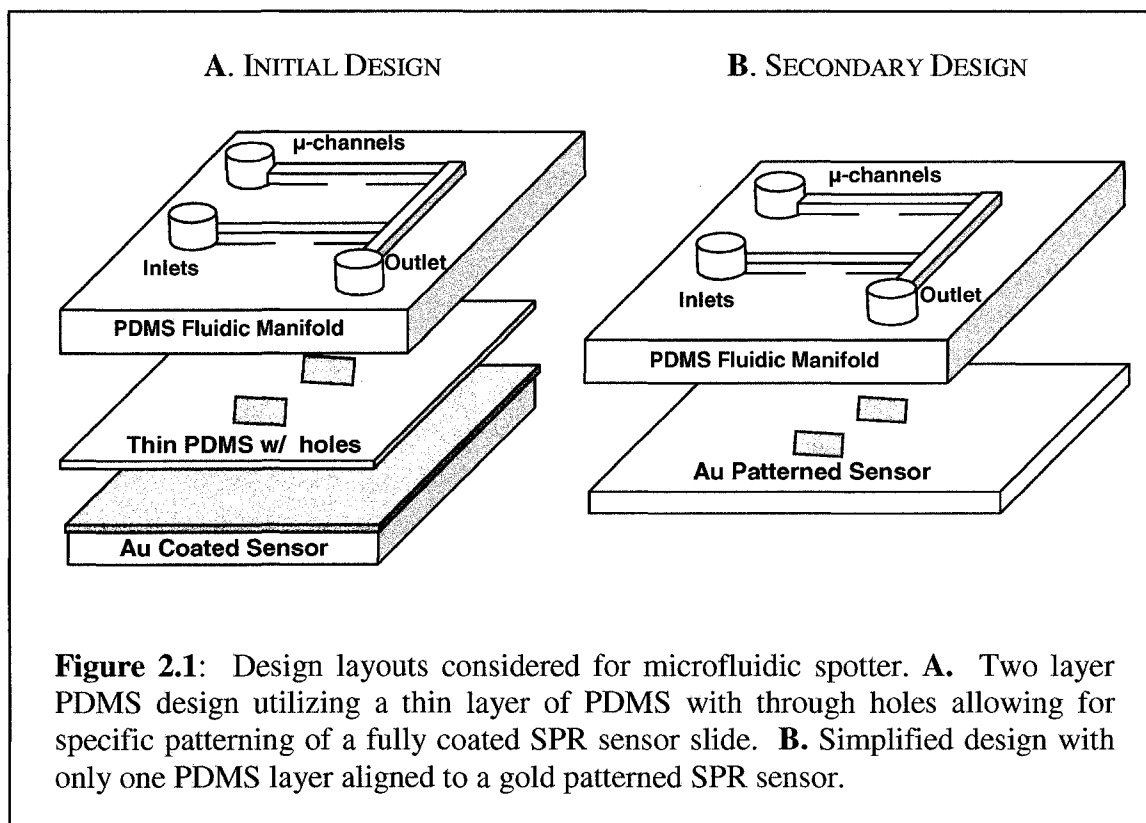
Furthermore, these devices are mounted in large volume flow cells that only allow one solution at a time to pass over the sensing surface. While a microfluidic flow cell, for small volume samples, has been demonstrated in the literature,¹² it was a single channel device used for single component analysis. A device that combines gold patterning to achieve high viewing contrast, allows for various solution types and limits the affect of drying and denaturation that occur with micro-spot patterning and allows for multiple simultaneous analyte solution introduction to the sensing surface, would be advantageous.

Due to the lack of large available protein libraries, and the increased cost and time for their development,¹³ many researchers and research areas focus on a limited subset of biomolecules of interest. Such low density sample requirements often do not justify the burdensome cost of high throughput systems, such as robotic pin printers, and their time consuming protocols, such as labeling and environmental controls. The material presented here in Chapter 2 will focus on the development of a robust micro-scale gold patterning technique for use with a unique microfluidic spotting device to create a convenient and customizable microarray platform for SPR imaging.

2.2 CHIP DESIGN

Figure 1.1 is a schematic of the proposed microfluidic spotting device. Initial designs focused on creating discrete areas of exposure from enclosed microchannels based on straight microchannels used in previous work.^{5, 10, 14} This required a 3-dimensional approach to the design and layout of the device, resulting in a multi-step fabrication and assembly procedure.¹⁵ This design and fabrication process ultimately proved successful but was very cumbersome and resulted in a low throughput of device fabrication. Since this initial design required the formation of a thin PDMS membrane for every device, much time and effort was needed in their assembly. To reduce difficulties in assembly and use of these early devices, new design features were incorporated. Gold (Au) sensing regions, to which analyte immobilization and detection occurs, were patterned on the SPR slide, providing areas of high detection contrast and good sealing properties to the PDMS. These sensing regions were aligned to a single 2-

deminsional polydimethylsiloxane (PDMS) microfluidic manifold thus eliminating multi layered fabrication methods.



While much time was spent on the initial design of the first prototype device (Figure 2.1A) experiences from this ultimately helped in future device iterations. The development of thin PDMS membranes with through-holes was effectively used for the surface patterning of the SPR sensors with gold. These membranes while difficult to fabricate for every device, were extremely durable for metal deposition and could be used multiple times for gold patterning. Also, to achieve a completed device based on Figure 2.1A, time was initially dedicated to the building of an alignment microscope specific for the SPR slides and microfluidic devices fabricated. This effort was then applied to future devices designed and since these devices were of a more straightforward design alignment became a routine step in the fabrication process.

PDMS was chosen as the substrate material for the microfluidic manifold because of its many advantageous features,¹⁶ such as its selfsealing conformal reversible/irreversible bonding properties, well known high fidelity replication

procedures and low cost. To provide a support for PDMS microchannel casting, positive relief photoresist silicon (Si) masters were fabricated. Photoresist masters have proven to be a reliable replication support for PDMS casting.¹⁷⁻¹⁹ There also exist routine procedures for photoresist processing on Si wafers.

The following chapter is divided into two main sections: 1 - device design and fabrication and 2 - evaluation and new designs. In the first section, the following are described; device dimensions and fabrication methods for both the PDMS microchannels and Au sensing regions. Dimensions for the Au sensing regions and subsequent channels were determined from two main factors; available total footprint (real estate) of SPR sensor and the optical unit on the SPR instrument. Available field of view and aperture settings of the optical unit ultimately limited the feature size of the sensing regions and the subsequent channel dimensions. Au patterning techniques utilized for SPR rely on machining shadow masks for Au depositions.¹¹ Machined shadow masks would not provide the necessary small sensing area needed in this work. Thus, alternate micro-patterning techniques were evaluated. To accommodate the height dimensions needed in the positive relief photoresist Si masters it was necessary to work with and determine a procedure for using thick photoresist. A commonly reported thick photoresist is the epoxy based negative resist SU-8, available from MicroChem Corporation (Newton, Mass. USA).²⁰⁻²³

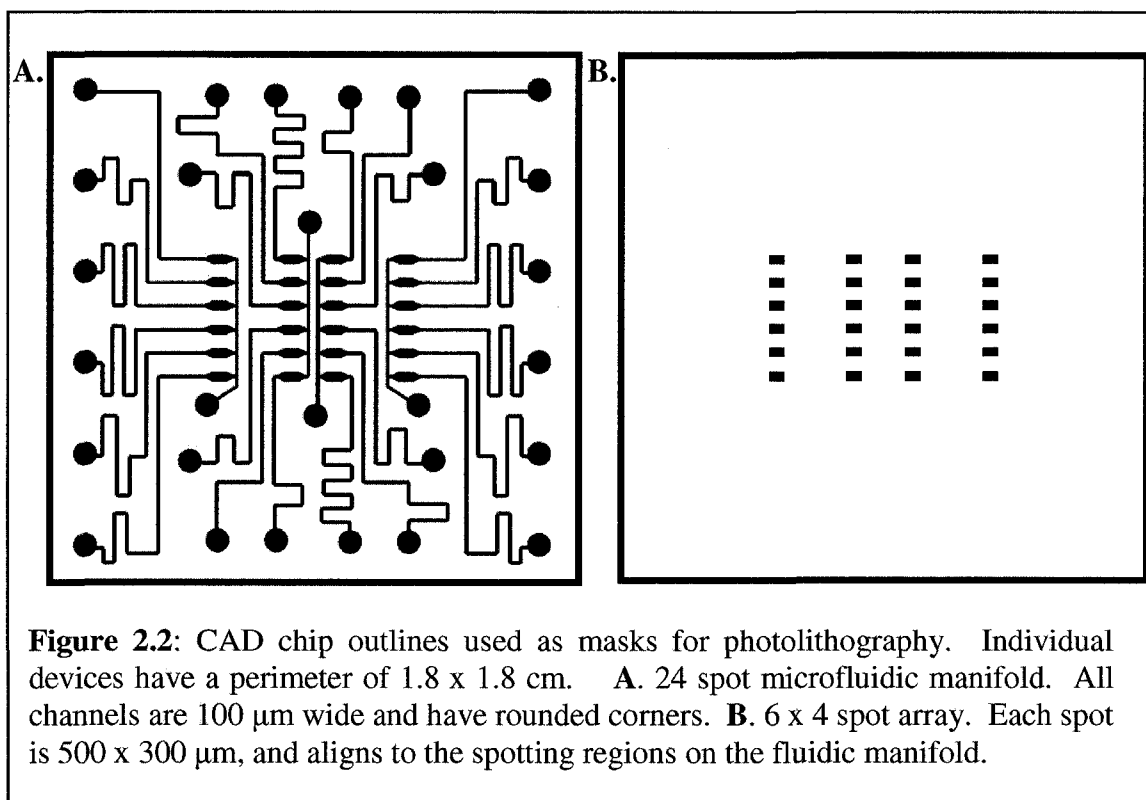
In the second section the following are described; procedures used to evaluate the performance of the fabricated devices and subsequent design changes to compensate for observed deficiencies. In an array format it is necessary to ensure that there is no spot-to-spot contamination. Since the design incorporates a common outlet examining and compensating for any spot-to-spot contamination is necessary. Evaluation of these prototype devices may also lead to better design and improved fabrication procedures.

2.2.1 Si MASTER PROCESSING

2.2.1.1 MASK DIMENSIONS

Figure 2.2 is a computer assisted design (CAD) illustration of the design for a 24 spot microfluidic spotting device used for the fabrication of positive relief photoresist masters on four inch Si wafers. The spot array mask is designed to align to the spotting

regions on the microfluidic manifold, therefore alignment marks were not necessary. To increase replication in the PDMS casting step, six devices were fabricated per Si wafer processed.



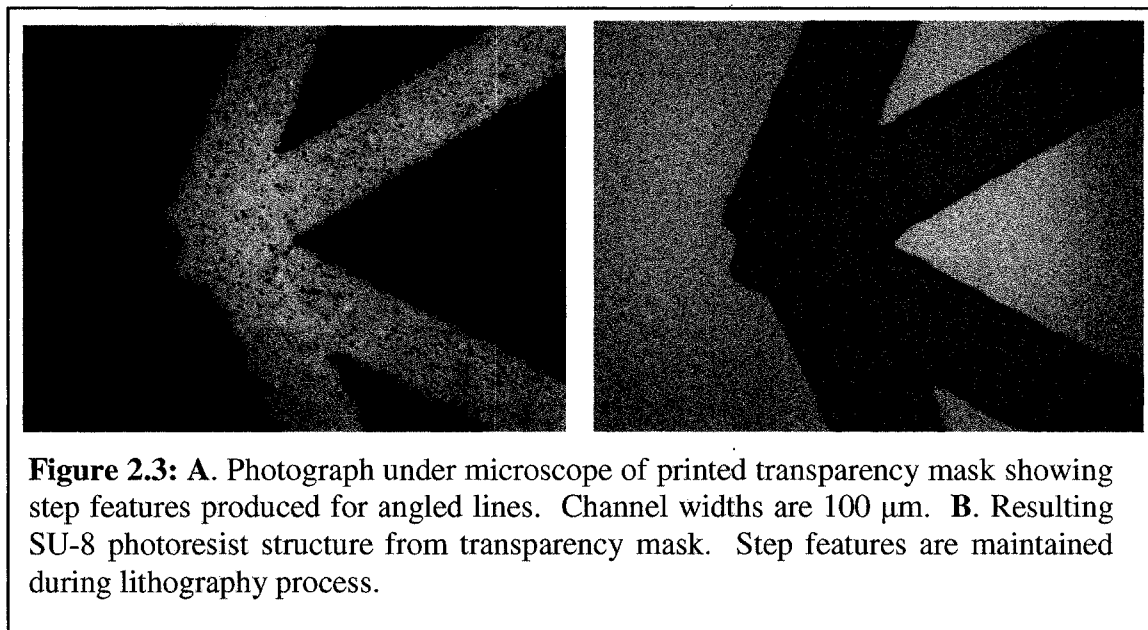
Dimensions are as follows; 1.8 x 1.8 cm perimeter, 100 μm wide flow channels and spotting regions 500 x 300 μm . These parameters were evaluated and chosen for their compatibility with both the fabrication methods and detection system.

The first consideration for a microfluidic spotting device design was the total footprint available. This footprint was defined by the area of the glass slide used in the SPR instrument and its prism and holder assembly. The area is predefined by the manufacture at 1.8 x 1.8 cm. For ease of fabrication and use, keeping the microfluidic device within this available area was deemed important.

To evaluate design, fabrication and operation procedures, 24 sensing spots in the array design were judged to provide an adequate number of array elements for a proof of concept device. Having too few spots would make understanding scaling issues involved

with a greater number of spots difficult. Having too many spots would complicate and overly burden the design and fabrication procedures.

To accommodate 24 array elements, channel widths were chosen as a balance between available spacing and compatibility to the mask printing techniques. Masks for positive relief photoresist Si wafer masters were printed on transparency film using high resolution printers (Quality Color, Edmonton AB). This was a low cost alternative to chromium soda lime glass masks, normally used for lithographic fabrication procedures, as it was envisioned that multiple masks would be designed and fabricated. Transparency film masks have their own drawbacks. They exhibited a lower limit of feature resolution of $\sim 50 \mu\text{m}$ and any angled lines consisted of step features that are reproduced lithographically (Figure 2.3). Therefore, channel widths were ideally maintained at $100 \mu\text{m}$ and straight channel lines were preferentially incorporated into the design.



Four aspects of the device are worth noting in the design. First, every six inlets has a common outlet, which reduced the total number of access holes required in the available area. Second, inlet channels to the spotting regions were lengthened for extra flow restriction to ensure solutions arrive at each spot at the same time. This potentially decreases the chances of trapping air within the microchannels due to solution arriving at the waste line at different times. Third, Au spot dimensions ($500 \times 300 \mu\text{m}$) are made

larger than the channel widths (100 μm) to accommodate for the plane of focus in the SPR optical system (discussed further in Section 2.2.2.1) Fourth, solutions flow through a spotting region with widening and narrowing flow paths, which allow for complete solution coverage of the larger 300 μm wide Au spots, while providing an architecture without 90° angles in order to minimize air trapping.

2.2.1.2 Si MASTER FABRICATION

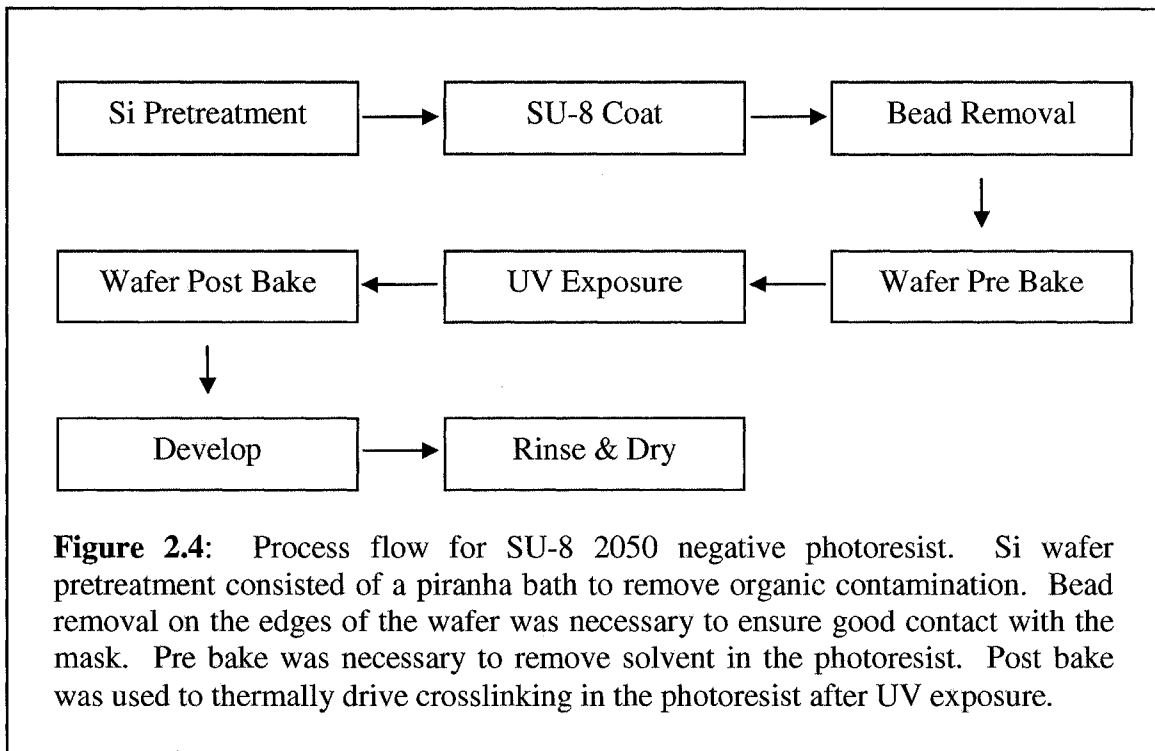
Photoresist Si masters were chosen as the PDMS casting support because of their well established fabrication protocols from the semiconductor industry. The Nanofab Facility at the University of Alberta is equipped with all necessary equipment and expertise for photoresist processing. Other methods of producing positive relief masters for PDMS casting, include: glass and Si etching. These methods were not used because of their relative expense, length of processing time and possible substrate surface roughness. Wet and dry etching processes over large areas can result in surface roughness which may result in poor PDMS sealing to the SPR glass slides. Lithographic methods of producing positive relief structures provide a smooth substrate surface for PDMS casting (the underlying Si wafer), are highly uniform over large areas (dependent on UV light source) and have fast processing times.

Photoresist compounds can be classified by the film thickness range they are capable of producing. As such, it is necessary to know what thickness is desired for any particular application. One of the most widely used photoresist materials is HPR 504, a positive photoresist that is used as a metal etching masking layer. It has a working thickness range of 100 nm to 2 μm . This is a suitable range for a metal masking layer; however, it is too thin for a microfluidic channel in PDMS.

The use of photoresist material as a support for casting PDMS results in the film thickness of the photoresist equaling the PDMS channel depths. The main consideration of PDMS channel depths was resistance to flow. With only one outlet per six inlets, elongated channel lengths and hydrophobic sidewalls from the PDMS, aqueous resistance to flow was thought to be a problem. Spotting regions were also cast in PDMS where curing occurs around a photoresist structure resulting in a through hole. The height of the photoresist column needed to be greater than 75 μm , the observed minimum thickness of

a thin film of PDMS for manipulation with fine tweezers (Dumont high precision grade tweezers, Ted Pella Inc.).

For the initial designs, a photoresist capable of thick structures was desirable. Meeting the thickness requirements of both the channel profile and spotting columns was MicroChem SU-8 2050 negative photoresist. It has a working thickness range of 40 – 170 μm . As a negative photoresist UV light exposure causes crosslinking and hardening of the epoxy polymer. Unexposed photoresist can be washed away leaving behind the patterned exposed resist. Figure 2.4 is a layout of the general steps used in a negative SU-8 2050 lithographic procedure.



Process development at the University of Alberta Nanofab for thick film SU-8 photoresist was necessary as it was a newly introduced photoresist to the laboratory. Three parameters were investigated; spin coat speed, prebake temperature and UV exposure time. These parameters proved to be the most important in developing a reliable SU-8 2050 lithographic process for Si wafer photoresist masters. The manufacturer's data sheet was used as a baseline for the determination of process parameters.²⁴

Two thicknesses were investigated, 50 μm for the channel depths and 100 μm for the spotting regions. The following parameters were determined.

Table 2.1: Comparison of Manufacturers and Experimentally Determined SU-8 Processing Parameters

	Experimentally Determined		Manufacturer	
	50 μm	100 μm	50 μm	100 μm
Spin coat (rpm)	3000	1500	3000	1800
Pre-bake (min, °C)	120 @ 60	120 @ 60	0-3 @ 65	5 @ 65
			6-9 @ 95	10-20 @ 95
UV exposure (s)	75	95	~ 5*	~ 6*

* Calculated from MicroChem reported exposure (exp) energy: 50 μm = 150 – 215 mJ/cm^2 , 100 μm = 215 – 240 mJ/cm^2 based on Nanofab Exposure Factor of 29.5 mW cm^{-2} using;

$$Exp\ t(s) = Exp\ Energy\ \left(\frac{\text{mJ}}{\text{cm}^2}\right) / Exp\ Factor\ \left(\frac{\text{mW}}{\text{cm}^2}\right) \quad \mathbf{2.1}$$

Deviation from the manufacturer’s baseline recommendations may have resulted from limitations in the pre-bake step. The outlined recommendations for the pre-bake used a step wise heating process on a hotplate with thermal contact between the plate and photoresist substrate. This process is important in drying the photoresist, by removing solvent, thereby hardening the photoresist. To achieve effective heating without disruption to the film thickness a hotplate with good temperature uniformity was needed. None of the available hotplates possessed such uniformity and wrinkling from thermal stress was observed. Figure 2.5 is a photograph of the observed wrinkling seen with hotplates in the Nanofab.

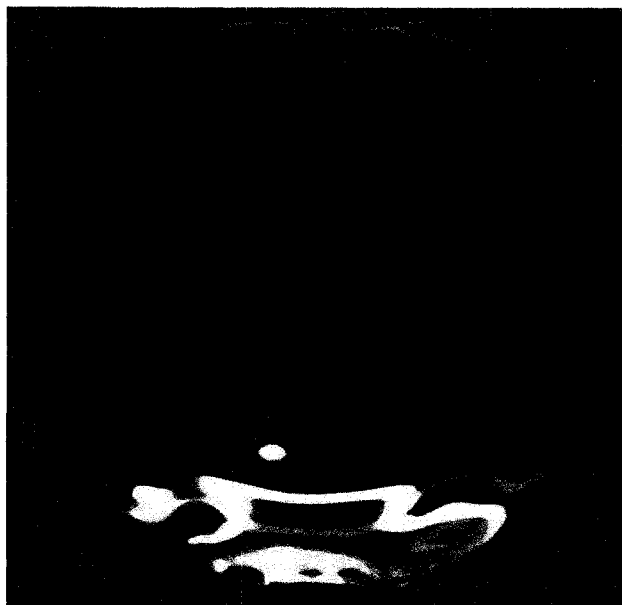


Figure 2.5: 100 μm thick SU-8 2050 coated Si wafer. Upon spinning of photoresist a pre bake was performed using the Nanofab hotplates at the manufacturer's specified temperature. Distortions in the film can be seen around the outside edges and as islands towards the center.

A convection oven was used as an alternative to a hotplate. The air circulation from the high temperature fan results in an even uniform temperature across the photoresist. However, the use of a convection oven also results in skin formation over the resist. This skin can inhibit the evolution of solvent and extend exposure times.²⁴ Drying and hardening of the SU-8 2050 photoresist was achieved in a convection oven with no disruption to the film integrity at 60°C for 2 hours. A minimum cool down period of 30 minutes was necessary to ensure proper setting of the photoresist as the film is still pliable upon removal from the oven.

Exposure time was based on the development of a latent image in the photoresist after UV light exposure, as outlined in the manufacturer's data sheet. The increased time of exposure compared to the baseline parameters given in the data sheet is thought to be from the differing method of pre-bake heating. Skin formation on the photoresist film from the use of a convection oven may change the absorption ability of the photoresist requiring longer exposure times. After exposure of 75 and 95 seconds for 50 and 100 μm photoresist films faint latent images of the mask pattern could be seen, indicating initiation of epoxy crosslinking. A post exposure bake (PEB) of 30 minutes at 65°C was

used to thermally drive the epoxy crosslinking to completion, followed by photoresist development with MicroChem's SU-8 developer (1-methoxy-2-propyl acetate), which removes all uncrosslinked photoresist. The PEB and development times were in line with the manufacturer's specified parameters. An outline of the full lithographic parameters used is presented in Table 2.2.

Table 2.2: Determined parameters for two SU-8 2050 film thicknesses

	Optimal Photoresist Thickness	
	50 μm	100 μm
Spin coat (s @ rpm)	10 @ 500	10 @ 500
	60 @ 30000	60 @ 1500
Pre-bake (min @ °C)	120 @ 65	120 @ 65
Exposure (s)	75	95
Post bake (min @ °C)	30 @ 65	30 @ 65
Development (min)	6	9

2.2.2 PDMS PROCESSING

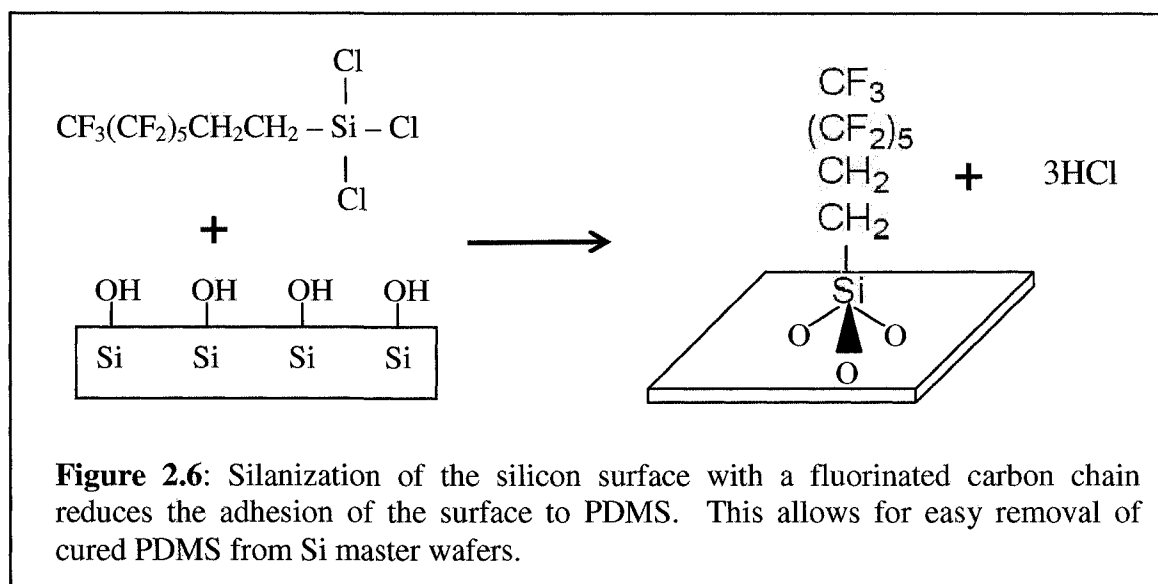
Polymers offer an attractive alternative to glass and silicon materials for fabrication of microfluidic systems, as they are less expensive and fragile than glass and silicon. The fabrication processes used to create plastic devices are based on replication (casting, embossing, or injection molding) and are faster and less expensive than those used on glass and silicon. PDMS is an elastomeric material that is readily used in microfluidics and has been employed for sorting of cells, sizing of DNA, patterning of biological and non-biological materials and electrophoretic separation of biomolecules.^{16, 25-27} It is an ideal material and fabrication method for rapid prototyping of microfluidic structures.²⁵

The final device consists of components from two PDMS curing steps on two photoresist masters. The first master contains the microchannel manifold, in which access holes are punched and allow for solution introduction and removal. The second master contains spot arrays, for which a novel PDMS curing procedure was developed in order to create thin PDMS membranes with microspot access holes. All PDMS

fabrication reported here used Sylgard 184 silicone elastomer (Dow Corning; Midland, MI).

2.2.2.1 MICROCHANNEL MANIFOLDS

Upon positive relief photoresist master fabrication, all Si wafers were gas phase silanized with trichloro(1H, 1H, 2H, 2H-perfluorooctyl)silane (97%, Sigma-Aldrich, St. Louis, MO). Wafers were placed overnight in a vacuum desiccator with 30 μ L of silane solution. Figure 2.6 illustrates the gas phase reaction between trichlorosilane and surface Si-OH groups on the Si wafer. The resulting fluorinated surface produced a surface with weakened adhesion to PDMS, facilitating easy removal of cured PDMS.



All PDMS handling was done under a clean hood utilizing a HEPA filter. PDMS curing was achieved according to established methods.^{28, 29} Briefly, a 10:1, prepolymer to cross-linker ratio, by weight, was mixed in a Teflon® weighing boat and placed under vacuum to remove trapped air bubbles. To provide a physical support for PDMS curing masters were affixed to the centre of a plastic Petri dish by curing a thin layer of PDMS between the Si wafer and dish. With air bubbles removed, the mixed PDMS was poured over the positive relief masters and again placed under vacuum, to remove any air bubbles introduced during pouring. To ensure uniformity over the full four inch diameter of the Si master the Petri dish was placed on a leveled plate for 1 hour. Subsequently, curing was achieved at 75°C for 1 hr. Upon removal from the oven, the cured PDMS was cooled at room temperature for 1 hr in a clean hood.

Each 1.8 x 1.8 cm device was cut from the bulk PDMS and access holes were punched through the PDMS using a 16 gauge needle whose tip had been flattened and sharpened in a lathe. This produced inlet/outlet reservoirs of 1 mm in diameter.

Fully cured PDMS contains uncrosslinked low molecular weight (LMW) chains. The LMW species are either uncrosslinked linear PDMS chains or residual crosslinking agent.³⁰ These species can diffuse to the surface of PDMS and onto supporting substrates. Since these microchannel PDMS devices are used for surface immobilization studies and with a surface sensitive optical detection system elimination of these LMW chains was deemed advantageous. Two methods primarily used for organic extraction of LMW chains from cured PDMS are thermal aging³¹ and organic extraction.³² Organic extraction was used because it was the least time consuming, hours compared to days for thermal aging.

Refluxed hexane in a Soxhlet setup was used for extraction of LMW chains in cured PDMS device. Briefly, 1.8 x 1.8 cm individually cured PDMS components, of the device (three at a time), were loaded into a Soxhlet extractor. The extractor is equipped with a condenser and attached to a flask containing the hexane solvent. The solvent is heated to reflux, condensing on the condensing arm and dripping back down into the chamber housing the PDMS devices. The chamber slowly fills with warm solvent and extracts LMW chains. When the Soxhlet chamber is filled it automatically empties by a siphon side arm with the solvent running back down to the distillation flask. Distillation continues with the extracted LMW chains remaining in the solvent. The cycle is allowed to repeat at least three times, approximately 3 hours.

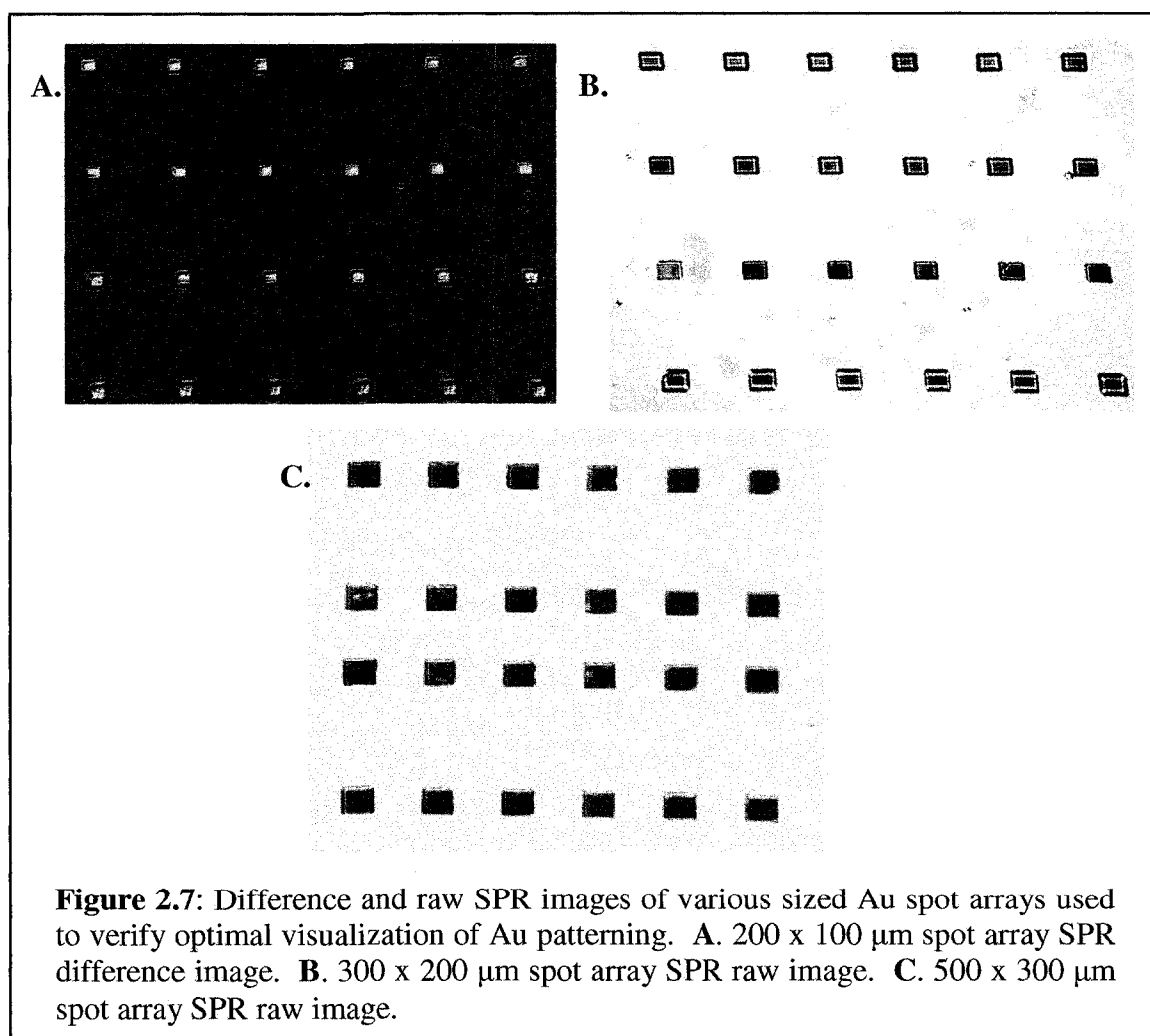
When removed from the extractor the PDMS devices are swollen due to the absorption of hexane. Each device is dried under nitrogen and placed on a glass slide over night under a clean hood to allow for complete solvent evaporation. Upon extraction and drying each device is ready for use.

2.2.2.2 MICROSLOT ARRAYS

SPR occurs only at the surfaces of noble metals when specific conditions of wavelength and incident angle are met. To localize the SPR response and minimize the background signal that is generated across the whole surface of a fully Au coated SPR

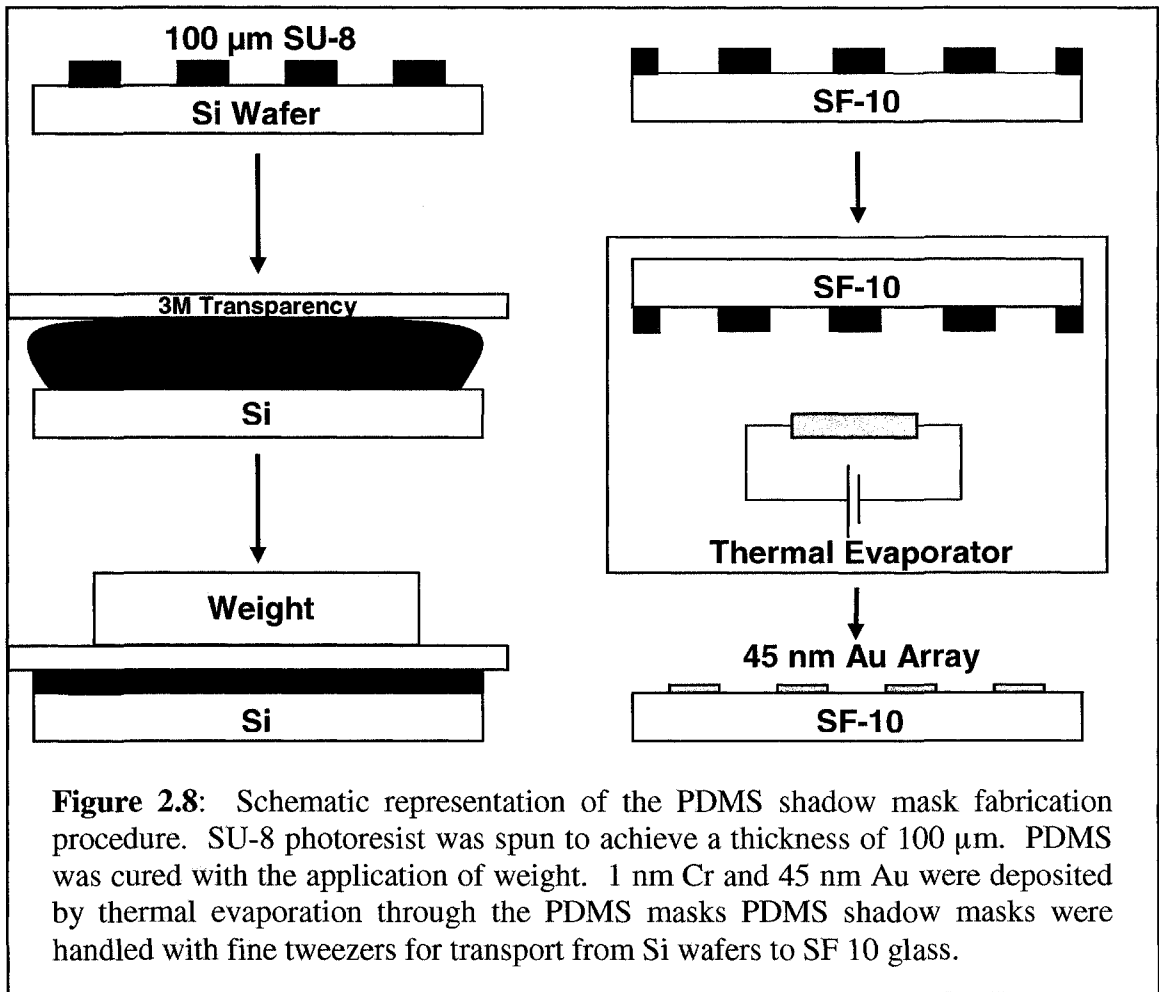
sensor chip, a pattern of Au spots was utilized. Ideal spot size was identified based upon ease of visualization with the SPR imager used. Figure 2.7 shows a comparison of SPR images for various Au sizes used to determine optimal spot area.

Due to the channel configuration and layout, the area of the spot array was 8 x 4 mm. For determining spot size, two competing factors needed to be balanced: 1. achieving focus of the Au spots across a field of view of 8 x 4 mm, and 2. maintaining spot sizes compatible with the widths of the microchannels. Meeting these criteria were the dimensions of 500 x 300 μm . At these sizes, machining reliable and consistent spots in a shadow mask holder for metal deposition on to the glass surface would prove to be difficult. Photolithographic techniques access Au patterns of this size easily.



Photoresist lift off is one technique used for metal patterning on glass substrates. This procedure uses photolithography to pattern photoresist on the substrate of interest. Upon UV exposure and development, metals can be deposited on the underlying substrate. Once deposition is completed, the remaining photoresist can be removed, leaving behind the patterned metal. To simplify the procedure and eliminate possible surface contamination of the substrate and metal from the chemical removal of photoresist, an alternative to the technique for microscale Au patterning was developed.

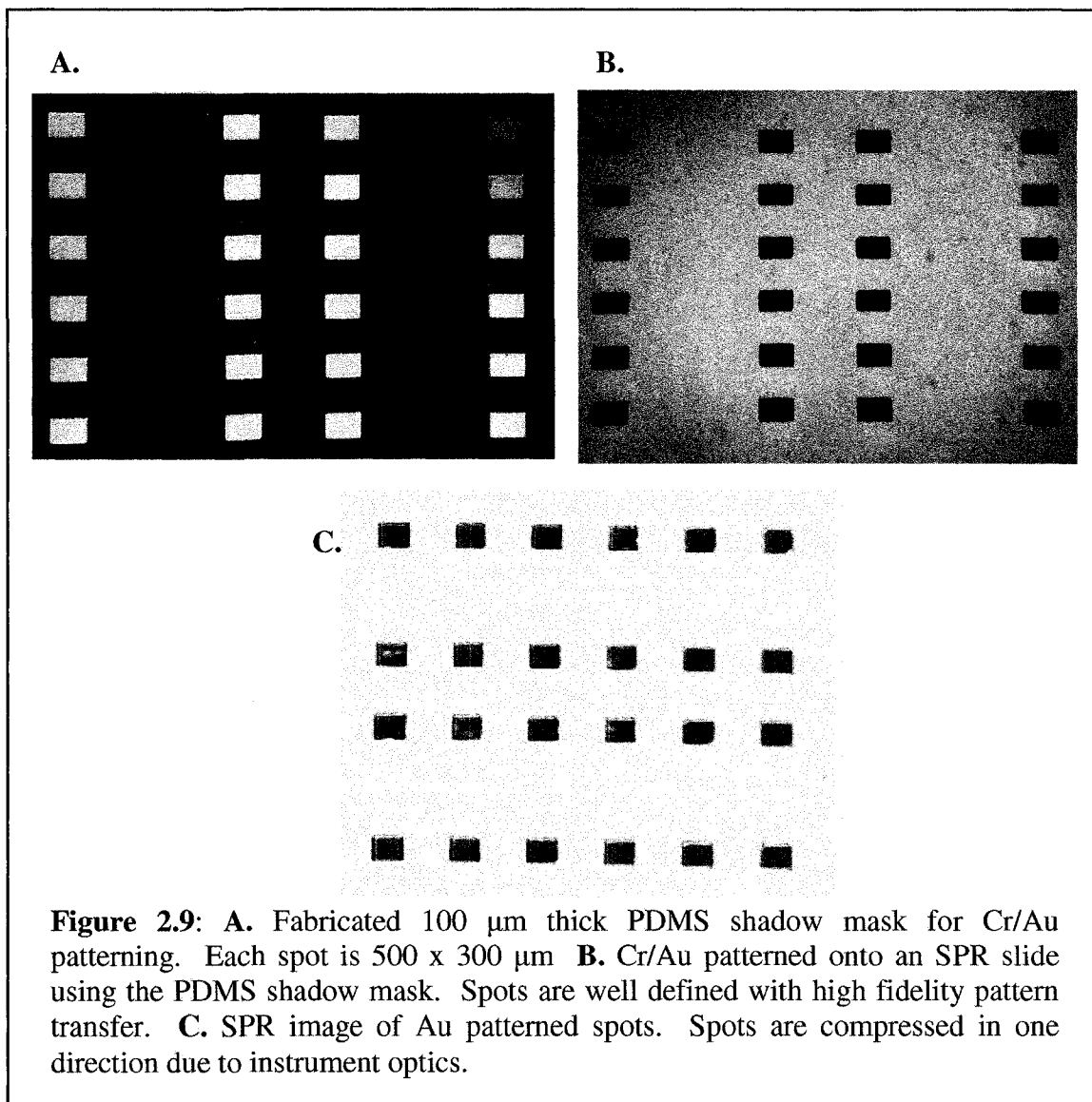
Our method involved the photolithographic fabrication of photoresist arrays of $500 \times 300 \mu\text{m}$ columns on Si wafers as moldings for PDMS casting. The height of these features was optimally $100 \mu\text{m}$. This proved to be the minimum height needed for easy manual handling with tweezers for thin PDMS membranes. Thinner PDMS membranes proved to be extremely fragile. Since PDMS is a soft elastomer, thin membranes ($< 100 \mu\text{m}$) often distorted or sagged easily, leading to deformed spot features. These positive relief photoresist column arrays served as reusable masters for the formation of thin PDMS shadow mask membranes, containing through holes formed from the curing of PDMS around the features. Figure 2.8 outlines the fabrication steps.



To avoid curing of PDMS over the features, and thus allow metal deposition to the substrate, weights were applied to remove excess PDMS from above the features. If sufficient pressure was not applied to the Si wafer, uncured polymer seeped between the features and weights, blocking the through holes. It was determined that a pressure of > 6 MPa, corresponding to a weight of ~ 13 kg, was necessary to ensure proper and reproducible sandwiching of the PDMS. Distortions of the photoresist features due to the pressure exerted on them was thought to be a concern, however no ill effects on the photoresist structures or their dimensions from multiple high pressure curing processes were detected. Curing was achieved at room temperature for 12 hours. This afforded enough time for the PDMS to set around the photoresist features so the weights could be removed and curing completed in an oven at 75°C for 1 hour.

3M transparency film sheets (CG 3460) were used to separate the PDMS liquid polymer from the weights. Due to the flexible nature of these sheets, they provided reliable contact to the photoresist structures during application of the weights. Other support materials were tested such as Si wafers, glass slides, Teflon® sheets, and plastic wrap. All proved to be too fragile (Si and glass) or too delicate (Teflon® and plastic wrap) to support the necessary applied weight. The 3M transparency sheets also exhibited less adhesion to the PDMS than the PDMS had to the Si wafer, thus facilitating easy removal of the transparency. Furthermore, the films did not exhibit any deleterious affects from heating at 75°C during final curing.

Upon curing the features of interest, 1.8 x 1.8 cm PDMS squares with arrays of through holes, were cut from the bulk PDMS membrane sheet. No cleaning procedures were used for these PDMS pieces. All handling and transferring of these thin membranes were done with fine tweezers. PDMS thin membranes were manual placed on glass SPR slides where conformal contact between the PDMS and glass provided a versatile seal allowing for localized metal deposition to the exposed areas while, being reversible to allow for the removal of the PDMS shadow masks for reuse in further metal depositions. When not in use, PDMS shadow masks were stored in a vacuum desiccator Au side down. Figure 2.9 shows images of the PDMS microspot shadow mask and Cr/Au patterned SPR slides resulting from the masks.



2.2.3 SPR SLIDE FABRICATION

SPR sensors consist of a thin layer of Au patterned onto glass slides. SF-10 glass (Schott Glass Technologies, PA, USA) is a high refractive index glass that is used as the substrate for fabricating SPR slides. Four inch square sheets of SF-10 glass are cut into 1.8 x 1.8 cm dyes using a diamond encrusted high precision table saw (Diamond Touch Dicing Saw, Texas, USA). Each cut sheet was stored under vacuum in a desiccator until needed for Au patterning.

Under a clean hood, pre-cut SF-10 dyes are cleaned in a piranha bath (3:1, $\text{H}_2\text{SO}_4:\text{H}_2\text{O}_2$ – caution should be observed when using acids and peroxides) for 20 minutes, rinsed in water and $\text{N}_{2(g)}$ dried. Using fine tweezers, PDMS microspot shadow

masks are positioned onto the glass dyes by hand. Each mask is positioned such that the features are placed approximately in the centre of the slide. Conformal contact is achieved immediately upon contact between the glass slide and PDMS, providing a seal between the two materials. Each device is then placed in a holder and loaded into the vacuum chamber of a thermal evaporator for Cr/Au metal deposition.

Au deposition is achieved using thermal evaporation (Torr International Inc., NY, USA). Samples are loaded in a chamber face down over two crucibles, one containing Au and the other chromium. Evaporation occurs through the resistive joule heating of the crucibles containing the metals. The released metal vapour then condenses on the cooler substrate surface forming a thin film. Low pressure, $10^{-6} - 10^{-7}$ torr is used to avoid reaction between the metal and atmosphere. A typical pressure used for metal deposition during SPR slide fabrication is 5×10^{-7} torr, the applied power is typically 40 watts and 19 watts for chromium and Au, respectively. The achieved deposition rates are 0.05 – 0.1 Å/s for Cr and 0.3 - 0.6 Å/s for Au. A 1 nm chromium adhesion layer is deposited first followed by a 45 nm Au layer.

Upon completion of deposition the chamber is allowed to cool to room temperature and the dyes are removed. The PDMS shadow masks are peeled from the surface using fine tweezers and both the masks and patterned dyes are stored in petrie dishes in a desiccator under vacuum. To ensure consistent sealing of the PDMS to glass each mask is stored Au side down limiting the exposure and contamination of the PDMS side. The PDMS shadow masks have been used many times (> 8 metal depositions) with no evidence of degradation.

2.2.4 DEVICE ASSEMBLY

The Au patterned SPR sensor slide and PDMS microchannel manifold were assembled prior to use. As stated previously alignment marks were omitted since the design had inherent alignment between the spots and spotting regions. Alignment of 500 x 300 μm features on two 1.8 x 1.8 cm dyes required a specially built alignment microscope. Figure 2.10 is a design schematic and photograph of the homebuilt alignment microscope for 1.8 x 1.8 cm die alignment.



Figure 2.10: **A.** Homebuilt alignment microscope with x, y, z and θ translation stages. **B.** Accessories used for alignment. A slot holder to hold the SPR slide stationary and a microscope slide to hold the PDMS manifold.

To align two die pieces it is necessary to hold one stationary while adjusting the other in the x, y and θ positions. Upon alignment one die can be moved in the z direction for bonding to the stationary substrate. Here the PDMS manifold is held stationary, affixed to a microscope slide, slotted into a holder with features facing down. The SPR slide is positioned in a slot holder on a micro-translation stage with the Au pattern facing upwards. The two substrates are brought into close proximity, but not contacting each other, so as to have both features (Au patterns on SPR slide and spotting regions on PDMS manifold) simultaneously in focus. To achieve a large non-contact depth of field (the distance from the nearest object plane in focus to that of the farthest plane simultaneously in focus) proper lens selection was needed. A microscope lens with a 6.3x magnification and numerical aperture of 0.2 was used. These parameters balanced the need for magnification to view micro-scale features and achieving an optimal depth of field. Figure 2.11 is a photograph of an aligned 24 spot SPR sensor with a microfluidic manifold. As can be seen, micro-

scale alignment with this homebuilt alignment microscope was achievable.

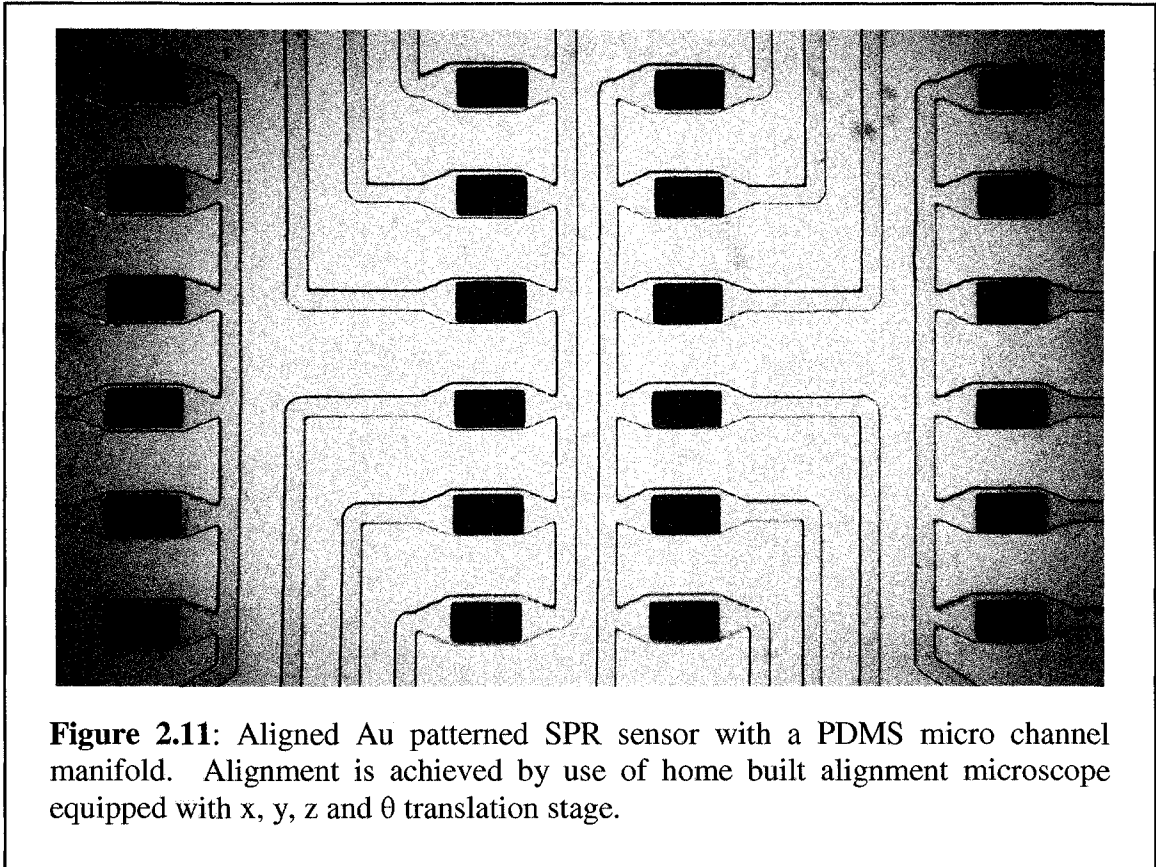
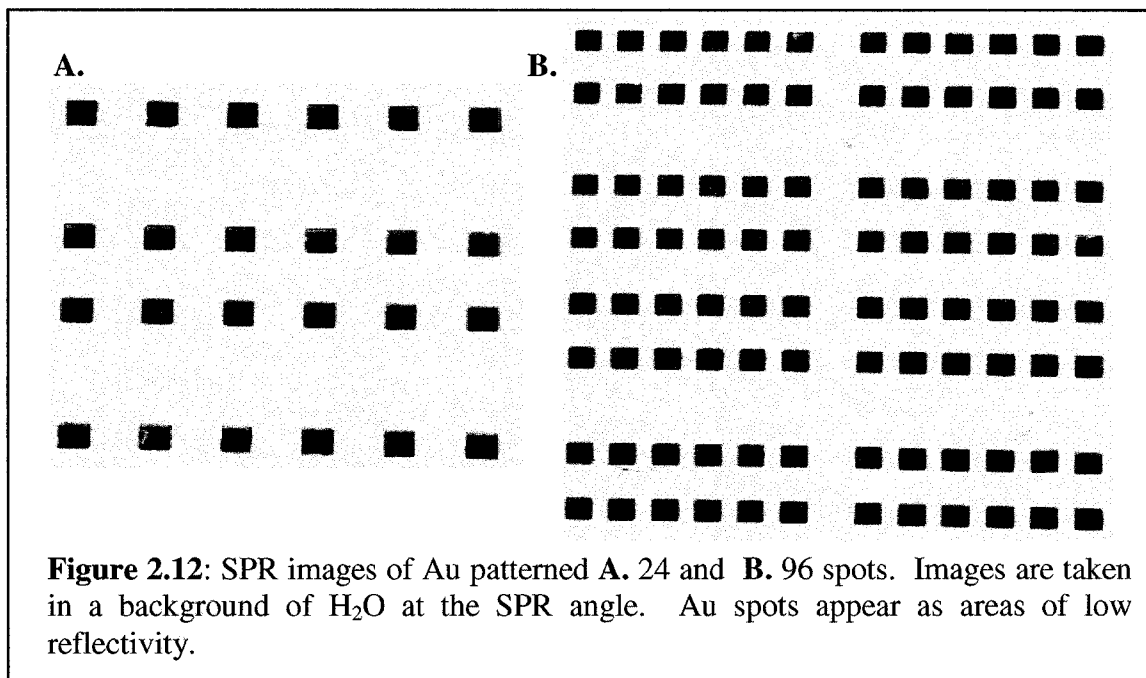


Figure 2.11: Aligned Au patterned SPR sensor with a PDMS micro channel manifold. Alignment is achieved by use of home built alignment microscope equipped with x, y, z and θ translation stage.

2.3 EVALUATION

To ensure no sensing complications arise from micro-sized Au patterned slides, Au spotted SPR slides, were mounted in the SPR to observe their localized signals. Figure 2.12 shows SPR refractive index images of a 24 and 96 spot sensor, respectively. Each image is taken with unmodified Au spots in a background solution of water. The angle is adjusted to the SPR angle resulting in minimum reflectivity of the Au spots for easy detection. The remaining, uncoated-glass background exhibits no surface plasmons due to the absence of the Au, resulting in maximum reflectance of the incoming light. Thus, areas of interest are clearly visible without the need for background blocking.



These raw SPR images show clearly visible boundaries of the Au spots thus showing the effectiveness of the PDMS masking layers used during metal deposition. This method results in well defined spots across a large surface area. Such fidelity of metal deposition results in even SPR signal strength across the array with no spatial dependence. These well defined areas also exhibit no shadowing effects from the metal deposition or due to the angled path of the incoming and reflecting light.

2.3.1 SPOT-TO-SPOT CONTAMINATION

Array systems require each sensing element be independent of neighboring elements. This ensures reactions and conditions at one element do not affect another and sensing of independent and different experimental parameters at each element is possible. In ELISA experiments this is achieved by physical separation of wells. In pin printing methods, it is achieved through moveable print heads that print to spatially separated areas, along with surface coating to avoid spot spreading. Within the microfluidic SPR sensor, spot separation is achieved by confining each spot to an individual inlet channel. However, each individual sensing region is connected by a common outlet channel. For this reason investigation of spot-to-spot contamination was necessary to observe the affect of a common outlet.

Figure 2.13 is a photograph of the 24 spot microfluidic device loaded with various dye solutions. As solution flows through the channels due to applied vacuum at the outlet, solution fidelity over the spots is maintained. As the vacuum is removed to allow for solution incubation, mixing can be seen to occur in the spotting regions. This mixing may arise from a back pressure difference along each channel and reservoir, which become apparent after removal of the vacuum, and diffusion of the solution over time.

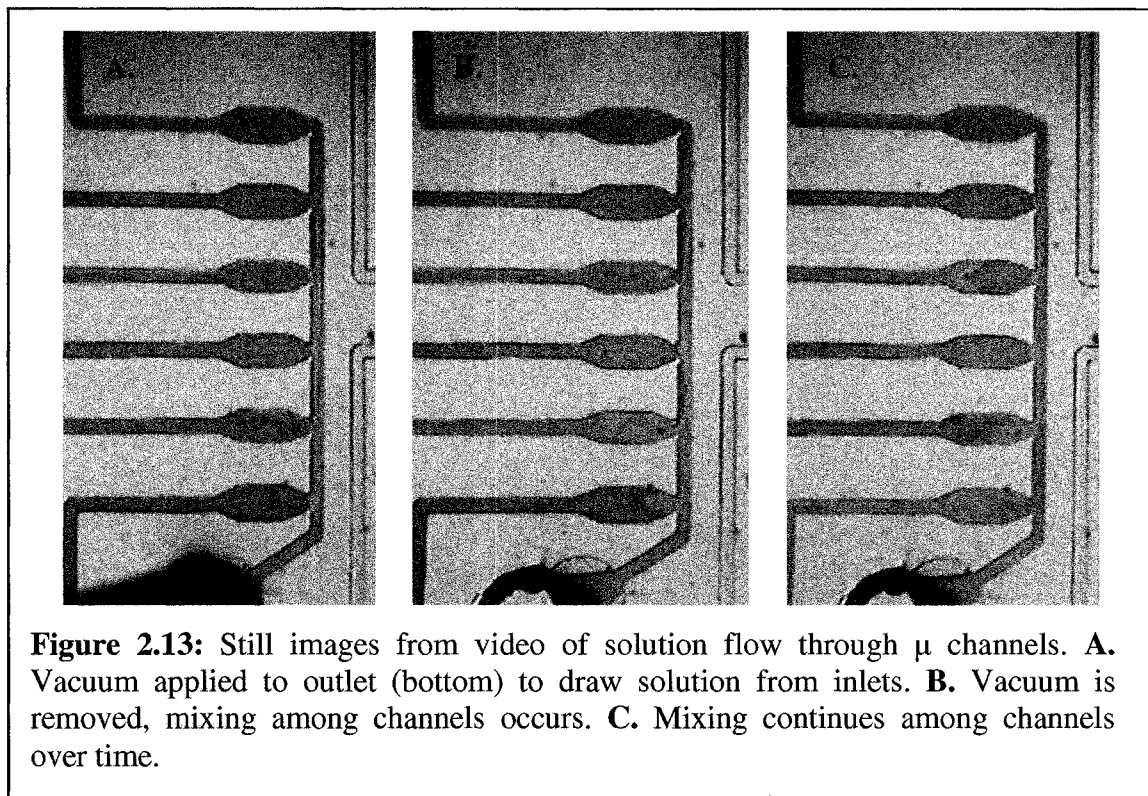


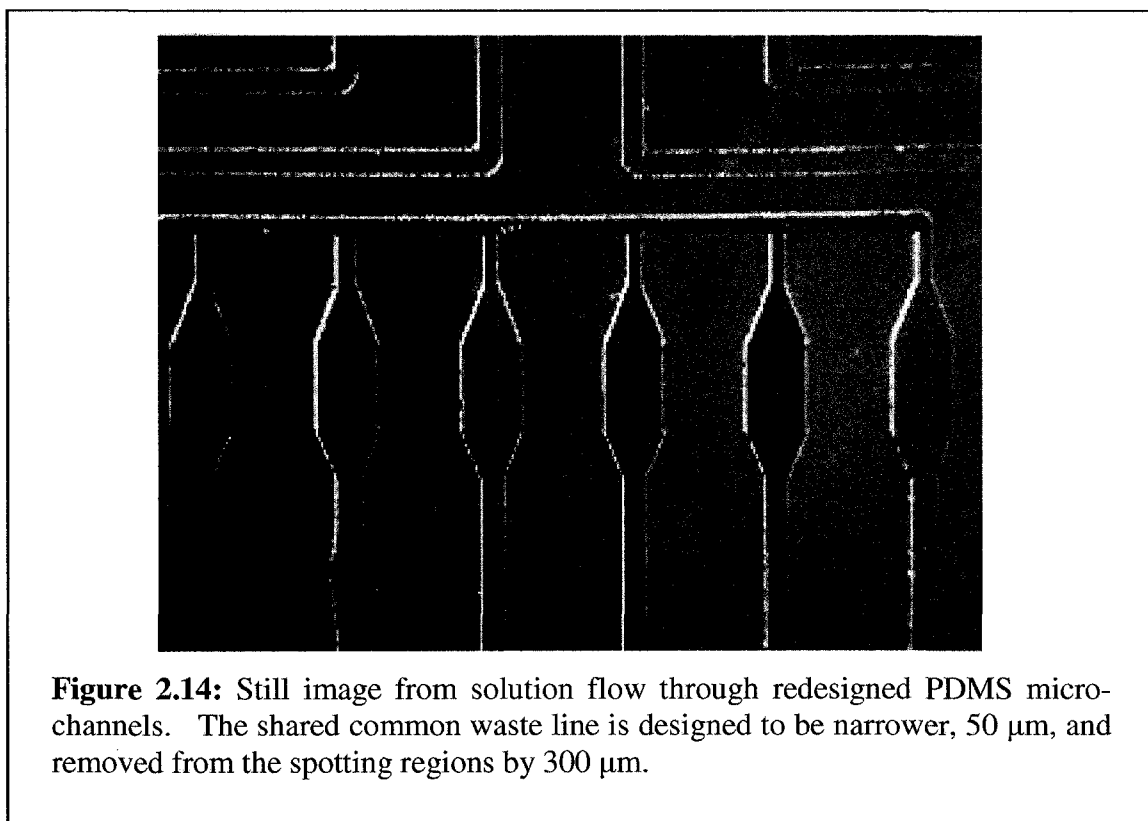
Table 2.3 outlines the potential longitudinal distances achieved by small molecule dyes ($D = 10^{-4} - 10^{-5} \text{ cm}^2 \text{ s}^{-1}$) and protein samples ($D = 10^{-6} - 10^{-7} \text{ cm}^2 \text{ s}^{-1}$) in aqueous solutions for typical diffusion coefficient ranges and experimental incubation times.

Table 2.3: Einstein calculation of diffusion longitudinal distance

Time (min)	Diffusion Coefficient ranges ($\text{cm}^2 \text{ s}^{-1}$)			
	10^{-4}	10^{-5}	10^{-6}	10^{-7}
10	346.4 μm	109.5 μm	34.6 μm	10.9 μm
30	600.0 μm	189.7 μm	60.0 μm	19.0 μm

D = diffusion coefficient; Einstein calculation: $\sigma = \sqrt{2 * D * t}$; where **D** = $\text{cm}^2 \text{ s}^{-1}$ and **t** = s 2.2

For a protein of ~ 100 kDa the diffusion coefficient is $\sim 10^{-6} \text{ cm}^2 \text{ s}^{-1}$. The calculated value of $60 \text{ }\mu\text{m}$ for longitudinal distance when $D = 10^{-6} \text{ cm}^2 \text{ s}^{-1}$ was used as a base for design changes. The original design consisted of $50 \text{ }\mu\text{m}$ spacing between the waste line and spotting region. This bordered on the observable limit of the mask printing method used. Thus, upon fabrication the outlet channel appears contiguous with the spotting region (Figure 2.13).

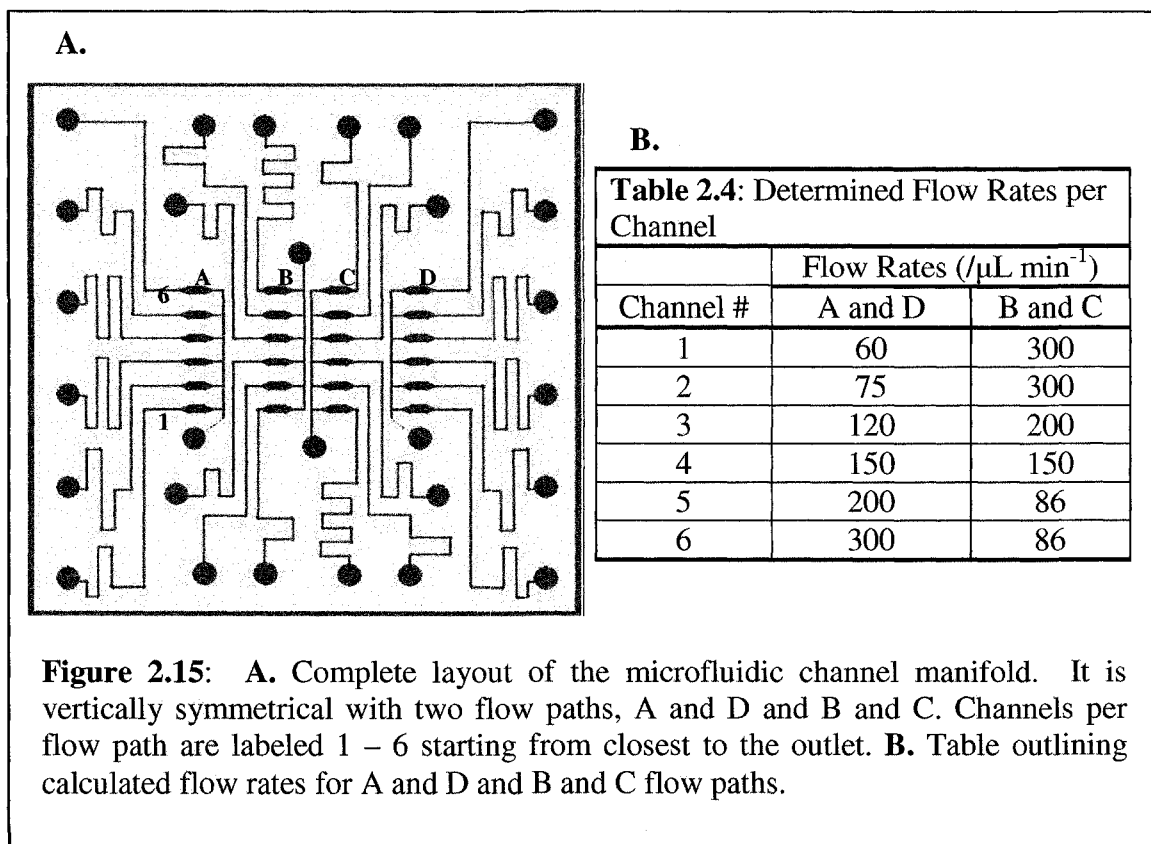


It was also important to compensate for any mixing occurring as a result of back pressure from the waste line to the spotting regions, which might be occurring upon vacuum removal. To compensate for possible diffusion and back pressure considerations, the distance between the common outlet and spotting regions was increased from 50 to $300 \text{ }\mu\text{m}$ and the width of the channel was narrowed from 100 to $50 \text{ }\mu\text{m}$. This results in an increased distance for longitudinal diffusion and increased resistance to flow for solution in the waste line. To compensate for diffusion a length of $150 \text{ }\mu\text{m}$ (2.5 times $60 \text{ }\mu\text{m}$) was used. To compensate for back pressure 2 times $150 \text{ }\mu\text{m}$ was used. The width was narrowed to $50 \text{ }\mu\text{m}$ based on the limit of mask printing

achievable. Figure 2.14 shows the completed device loaded with dye solutions illustrating the elimination of spot-to-spot contamination due to a narrow elongated connecting channel.

2.3.2 RESISTANCE TO FLOW

Upon redesign and fabrication of the 24 spot microfluidic device and elimination of spot-to-spot contamination, resistance to flow inequalities among the channels was observed. To ensure equal contact time during continuous injection and equal injected sample volumes per sensing element, volume flow rates must be made equal among the channels. Volume flow rates were determined by injecting 10 μL of water in each inlet, applying vacuum and recording the elapsed time the solutions take to cross a defined point. The vacuum applied was the house vacuum in the Gunning/Lemieux Chemistry building. Figure 2.15 outlines the volume flow rates determined for each flow path. Since the device is symmetrical along the center these values are assumed to hold for the remaining channels not tested.



The flow rates increase for channels with spotting regions closer to the outlet reservoir, even though the total length (inlet to outlet) of the channels is approximately equal. To understand this observation, resistance to flow calculations were performed for the channels. The Hagen-Poiseuille equation is a solution to the Navier-Stokes equation that describes fluid flow through an enclosure. For flow through a rectangle, as defined by the geometry of the channels formed in PDMS, it has the form;

$$\frac{\Delta P}{Q_v} = R_{flow} = \frac{4\eta L}{WD^2} \quad 2.3$$

Where, ΔP = pressure drop along channel, Q_v = volume flow rate, R_{flow} = resistance to flow, η = viscosity, L , W , D = length, width, depth. The total length of any given channel in the design is made up of two size regimes. From the inlet to the end of the spotting region the channel has a width of 100 μm . From the end of the spotting region to the outlet reservoir the channel has a width of 50 μm . The total resistance to flow in one channel can be estimated as the sum of each size regime. Table 2.5 and 2.6 outline the calculated resistance to flow for each channel flow path.

Channel #	Pre-Spot Distance (μm)	Post Spot Distance (μm)	$R_{flow, pre}$ ($/10^{12}$)	$R_{flow, post}$ ($/10^{12}$)	R_{total} ($/10^{12}$)
1	13900	296	2.22	0.189	2.41
2	13244	1096	2.12	0.701	2.82
3	12367	1896	1.98	1.21	3.19
4	11500	2696	1.84	1.73	3.57
5	10948	3496	1.75	2.24	3.99
6	10100	4296	1.62	2.75	4.37

Channel #	Pre-Spot Distance (μm)	Post Spot Distance (μm)	$R_{flow, pre}$ ($/10^{12}$)	$R_{flow, post}$ ($/10^{12}$)	R_{total} ($/10^{12}$)
1	12288	296	1.97	0.189	2.16
2	11591	1096	1.85	0.701	2.56
3	10233	1896	1.64	1.21	2.85
4	9729	2696	1.56	1.73	3.28
5	8900	3496	1.42	2.24	3.66
6	8438	4296	1.35	2.75	4.10

- No consideration is given for the geometry of the spotting region.
- $\eta_{H_2O} = 1 \times 10^{-3} \text{ Pa}\cdot\text{s}$,

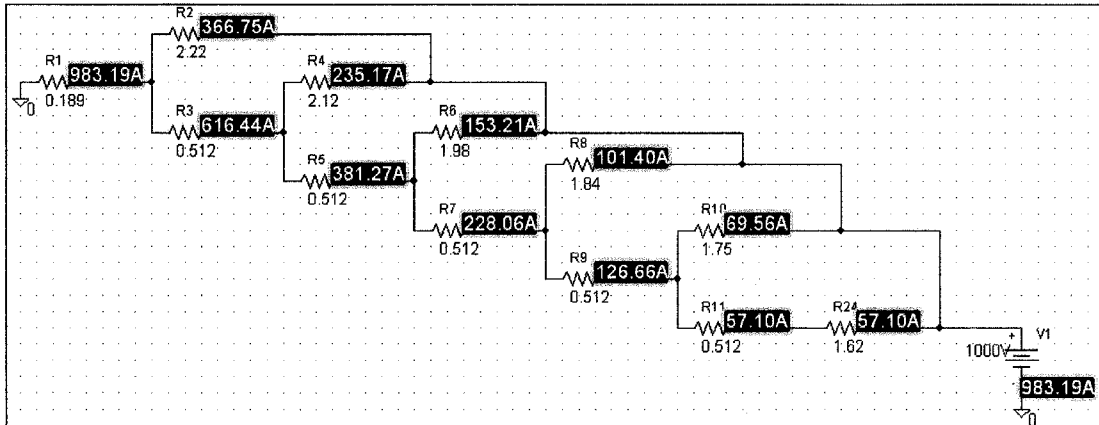
This is a simplified calculation which assumes all channels are independent of each other. For total resistance to flow the calculations agree qualitatively with the observed trend in flow rates. As the spotting region distance from the outlet increases so does the total resistance to flow for the channel and the volume flow rate decreases. These calculations also explain differences between volume flow rates reported for the different columns of spotting regions. Column B and C calculations show lower resistance to flow as evidenced with the observed flow rates. These calculations also show that resistance to flow behaves inversely before and after spotting regions.

A more complete analysis of the microfluidic device flow behavior, taking into account the connectivity of the flow paths can be achieved by using PSpice (9.1 Student Version, Cadence Design Systems, Berkshire UK) simulation software. PSpice is an electronics design and modeling program that has been successfully utilized previously to elucidate flow behavior in microfluidic devices.^{33, 34} Since, the channels are filled with the same solutions the resistance values for each channel are proportional to channel L /cross sectional area. The determined current is proportional to flow in each channel. A circuit layout of one set of 6 channels is shown in Figure 2.16 along with the associated channel resistances calculated in Table 2.5.

Two operational states of the flow channels are depicted using the PSpice modeling software: 1. The common outlet filled with air and possessing a resistance of 0 with the pre-spot channels filled with H_2O and 2. All channels filled with H_2O . An initial state of operation would have all channels filled with air followed by injection of solution. Initially, the solution fills the pre-spot channels. Figure 2.16 shows that the channels fill fastest for the channel furthest away from the outlet. When all channels are filled with solution, including the outlet channel, the simulation model shows that the flow rate then increases for the channel closest to the outlet.

To confirm the resistance to flow calculations and simulations, solution flow was monitored under a microscope. Figure 2.17 are still images taken from videos of solution flow through the redesigned 24 spot microfluidic device. Each image is a still from a different time during one solution injection cycle.

A. All channels filled with H₂O



B. Pre spotting regions filled with H₂O. Post spotting regions filled with air.

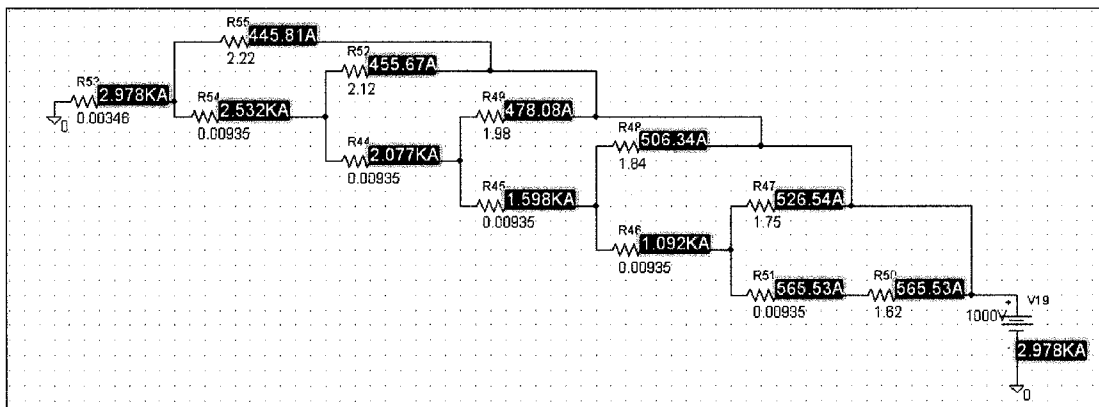


Figure 2.16: PSpice flow simulation of the A and D flow path. Inlet and outlet of the channel are represented by the voltage source and ground, respectively. **A.** Simulation with all channels filled with H₂O. Flow (current) is greatest for the channel closest to outlet. **B.** Simulation for post spotting region channels filled with air and pre spotting regions filled with H₂O. Flow is greatest for channels furthest from outlet. Channel resistance due to air calculated with $\eta_{\text{air}} = 1.8 \times 10^{-5}$ Pa·s.

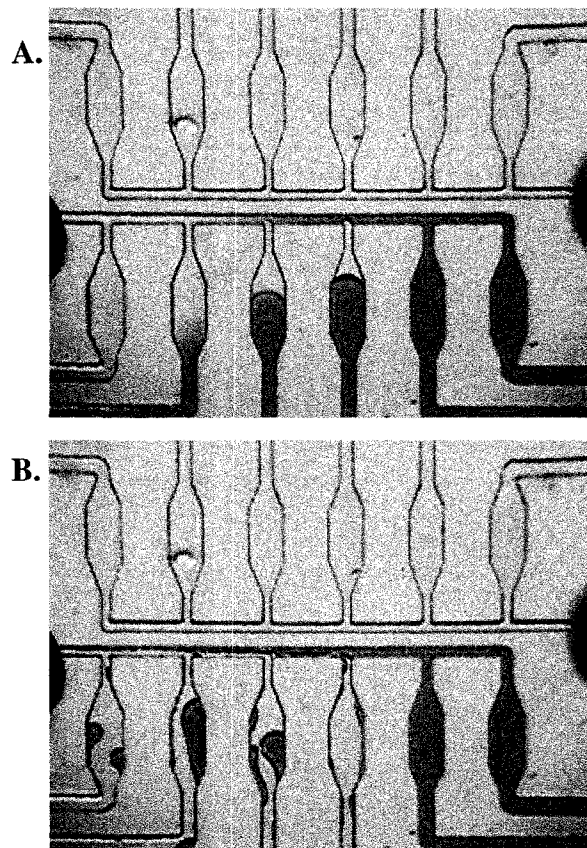


Figure 2.17: Photographs of dye solution flowing through one set of channels upon application of vacuum. Outlet reservoir is located on left side of images. **A.** Solution arrives at the outlet channel first for channels furthest from vacuum. **B.** Channels closest to the vacuum outlet have solution removed first.

10 μL droplets of dye solutions are loaded into each inlet reservoir. Vacuum is applied at the common outlet of the 6 inlets and solution is drawn through the channels and spotting regions. Figure 2.17A is a still image as the solutions first approach the spotting regions. The solutions arrive at the spotting regions staggered as indicated by the resistance to flow calculations. Figure 2.16B is a still image as the channels are emptied of the 10 μL solutions. The channels are emptied of solutions in the reverse order in which they arrived at the spotting regions, following the resistance to flow calculations and simulations. This result confirms the resistance to flow calculations and simulation showing varied resistance to flows before and after the spotting region due to the narrowing of the common outlet channel.

The varied resistance to flow among the channels does not easily allow this device to be used as a surface patterning device or integrated flow cell for simultaneous multiple injections and detection of sample solutions. Differences in flow can lead to premature draining of channels during filling of other channels, varied sample usage per channel and possible clogging of channels with weaker flow.

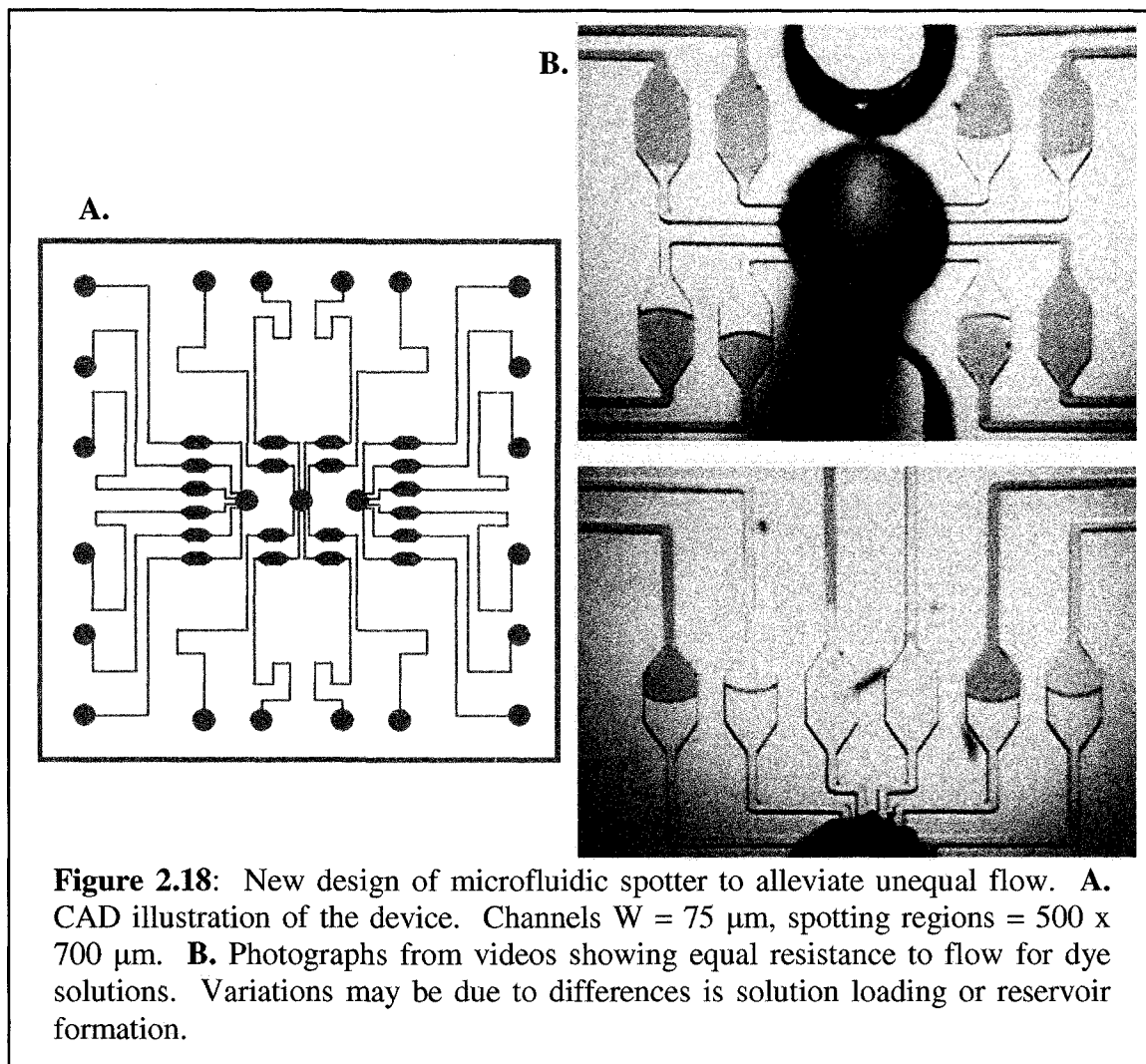
2.4 NEW DESIGNS

To alleviate flow restriction problems encountered with early devices, new prototype designs were developed. Sharing a common waste line among a group of inlets was initially used in designs as a means to decrease the number of access holes needed for the available area. Individual outlets per inlet would require a lot of space. While successful at minimizing space, the final design resulted in varied flow rates among common inlets per outlet, as described in Section 2.3.2. A new design maintaining the benefits of reduced space while achieving equal resistance to flow was desired.

Initially it was thought that decreasing the number of inlets per outlet ratio by half (3:1 from 6:1) would balance volume flow rates as differences in flow rates among sets of three array spots were not as drastic. However, that would also double the number of outlet reservoirs from 4 to 8, strain the layout due to total area restrictions (1.8 x 1.8 cm) and require a complete redesign of the underlying spot array to accommodate for the extra outlets. Furthermore, to truly equilibrate the flow rates among the channels it would be necessary to ensure that the cross sectional area as well as the total lengths of the outlet channel equaled that of the inlet channels.

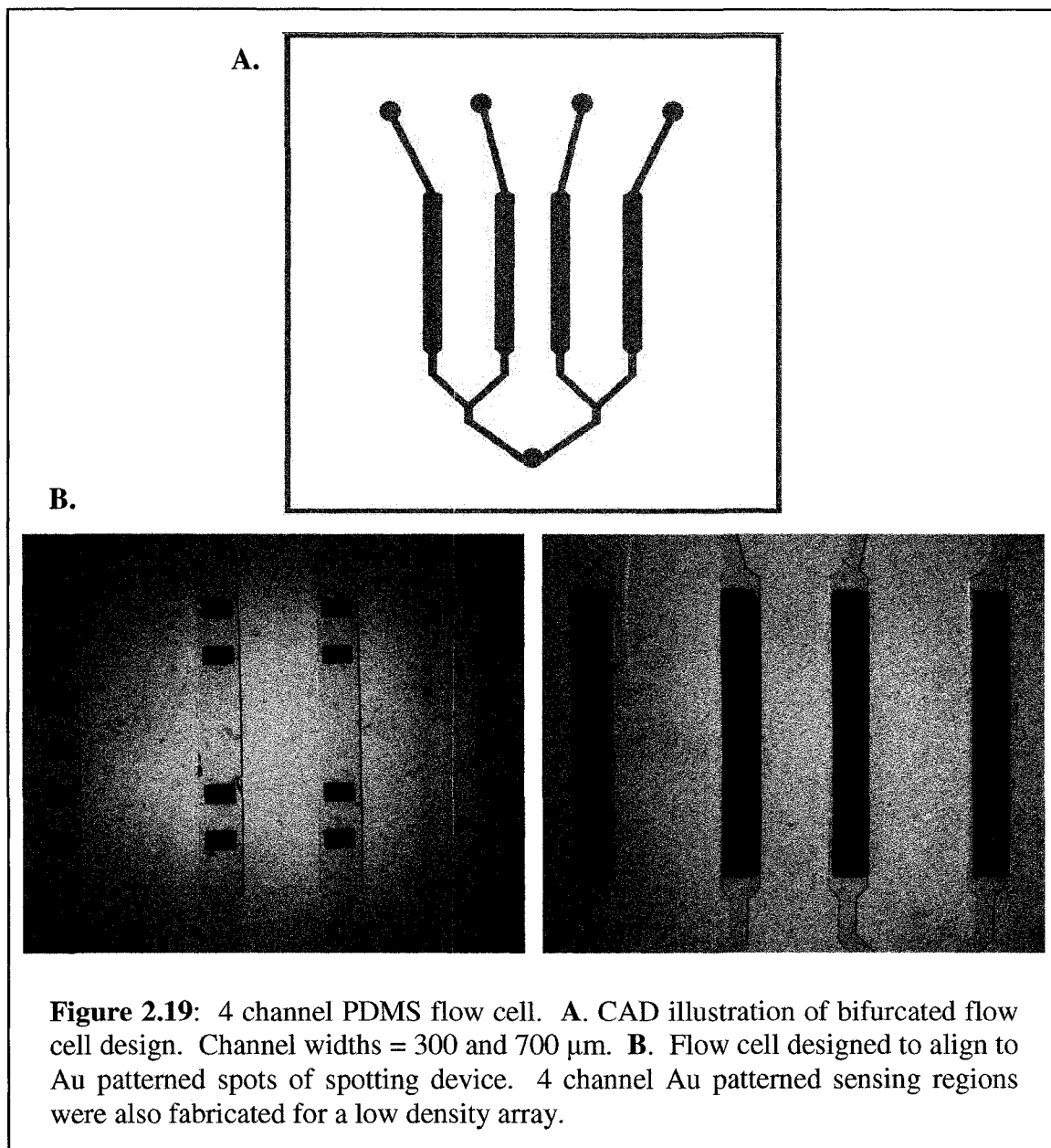
Maintaining a common outlet would require either decreasing the width of the inlet channel or increasing the width of the outlet channel. Increasing the width of the common outlet channel could result in spot-to-spot contamination, while decreasing the inlet channel width would increase the resistance to flow. At a 50 μm width, equal to the width of the outlet channel, the resistance to flow increases to 9.1×10^{12} , more than doubling the largest calculated resistance to flow value in Table 2.5 and 2.6. This would significantly reduce the volume flow rates achievable.

An alternative approach was taken in considering a redesign. Common outlets were maintained for sets of inlets however, the common outlet channel was replaced with discrete outlet channels. Thus, each flow path is made up of an inlet channel opening onto a spotting region and an outlet channel directly leading waste away to the outlet reservoir with no other intersections. This had multiple benefits. First, spot-to-spot contamination was eliminated, as each solution flows through individual channels. Second, decoupling of the spots from a common outlet allowed for equalizing the pre and post spotting region channel dimensions. This results in channel length being the only variable in calculating equal resistance to flow. Since length is the only factor in ensuring equal resistance to flow it was necessary to position the outlet reservoirs in the center of the device. This ensured having as little as possible length discrepancy between the various inlet paths. By placing three outlet reservoirs in the center of the device it was necessary to remove four Au spots. A redesign of the spot array was not necessary as the remaining Au spots maintained their positions. Figure 2.18 is a CAD representation of the device layout along with photograph images showing balanced flow resistance. The variation in flow seen in Figure 2.18B could potentially be due to differences in the loading of the dye solution in the inlet, or variations in the punched hole that defines the inlet. By calculating the volume difference of the channels from the various solution fronts, and using the difference in the times between the images a semi-quantitative analysis of the flow rate could be determined. This was not done as visual confirmation of equal flow among the different channels was sufficient. Future designs may benefit from a more detailed analysis of the channel flow rates.



An additional improvement to the design was obtained by increasing of the size of the spotting regions, to $500 \times 700 \mu\text{m}$. This allowed easier alignment between the Au patterned spots ($300 \times 500 \mu\text{m}$) of the array and the microfluidic manifold, by providing $100 \mu\text{m}$ of extra spacing on each side of the Au spots. A drawback still present in this design is the number of reservoirs. To allow for this device to be used as a sample flow cell it is either necessary to pipette sample into each reservoir or apply tubing to each reservoir for sample introduction from a vial. Pipetting 20 samples individually is tedious, while mounting connection tubing to each inlet becomes cumbersome. Thus, a low density microfluidic flow cell was developed for coupling to the 20 spot array for easy delivery of samples.

Applying the knowledge and experience garnered through the development of a microfluidic spotting device, production of a low density microfluidic flow cell was achieved. The device consists of four channels aligned to the four rows of spots forming the array. Each channel would allow for sample flow over 4 or 6 spots from an individual inlet towards a shared outlet. In this way fewer tubing connections or pipetting events are necessary to introduce samples. Only two design aspects were necessary for consideration: 1. maintaining equal resistance to flow and 2. allowing for easy alignment between spots and channels. Equal resistance to flow was achieved by balancing channel length. With a shared outlet this was achieved by having a bifurcated channel design at the outlet. Easy alignment was achieved by designing the channel dimensions to be wider than the spots. During fabrication it became possible to easily fabricate an accompanying low density SPR Au patterned sensor based on the channel flow cell design and using our Au patterning technique discussed above (Section 2.2.2.2) Figure 2.19 is a schematic outline of the flow cell design with photographs of aligned Au patterned SPR sensors with the 4 channel PDMS device.

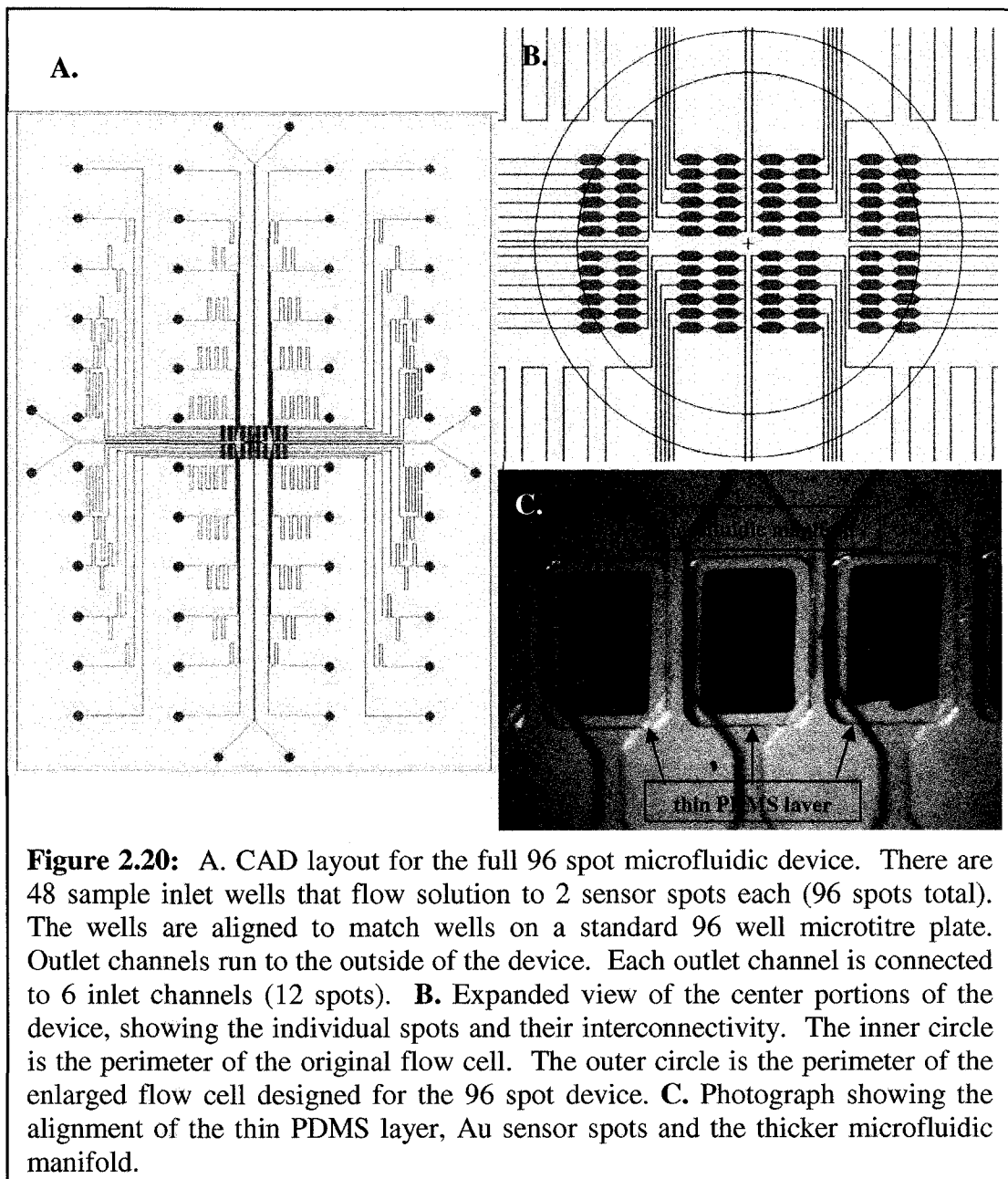


2.5 96 SPOT MICROFLUIDIC SPR ARRAY

Employing the acquired knowledge and experience in designing and fabricating the 4 channel and 20 spot microfluidic SPR sensors, development of a higher spot density array was undertaken. 96 well microtitre plates are the most commonly used platform for immunoassay analysis, typically in ELISA format. For that reason, work was initiated to attempt coupling a 96 well microtitre plate to a 96 spot SPR sensor utilizing

microfluidics. This would have the benefit of allowing known protocols and instrumentation used with microtitre plates to interface with microfluidic devices.

The proposed design required conventional micro-pipettors to interface with a 96-well reservoir layout that would connect each microtitre plate well to an inlet for sample being drawn through individual microfluidic channels to a Au sensor assigned to that particular well. The Au sensing elements were centrally located on the SPR sensor. Since the SPR sensor is fixed in size at 1.8 x 1.8 cm, solution flow from the much larger microtitre plate occurs off of the SPR sensor region. The PDMS microfluidic manifold was of the same dimensions as the microtitre plate. Thus, to ensure sample exposure only at the Au sensing elements a thin PDMS membrane was used to allow for solution to be transported over long distances from the microtitre plate wells to the SPR sensor. The PDMS membrane contained through holes, aligned to the spotting regions of the microfluidic manifold and the fabricated Au spot array on the SPR sensor. These through holes allowed for solution deposition to the specific sensor elements. This design is conceptually similar to the first proposed microfluidic SPR sensor illustrated in Figure 1.1A. Figure 2.19A-C is a CAD illustration of the 96 spot device along with a photograph of three aligned sensors.



While 96 Au spots are patterned, limitations in the dimensions of spotting regions and channel widths ultimately limited the total number of inlets. Channels were limited to 75 μm widths to ensure an adequate volume flow rate. A smaller width would result in increased resistance to flow, as well as being more difficult to produce with high resolution printing. Au spots were maintained at 500 x 300 μm , the optimally determined size for adequate viewing. The spotting regions were 700 x 500 μm to ease alignment of the microfluidic channels and SPR sensors. Each inlet well and channel connects to 2

adjacent spotting regions, with 6 inlets (12 total sensor spots) coupled to one outlet, located at the periphery of the completed device. The original flow cell had an internal diameter of 1.2 cm while a new flow cell was needed with an internal diameter of 1.5 cm to accommodate for the higher number of sensing spots. This larger flow cell was fabricated in the Department of Chemistry Machine Shop using the original flow cell as a template.

2.5.1 FABRICATION

Positive photoresist masters on Si wafers were used as the negative templates for PDMS curing. Photoresist processing, PDMS curing and thin PDMS membrane fabrication were carried out as described previously in Section 2.2.1 and 2.2.2. However, adjustments to the fabrication procedure accounting for the larger device dimensions were necessary.

Five inch Si wafers were required as the support substrate for the PDMS photoresist masters. Both the microfluidic manifold and thin PDMS membranes with through holes possessed the same dimensions as a standard 96 well microtitre plate (12 x 8 cm), resulting in the need for the larger support substrate. At the time of experimental work the University of Alberta Nanofab Facility was not fully equipped for larger wafer processing making fabrication tedious and time consuming. Also, curing the PDMS over a larger 5 inch diameter area for the microfluidic manifold required the construction of a special clamp holder. This consisted of a 5 inch diameter ring with a fitted rubber O-ring on the bottom. The ring would be positioned around the outer diameter of the wafer and clamped against a support plate creating a seal. A 10:1, polymer:curing agent mixture, could then be poured over the wafer features to a desired thickness.

To ensure a consistent thickness of the PDMS membrane over the relatively large area of 12 x 8 cm, a glass slide of the same dimensions was positioned between the transparency film and weights. Attempts to fabricate this large area membrane without the glass slide resulted in a wavy membrane that was difficult to bond to the microfluidic manifold and SPR sensor. Irreversible O₂ plasma bonding was used to bond the thin PDMS membrane to the microfluidic manifold. Alignment was achieved using the homebuilt alignment microscope described in Section 2.2.4. After alignment and

bonding of the PDMS thin membrane and microfluidic manifold it was stored under vacuum upside down until needed.

Alignment to a 96 spot Au patterned SPR slide was achieved by using a aluminum (Al) holder of the same dimensions as the bonded PDMS thin membrane and microfluidic manifold. This hole had an opening in the middle machined to the dimension of the SPR slide so that the patterned sensor was flush with the Al plate surface. This allowed for the bonded PDMS device to be aligned to the 1.8 x 1.8 cm SPR sensor. The Al holder acted as a support for the completed device. Sample could be injected by use of a single tip pipet or a 12 tip pipet directly to the inlets or through a coupled microtitre plate. Figure 2.20 shows the completed 96 spot SPR sensor device.

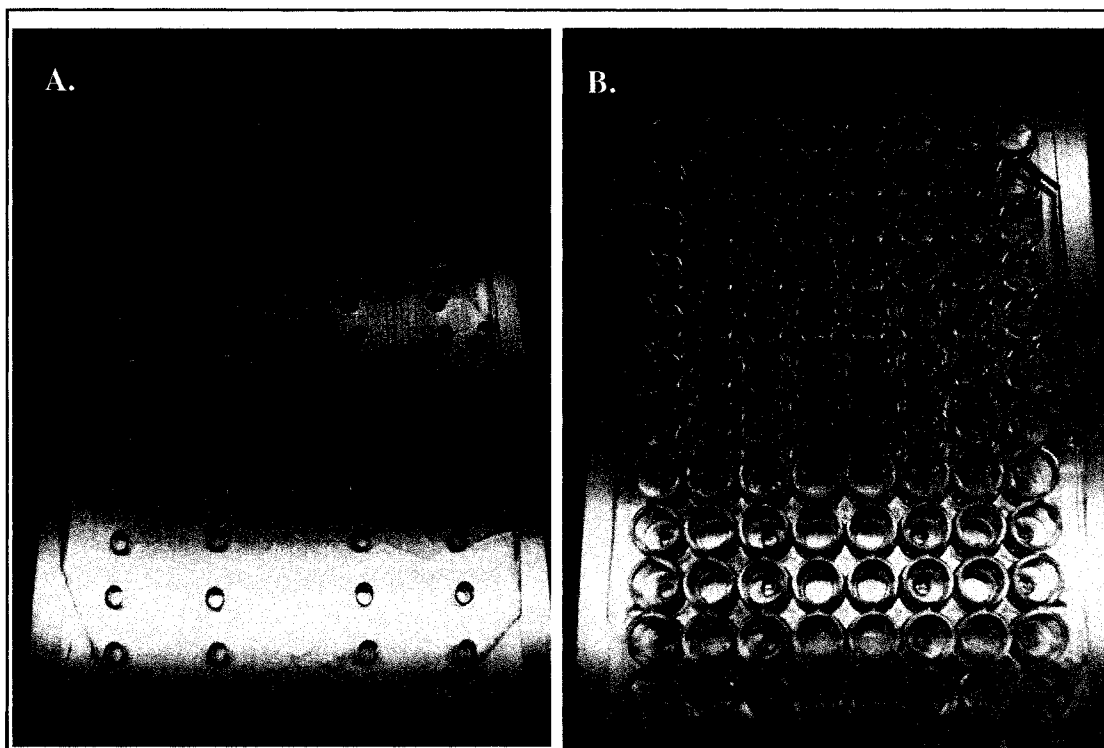
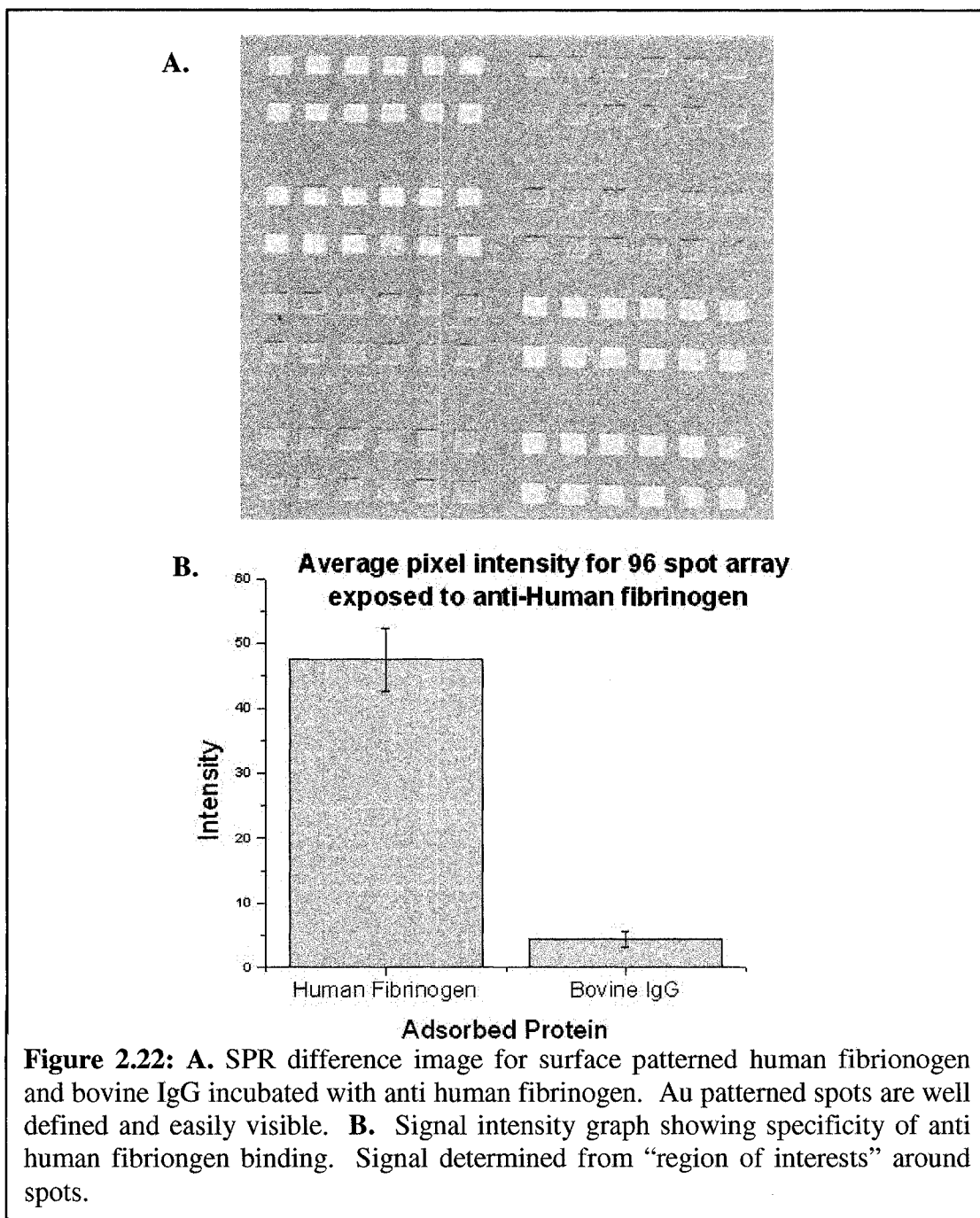


Figure 2.21: Photographs showing the completed 96 spot microfluidic SPR sensor device. **A.** The Al plate acts as a support holding the Au patterned SPR sensor. The bonded PDMS device is aligned to the Au patterned spots on the sensor. Outlets are positioned to the periphery of the device each outlet is connected to six inlets. **B.** Coupling of a 96 well microtitre plate to the PDMS device. Holes are drilled in the well to a smaller diameter than the punched inlet holes in the PDMS. This ensures that the wells of the plate sit in the PDMS inlets reducing leakage.

2.5.2 EVALUATION

To evaluate the performance of the fabricated 96 spot microfluidic SPR sensor a straightforward binding experiment was performed. A 96 spot SPR sensor was first ozone cleaned and incubated overnight in 5 mM mercaptoundecylamine (HS-(CH₂)₁₁-NH₂) in 100% ethanol. This created an amine terminated self assembled monolayer at the surface of the Au spots. The SPR sensor was rinsed with ethanol and N₂ dried. It was then aligned and reversibly bonded to the two layer 96 spot PDMS microfluidic manifold. Using vacuum, 160 µg mL⁻¹ human fibrinogen and 100 µg mL⁻¹ bovine IgG were flowed through the channels of the device and physisorbed over the Au spots. After incubation for approximately 1 hour a rinsing step with buffer was performed. The PDMS channels were then emptied of solution by vacuum and the PDMS device was removed from the SPR sensor. The SPR sensor was then coupled to the glass prism and larger flow cell for loading into the SPR imager. Anti human fibrinogen (20 µg mL⁻¹) was incubated in the flow cell for 15 minutes and a difference image was taken after rinsing with buffer. Figure 2.21 is the difference image of the 96 spot SPR sensor for anti human fibrinogen binding to immobilized human fibrinogen.



2.5.3 IMPROVEMENTS

While the proof-of-concept of a 96 spot SPR sensor was demonstrated, wider adoption of this design was limited. During the course of the work presented here the ability to pattern 48 separate samples was not a necessity. Thus, beyond demonstrating

proof of concept, not much effort was directed toward this design or device. Instead, effort was focused on the lower density 1.8 x 1.8 cm arrays.

Should the need for patterning larger arrays arise, improvements to the usability and design of the 96 spot array are recommended. They include the possibility of coupling the SPR prism directly to the backside of the SPR sensor as it is sitting in the Al holder. This would allow for the use of the PDMS microfluidic manifold as the flow cell and limit transfer steps of the SPR sensor. Also, the setup of an 8 port vacuum system would be highly advantages. Currently, vacuum is applied to each outlet manually and in a linear fashion. Setting up of an eight port variable vacuum connection would allow for simultaneous flow through the channels at controlled volume flow rates. This would ease operational use of the device.

2.6 CONCLUSIONS

Microfluidics has been utilized as a method for surface patterning. Devices have been designed to be used in conjunction with SPR detection. A novel micro-scale metal patterning method was developed to achieve uncontaminated Au sensing regions for coupling to a microfluidic manifold. To achieve optimally sized Au sensing regions, consideration of the detection instruments optical system was necessary. Fluid paths were formed in PDMS using positive relief photoresist masters. This approach allowed for fast and inexpensive prototyping of designs and provided a versatile material compatible with a wide variety of solutions and biological fluids.

Coupling metal patterned sensors to microfluidic channels required design elements for effectively linking narrow channels to larger detection regions. This was achieved using expanding and narrowing channel widths over the detection regions. Due to the large number of channels, evaluation of the resistance to flow was necessary to achieve uniform performance. Due to the sharing of a common outlet, resistance to flow calculations confirmed the importance of maintaining an equal cross sectional area across the full length of a fluid path. This was achieved by providing discrete waste channels converging on a common waste reservoir, thus providing equal resistance to flow and minimizing the number of reservoirs.

Along with a spotting device a low density channel device was fabricated that could be used for both patterning to a 4 channel Au patterned SPR sensor or as a novel SPR flow cell. By aligning the 4 channel bifurcated PDMS device to the Au pre-patterned SPR sensors, up to 4 samples can be investigated against the patterned SPR sensor surface. The utilization of a multi channeled flow cell allows for greater sample throughput and a reduction of sample volume.

2.7 REFERENCES

- (1) Nelson, B. P.; Grimsrud, T. E.; Liles, M. R.; Goodman, R. M.; Corn, R. M. *Analytical Chemistry* **2001**, *73*, 1-7.
- (2) Kyo, M.; Yamamoto, T.; Motohashi, H.; Kamiya, T.; Kuroita, T.; Tanaka, T.; Engel, J. D.; Kawakami, B.; Yamamoto, M. *Genes to Cells* **2004**, *9*, 153-164.
- (3) Shumaker-Parry, J. S.; Zareie, M. H.; Aebersold, R.; Campbell, C. T. *Analytical Chemistry* **2004**, *76*, 918-929.
- (4) Wegner, G. J.; Wark, A. W.; Lee, H. J.; Codner, E.; Saeki, T.; Fang, S. P.; Corn, R. M. *Analytical Chemistry* **2004**, *76*, 5677-5684.
- (5) Kanda, V.; Kitov, P.; Bundle, D. R.; McDermott, M. T. *Analytical Chemistry* **2005**, *77*, 7497-7504.
- (6) Wolf, L. K.; Fullenkamp, D. E.; Georgiadis, R. M. *Abstracts of Papers of the American Chemical Society* **2005**, *230*, U1041-U1042.
- (7) Kim, M.; Park, K.; Jeong, E. J.; Shin, Y. B.; Chung, B. H. *Analytical Biochemistry* **2006**, *351*, 298-304.
- (8) Fischer, B.; Heyn, S. P.; Egger, M.; Gaub, H. E. *Langmuir* **1993**, *9*, 136-140.
- (9) Brockman, J. M.; Frutos, A. G.; Corn, R. M. *Journal of the American Chemical Society* **1999**, *121*, 8044-8051.
- (10) Kanda, V.; Kariuki, J. K.; Harrison, D. J.; McDermott, M. T. *Analytical Chemistry* **2004**, *76*, 7257-7262.
- (11) Lee, H. J.; Nedelkov, D.; Corn, R. M. *Analytical Chemistry* **2006**, *78*, 6504-6510.
- (12) Wegner, G. J.; Lee, H. J.; Corn, R. M. *Analytical Chemistry* **2002**, *74*, 5161-5168.
- (13) Ptacek, J.; Devgan, G.; Michaud, G.; Zhu, H.; Zhu, X. W.; Fasolo, J.; Guo, H.; Jona, G.; Breitreutz, A.; Sopko, R.; McCartney, R. R.; Schmidt, M. C.; Rachidi, N.; Lee,

- S. J.; Mah, A. S.; Meng, L.; Stark, M. J. R.; Stern, D. F.; De Virgilio, C.; Tyers, M.; Andrews, B.; Gerstein, M.; Schweitzer, B.; Predki, P. F.; Snyder, M. *Nature* **2005**, *438*, 679-684.
- (14) Lee, H. J.; Goodrich, T. T.; Corn, R. M. *Analytical Chemistry* **2001**, *73*, 5525-5531.
- (15) Anderson, J. R.; Chiu, D. T.; Jackman, R. J.; Cherniavskaya, O.; McDonald, J. C.; Wu, H. K.; Whitesides, S. H.; Whitesides, G. M. *Analytical Chemistry* **2000**, *72*, 3158-3164.
- (16) Duffy, D. C.; McDonald, J. C.; Schueller, O. J. A.; Whitesides, G. M. *Analytical Chemistry* **1998**, *70*, 4974-4984.
- (17) Duffy, D. C.; Schueller, O. J. A.; Brittain, S. T.; Whitesides, G. M. *Journal of Micromechanics and Microengineering* **1999**, *9*, 211-217.
- (18) Kim, J. S.; Knapp, D. R. *Electrophoresis* **2001**, *22*, 3993-3999.
- (19) Eteshola, E.; Leckband, D. *Sensors and Actuators B-Chemical* **2001**, *72*, 129-133.
- (20) McDonald, J. C.; Metallo, S. J.; Whitesides, G. M. *Analytical Chemistry* **2001**, *73*, 5645-5650.
- (21) Ruano-Lopez, J. M.; Aguirregabiria, M.; Tijero, M.; Arroyo, M. T.; Elizalde, J.; Berganzo, J.; Aranburu, I.; Blanco, F. J.; Mayora, K. *Sensors and Actuators B-Chemical* **2006**, *114*, 542-551.
- (22) del Campo, A.; Greiner, C. *Journal of Micromechanics and Microengineering* **2007**, *17*, R81-R95.
- (23) Abgrall, P.; Conedera, V.; Camon, H.; Gue, A. M.; Nguyen, N. T. *Electrophoresis* **2007**, *28*, 4539-4551.
- (24) MicroChem *Permanent Epoxy Negative Photoresist: Processing Guidelines*, <http://www.microchem.com/products/pdf/SU-82000DataSheet82025thru82075Ver82004.pdf>.
- (25) McDonald, J. C.; Duffy, D. C.; Anderson, J. R.; Chiu, D. T.; Wu, H. K.; Schueller, O. J. A.; Whitesides, G. M. *Electrophoresis* **2000**, *21*, 27-40.
- (26) Ren, X. Q.; Bachman, M.; Sims, C.; Li, G. P.; Allbritton, N. *Journal of Chromatography B-Analytical Technologies in the Biomedical and Life Sciences* **2001**, *762*, 117-125.
- (27) Horvath, J.; Dolnik, V. *Electrophoresis* **2001**, *22*, 644-655.

- (28) Rowe, C. A.; Scruggs, S. B.; Feldstein, M. J.; Golden, J. P.; Ligler, F. S. *Analytical Chemistry* **1999**, *71*, 433-439.
- (29) Delamarche, E.; Bernard, A.; Schmid, H.; Michel, B.; Biebuyck, H. *Science* **1997**, *276*, 779-781.
- (30) Hillborg, H.; Gedde, U. W. *Polymer* **1998**, *39*, 1991-1998.
- (31) Eddington, D. T.; Puccinelli, J. P.; Beebe, D. J. *Sensors and Actuators B-Chemical* **2006**, *114*, 170-172.
- (32) Kim, J.; Chaudhury, M. K.; Owen, M. J. *Journal of Colloid and Interface Science* **2000**, *226*, 231-236.
- (33) Qiu, C. X.; Harrison, D. J. *Electrophoresis* **2001**, *22*, 3949-3958.
- (34) Attiya, S.; Jemere, A. B.; Tang, T.; Fitzpatrick, G.; Seiler, K.; Chiem, N.; Harrison, D. J. *Electrophoresis* **2001**, *22*, 318-327.

CHAPTER 3	SPR PLASMA PROTEIN ADSORPTION STUDIES
3.1 INTRODUCTION	84
3.2 EXPERIMENTAL	86
3.2.1 REAGENTS AND SOLUTIONS	87
3.2.2 INSTRUMENTATION	88
3.2.3 PROCEDURE	89
3.3 RESULTS	93
3.3.1 HUMAN PLASMA PROTEIN ISOTHERMS	93
3.3.2 THIOL REFRACTIVE INDEX CHANGES	102
3.4 CONCLUSIONS.....	107
3.5 REFERENCES	108

3.1 INTRODUCTION

Protein adsorption and bimolecular interactions on solid surfaces are phenomena with significance in various research fields. Understanding of adsorption to various materials is important for in vivo implantation technologies, biological sensors, bioseparation and medical understanding of thrombosis (clotting). Protein adsorption is a complex and dynamic process involving many noncovalent interactions, including hydrophobic interactions, electrostatic forces, hydrogen bonding, and van der Waals forces.¹ The adsorption process is affected by both protein parameters, including primary structure, size, and structural stability, as well as properties of the binding surface such as surface energy, roughness and chemistry.^{2, 3} In particular, surface chemistry greatly influences the type of protein adsorbed, quantity, conformation and stability.⁴⁻⁶ As an example, it has been shown that adsorption of fibronectin on different surfaces can alter protein structure and affect adhesion and spreading of cells.⁷

To investigate protein adsorption to various surfaces, many reports have focused on the studying of surfaces formed by self assembled monolayers (SAMs) from solutions containing ω - functionalized alkyl thiols⁸⁻¹² on noble metal surfaces, predominately Au. Long chain alkanethiols, HS-(CH₂)_n-X, spontaneously form stable and well-organized monomolecular layers on gold.^{13, 14} They also possess the benefit of being quasi crystalline, stable and reproducible. The terminal X functional group allows for control of the surface structure and chemistry at a molecular level, thus allowing for tuning of the surface to a desired state. These surfaces represent model systems of homogeneity that have been extensively used for the systematic investigation of the affects of surface chemistry on protein adsorption and cell adhesion.¹⁵⁻¹⁷

Sensitive surface detection methods are required for monitoring protein adsorption as the thickness of a fully formed monolayer coverage of adsorbed proteins has been reported in the range of 2 – 10 nm.⁶ Detection techniques such as ellipsometry,⁶ total internal reflection fluorescence spectroscopy,¹⁸ quartz crystal microbalance,¹⁹ atomic force microscopy²⁰⁻²² and radioactive isotope labeling methods,^{23, 24} have all been used previously for the monitoring of protein adsorption to alkanethiolates on gold. However, surface plasmon resonance (SPR) has recently emerged as the preferred method of monitoring protein adsorption to surfaces.²⁵⁻²⁸ SPR provides a convenient

method for the *in situ* investigation of protein adsorption over time. It directly monitors surface binding events without the need for labeling of analytes, and allows for the determination of the kinetics of surface interactions in real time.

SPR can be utilized as a spectroscopic method or imaging method. SPR spectroscopy monitors the angle shift of the SPR angle during binding events on gold surfaces. SPR imaging monitors changes in reflectivity, due to binding events, at a fixed angle. This allows for the monitoring of simultaneous adsorption events across a patterned surface in an array format. Much of the work involving protein adsorption studies with SPR has utilized SPR spectroscopy,^{9, 29-31} this method allows for only the serial monitoring of adsorption to various functionalized surfaces. As such, this technique increases the number of experiments needed when investigating responses to various surface modifications, possibly influencing experimental comparisons as conditions may change from experiment to experiment. It has been reported that preparations of surfaces and conditions of mass transport significantly influence protein adsorption.³² Therefore, allowing for the simultaneous monitoring of binding events to different surfaces, in a controlled array format, can decrease the number of individual experiments and allow for easier comparison of results.

Though there have been reports focusing on adsorption to many different types of surfaces,^{9, 30, 33} many have focused on single concentrations. Surface adsorption studies have predominantly focused on single concentration analysis, both at low and high protein concentrations. While information can be gained from these studies, including specificity of adsorption and possible mechanistic information, focusing on the surface response to a single concentration, rather than examining a range of concentrations, may be providing only limited information. Through examination of a range of protein concentrations to adsorption on a surface, a Langmuir binding isotherm can be constructed and an adsorption coefficient (K_{ads}) determined.³⁴ This can be achieved by fitting the adsorption signal for various concentrations to the Langmuir adsorption isotherm;

$$\theta = \frac{\Delta\%R}{\Delta\%R_{max}} = \frac{K_{ads}[C]}{1 + K_{ads}[C]} \quad 3.1$$

where θ is the fractional coverage of surface sites resulting from the ratio of $\Delta\%R$ for each concentration to the maximum $\Delta\%R_{\max}$ determined from the fit. K_{ads} is the adsorption coefficient and $[C]$ is the bulk solution concentration of the analyte. While not equivalent to binding association constants, K_{ads} can be helpful in ranking binding strengths as they have been shown to be inversely related to dissociation constants.³⁵ When the fractional surface coverage is half the maximum coverage ($\theta = 0.5$) the bulk concentration equals the inverse of the adsorption coefficient, $[C] = K_{\text{ads}}^{-1}$. Therefore, the values of the adsorption coefficient are determined from the inverse of the bulk concentration corresponding to half maximum surface coverage.

Proteins of interest for surface adsorption studies have usually focused on proteins providing a range of properties such as size, charge and shape.^{36, 37} These studies can provide model responses for various surfaces to the differences in protein properties and have been utilized in studies interested in determination of antifouling surfaces. Other studies have focused on the adsorption of whole plasma or serum.^{38, 39} This is important for biomedical fields when investigating the response of thrombosis to implanted surfaces. To the knowledge of this author there has yet not been a systematic study of the adsorption of the component proteins that make up human plasma. By decoupling the adsorption of individual proteins that make up the complicated and dynamic mixture of human plasma a baseline of response to specific surfaces can be achieved.

The purpose of this work is to examine, by SPR imaging, the simultaneous real time adsorption of the protein components of human plasma to functionalized gold surfaces modified by alkyl thiols over a range of concentrations. The protein components of human plasma investigated are human IgG, IgA, IgM, fibrinogen and albumin. These proteins make up approximately >99% of the protein complement of plasma. Their adsorption was monitored to the alkyl thiol terminal functional groups; $-\text{NH}_2$, $-\text{COOH}$, $-\text{CH}_3$ and $-\text{OH}$. These functional groups were chosen because they represented surfaces of opposite charges and hydrophobicities, thus providing a range of possible responses.

3.2 EXPERIMENTAL

Arrays were imaged using GWC Instruments SPRImager II (GWC Instruments; Madison, WI) as has been described in detail elsewhere.⁴⁰ The array sensor was

constructed from the thermal evaporation of a 45 nm gold (Au) film deposited on SF-10 glass (Schott; Toronto, ON, Canada) with a 1 nm adhesive chromium layer through a PDMS shadow mask, as described in Chapter 2.2.3. Alignment to a PDMS microfluidic manifold was achieved through the use of a homebuilt alignment microscope, described in Chapter 2.2.4. Upon activation of the Au sensor regions with functionalized alkyl thiol chains the sensor was mounted within a flow cell through which solutions were introduced to the entire surface via a peristaltic pump. The flow cell was filled with running buffer for the determination of the SPR angle. This angle was maintained throughout the course of the experiment unless otherwise stated. A reference image was taken in the running buffer from the averaging of 30 individual images.

Difference images were determined by subtracting the image taken after a binding event from the reference image taken prior to the binding event. Since the SPR angle was maintained, any differences between the images, as a result of binding from the incubation solution, appear as illuminated areas. The value of $\Delta\%R$ (percent change in reflectivity), is obtained, as specified by the manufacturer, by $\Delta\%R = 0.85(I_p/I_s) \cdot 100\%$ where I_p and I_s are the reflected light intensities detected using p and s polarized light.

3.2.1 REAGENTS AND SOLUTIONS

All human serum proteins (IgG, IgA, IgM, albumin, fibrinogen) used were purchased in the highest available purity from Sigma Aldrich and used as received. Lyophilized proteins (IgG, IgA, albumin, fibrinogen) were dissolved in phosphate buffered saline (PBS; 10 mM Na_2HPO_4 , 1.5 mM KH_2PO_4 , 137 mM NaCl, 2.7 mM KCl) pH = 7.4 from which they were aliquoted to their appropriate concentrations determined from the measured weight and accurate molecular mass. PBS buffer was prepared as a stock solution using ultra pure, 0.2 μm filtered, Milli Q de-ionized water and refrigerated until needed. Working buffer was prepared by 10x dilution with ultra pure water as needed. Concentrations for proteins provided as liquids (IgM) were determined by dilution, with PBS, of the received commercial antisera.

11-mercaptoundecylamine hydrochloride was obtained from Dojindo Laboratories (Japan); 11-mercaptoundecanoic acid, 11-undecanethiol, 11-mercapto-1-undecanol were all purchased from Sigma Aldrich. All thiols were prepared as 100 mM

stock solutions using anhydrous ethanol and stored in a freezer at -4° C. Working solutions were prepared as needed by dilution of the stock solution with anhydrous ethanol.

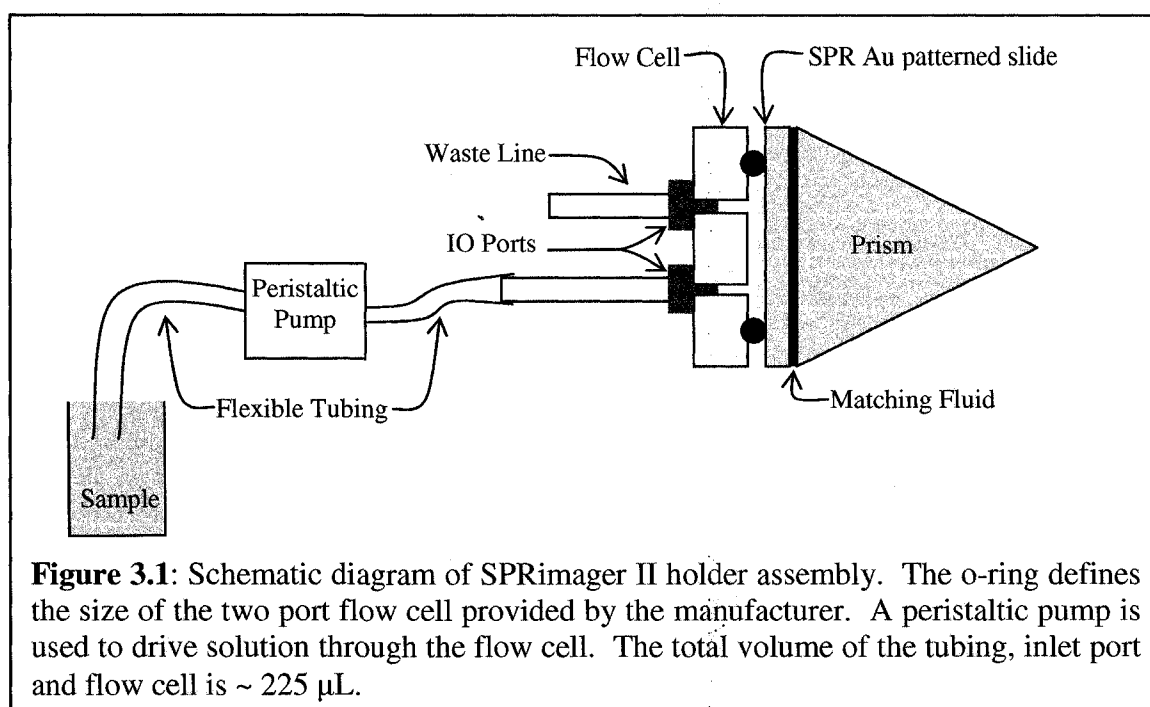
3.2.2 INSTRUMENTATION

SPRImager II (GWC Instruments; Madison, WI) was used for the surface sensitive detection of protein films on thiol activated Au sensor regions. A brief description of the instrumental setup and protocol will be given here.

As described previously, Au patterned SPR slides were formed using thin PDMS shadow masks in a thermal evaporator. These SPR slides can then be reversibly and conformally bonded to PDMS cast microfluidic manifolds. These manifolds contain channel structures, for the delivery of solutions, and spotting regions, for alignment to the Au patterned spots. Upon deposition of solutions of interest to the Au spots, the microfluidic manifold is removed and placed on the SPR holder Au side down. The SPRImager II requires the sensor assembly be in the Kretschmann geometry.⁴¹ Here a thin metal film is evaporated on the base of a prism for which photons from incident light at angle θ couple with the metal resulting in surface plasmon resonance at the Au film. To achieve this type of configuration, a glass prism is placed on top of the backside of a Au patterned SPR glass slide. To ensure no attenuation of photons through the prism/slide assembly the same type of glass, SF-10, is used for both pieces. This ensures a consistent refractive index. To compensate for the air glass boundary between the SPR slide and prism, a refractive index matching fluid is used to ensure a consistent index of refraction through the completed assembly. A single drop of matching fluid ($\sim 5 \mu\text{L}$) is placed on the leading edge of the glass slide. The prism is then positioned at this edge and slowly lowered causing the matching fluid to spread evenly between the slide and prism. This ensures no trapped air bubbles. The index of refraction of the SF-10 glass and matching fluid is 1.720.

Upon assembly, a two port (inlet and outlet) flow cell is mounted over the front of the SPR slide thus allowing for solution coverage of the Au regions. The flow cell consists of a 1.2 cm diameter 0.1 cm deep reservoir defined by a rubber o-ring. This o-ring ensures a tight seal with the SPR slide and results in an approximate flow cell

volume of 100 μL . The diameter of the o-ring also defines the maximum viewable area for the SPRImager II. The flow cell is held in place with four mounting screws to the SPR holder. Solutions are passed through the flow cell through 1/16" tubing screwed into an inlet and outlet port on the fluid cell. The inlet port tubing is connected to peristaltic pump tubing (ID = 1/32") whose inlet is placed inside a vial of solution. The peristaltic pump drives solution flow through the fluid cell. The total volume of solution required to fill the pump tubing, fluid cell tubing and fluid cell is $\sim 225 \mu\text{L}$. The peristaltic pump was operated at a volume flow rate of $\sim 100 \mu\text{L min}^{-1}$. A schematic diagram of the SPR holder assembly is provided in Figure 3.1.



3.2.3 PROCEDURE

A 24 spot microfluidic spotting device was used for patterning of the sensor surface. A representative aligned SPR sensor and PDMS microfluidic manifold is shown in Figure 3.2.

Activation of the Au sensors was achieved by incubation with 5 mM ω -alkyl functionalized thiol solutions in an anhydrous ethanol solvent for 2 hours. Due to the interconnected nature of the channels spreading of the thiol solutions in ethanol occurred quickly. Aliquots of 7 μL were pipetted into the outlet reservoir. Upon spreading of the solution throughout the interconnected channels due to capillary forces, each inlet

reservoir was capped with 3 μL of appropriate thiol solution. As a result of the design and spreading of ethanol-based solutions, only 4 different functionalized alkyl thiols could be patterned on one device, with each thiol solution coating 6 Au spots. It is important to note that leakage was not observed for these ethanol solutions within our microfluidic device. This may be attributed to the relatively strong conformal interaction between glass and PDMS compared to Au and PDMS. Interfaces of Au and PDMS have been observed to leak with the use of organic solutions.

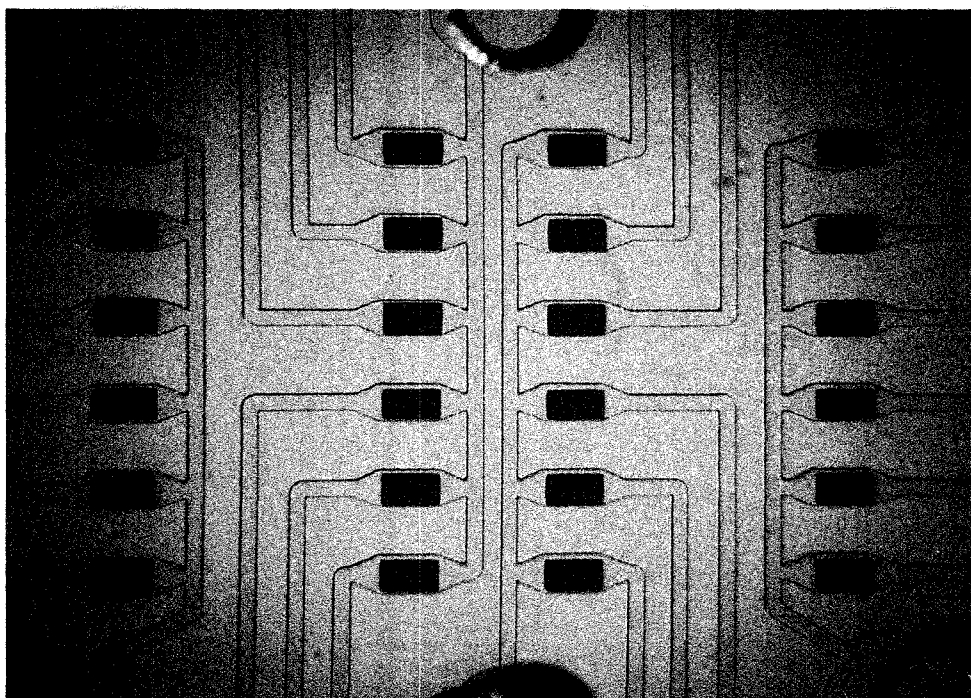


Figure 3.2: Photography of aligned 24 Au spot SPR slide and PDMS microfluidic manifold used throughout this study. Au spot size = 500 x 300 μm ; PDMS channel W = 100 μm , D = 50 μm . Native reversible bonding between glass slide and PDMS manifold were used for attachment.

After incubation with the 4 various thiol solutions, vacuum was applied to each of the four outlets for removal of the solutions. A washing step was applied, where 7 μL of anhydrous ethanol was aliquoted to each inlet and removed by vacuum through the outlet. This was repeated three times for each inlet reservoir. On the final ethanol rinse, vacuum was applied until all channels were evacuated. Using fine tweezers the PDMS manifold was removed from the glass SPR slide and discarded. The thiol patterned SPR slide was then immediately mounted to the SPR holder and coupled to the prism, through index matching fluid, and subsequently to the two port flow cell (Figure 3.1). The assembled

unit was then placed into the SPR where inlet and outlet tubing was connected and buffer solution was immediately introduced to the flow cell. This immediate mounting and filling of the flow cell limited the exposure of the thiol patterned SPR slide to ambient laboratory conditions.

Upon loading of the sample holder the SPR viewing angle was set. Once an appropriate angle is achieved it is maintained during the course of the experiment. At this angle a reference image is taken in a background of running buffer and is used for comparison to all subsequent images taken after binding events.

PBS running buffer is pumped through the flow cell and over the surface of the activated Au spots of the SPR slides for ~ 10 minutes. This is a conditioning step, insuring a constant background response from the running buffer. After conditioning, an angle adjustment can be made if necessary (due to changes caused by conditioning), and a new reference image is taken (better representing the baseline response). Solution switching to an appropriate protein sample is achieved by using a pair of tweezers to move the inlet tubing from one vial to another. First the peristaltic pump is switched off. Then tweezers are used to constrict the tubing prior to removal from one solution and are released after the tubing has been placed into another solution. This limits the possibility of introduction and trapping of air into the SPR tubing and flow cell. Finally, the pump is switched on and the new solution begins flowing to the flow cell. All solutions are injected and pumped through the flow cell at a rate of $150 \mu\text{L min}^{-1}$.

Isotherm data is collected by introducing increasing concentrations of protein solutions to the flow cell for incubation with the functionalized thiol coated Au spots. 1 mL of protein solution is injected into the flow cell. After injection of 1 mL of analyte the solution is allowed to incubate over the surface of the SPR slide for 60 minutes to allow for equilibrium. Between each protein solution a rinsing step corresponding to 3 volume rinses of the flow cell with running buffer is done to ensure a proper solution background for image capture. After rinsing with running buffer an image is taken. A new protein solution of higher concentration is injected into the flow cell in the same manner and these steps are repeated for subsequently increasing protein concentrations.

For each concentration of protein there is a corresponding SPR image, taken in background of running buffer, for the binding that occurs during the incubation. The

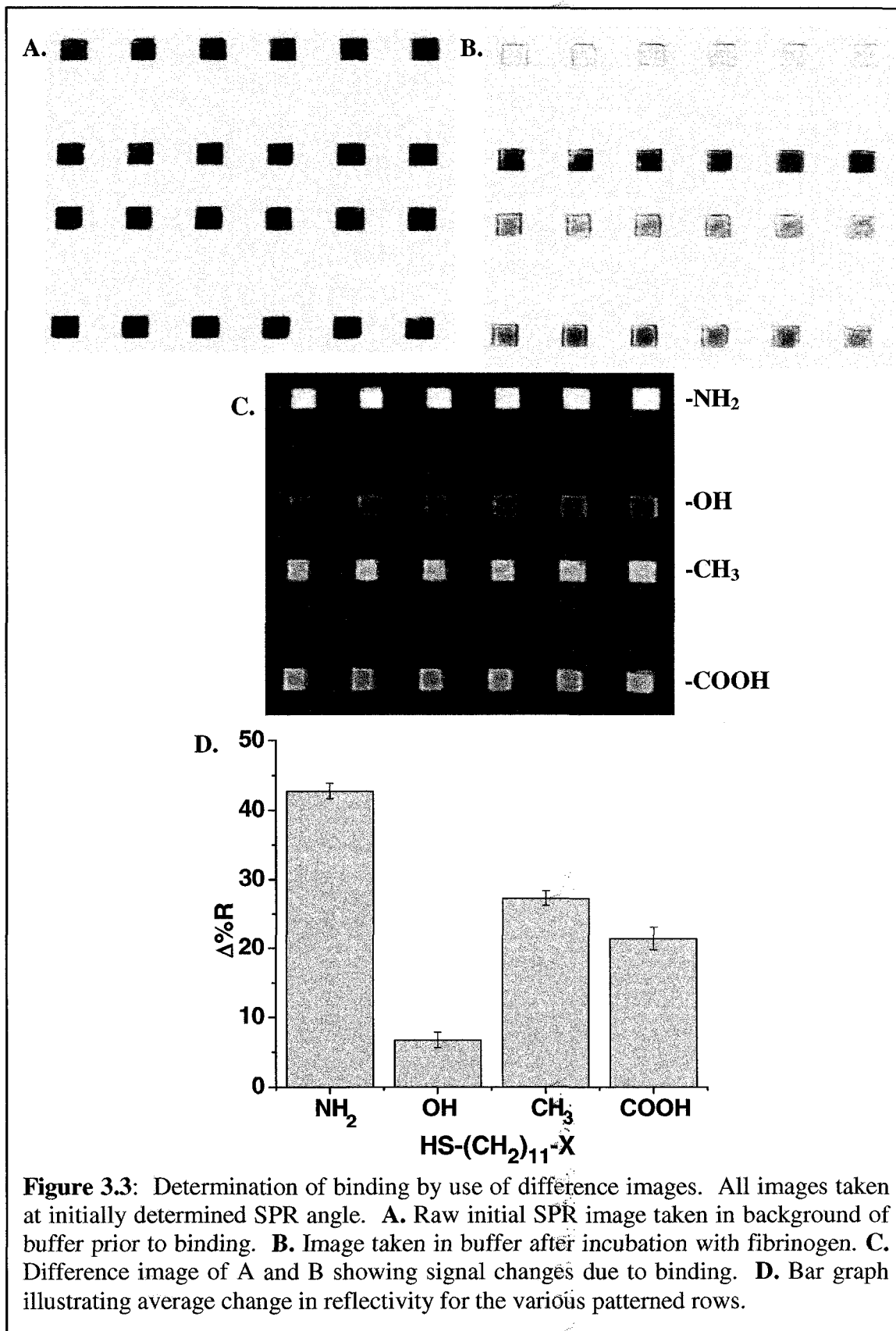


Figure 3.3: Determination of binding by use of difference images. All images taken at initially determined SPR angle. **A.** Raw initial SPR image taken in background of buffer prior to binding. **B.** Image taken in buffer after incubation with fibrinogen. **C.** Difference image of A and B showing signal changes due to binding. **D.** Bar graph illustrating average change in reflectivity for the various patterned rows.

binding that occurs during the incubation. The reference image is subtracted from the binding image to achieve an SPR image of the distinct binding that occurs for the analyte. Binding appears as areas of high intensity and areas of no binding appear as dark areas. For each concentration statistical analysis is applied to the 6 Au patterned spots. Figure 3.3 shows the various types of SPR images taken and the resultant difference image.

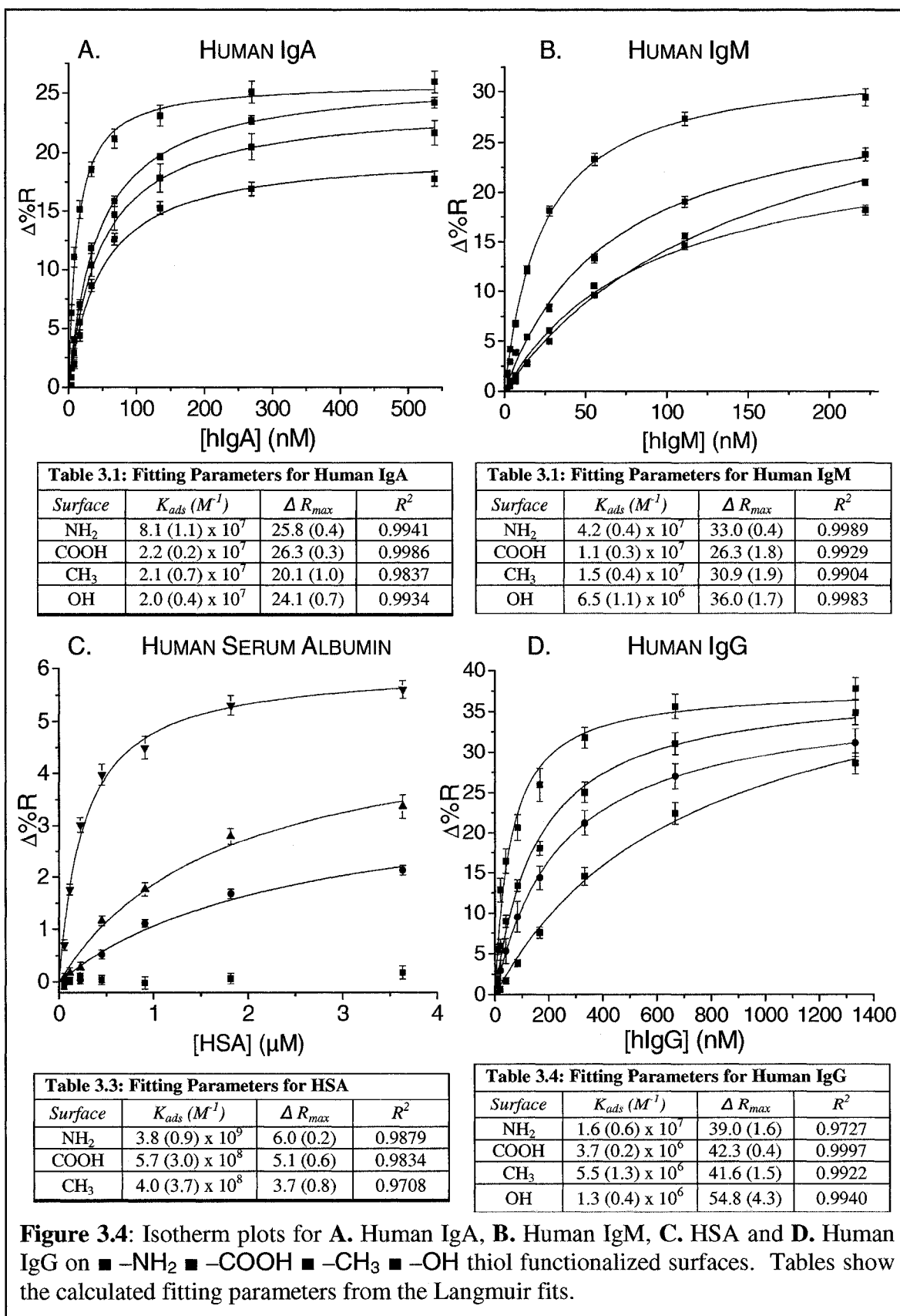
3.3 RESULTS

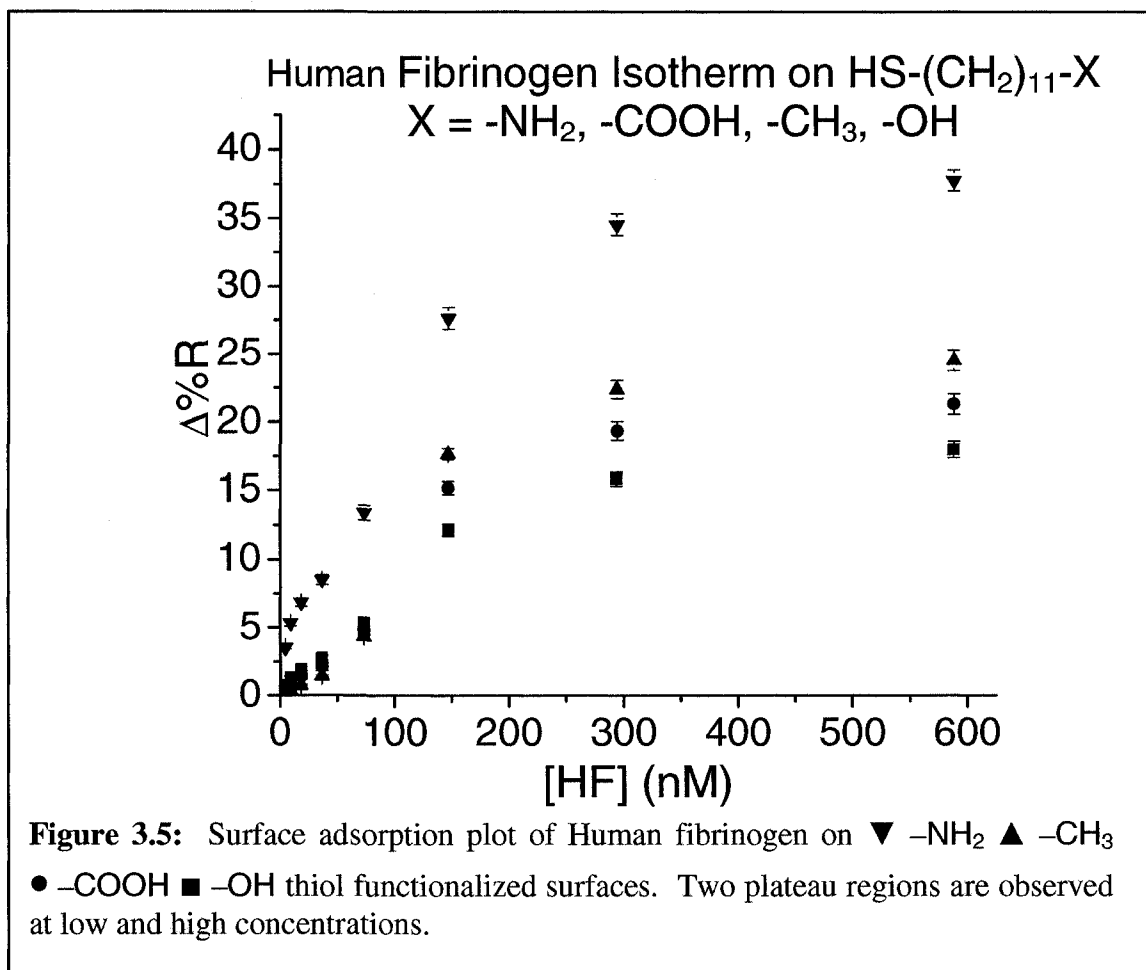
3.3.1 HUMAN PLASMA PROTEIN ISOTHERMS

Protein binding to solid supports is complex and can be affected by the interplay of a variety of factors such as buffer composition, pH and surface chemistry.^{9, 42} Of these the non-specific forces arising from the substrates physicochemical characteristics have been shown to be an important factor.⁹ In this study, the affect of specific chemical functionalities on the binding of human plasma proteins was investigated using a set of well characterized, chemically functionalized surfaces of self assembled alkanethiolates on Au surfaces.

Five human plasma proteins (IgG, IgA, IgM, albumin and fibrinogen), comprising > 99% of the protein composition of human plasma – the remaining < 1% consisting of low abundant IgD, IgE and regulatory proteins – were investigated. Langmuir binding isotherms were collected for each protein using SPR imaging over a concentration range of 1.5 to 200 $\mu\text{g mL}^{-1}$. These isotherms were collected on SPR slides patterned with four rows of six Au spots. Each row of six spots was functionalized with a different C₁₁ alkyl thiol SAM. Images were collected in PBS for each protein concentration after rinsing with buffer. A rinsing step is used to remove bulk refractive index changes due to the protein solution and any weakly bound species. A difference image for each concentration was generated by subtracting the reference image of the thiol patterned SPR chip in PBS. Average signal and standard deviation were determined from the six spots of each thiol patterned row. In this way isotherms for four thiol patterned surfaces could be constructed simultaneously.

Figure 3.4 consists of the isotherms constructed for the various human plasma proteins investigated. They are plots of percent reflectivity change versus solution concentration. Each isotherm is formed from the incubation of 1.563, 3.125, 6.25, 12.4,





25, 50, 100, 200 $\mu\text{g mL}^{-1}$ of the corresponding protein. The curve through the data points is the Langmuir fit for protein binding to each type of surface chemistry. Fitting was achieved using Origin 8 analysis software from OriginLab Corp. (Northampton, USA). While binding curves have been constructed for protein binding to various SAM surfaces in literature reports, they are often of one protein to one type of model surface.³⁴ There are also limited examples of these binding curves in the literature, where surface adsorption experiments are often conducted at one concentration for comparison. To the best of the author's knowledge, these are the first binding curves to be reported for simultaneous adsorption to various surface chemistries for a specific class of proteins. This allows for direct comparison of adsorption results both for the behavior of the surface chemistry and the various components comprising human plasma.

It is important to note that for SPR imaging detection the $\Delta\%R$ signal determined for adsorption events to the surface is only linear with surface concentration for

approximately 10% or less reflectivity change.³⁵ While the Langmuir fits for the data shown (Figure 3.4) exceed the 10% maximum limit for a linear response to adsorption events it is still useful in examining the relative binding behavior between the various surfaces and proteins investigated.

As SPR is a surface sensitive technique, these isotherms further confirm the observation that surface concentration of adsorbed proteins can be controlled by varying their concentration in solution.^{34, 43} This can be achieved to a maximum saturation point dependent on the type of surface. These isotherms also demonstrate that for human plasma proteins, it is the physiochemical property of the substrate surface that affects their non-specific adhesion to the surface. Since the protein conditions of pH, concentration, buffer composition and temperature are identical for each data point, differences of adsorption, for these experimental conditions, must be due to differences between the surface.

For each plasma protein investigated $-NH_2$ surface exhibits the greatest sensitivity to adsorption and greatest degree of protein adhesion compared to $-CH_3$, $-COOH$ and $-OH$. Observations of greater adsorption to amine functionalized surfaces is consistent with literature reports for peptide, protein and cell adsorption on aliphatic amine functionalized and poly-L-lysine surfaces.⁴⁴ However, this is the first systematic study of plasma protein binding across various surface chemistries showing $-NH_2$ surface as the preferred binding surface when compared simultaneously to $-CH_3$, $-COOH$ and $-OH$ functionalized surfaces. This effectively shows the absolute greater degree to which these proteins can physisorb to an $-NH_2$ terminated monolayer.

The greater degree of adsorption to an $-NH_2$ monolayer may possibly be explained by the electrostatic interactions of the protein and monolayer that arise at pH 7.4. For the proteins investigated here the reported pI values are as follows; human fibrinogen 5.5,⁴⁵ human albumin 5.4 – 5.8, IgG 6.6 – 10.0,⁴⁶ IgA and IgM 4.5 – 6.5.⁴⁷ The pK_a value of a terminal end amine group of an alkyl chain is approximately 10 (taken from the reported pK_a value of the side chain amine group of the lysine amino acid; reported as 10.53). Therefore at a buffer pH of 7.4 the amine surface will be dominated by positive charges from protonated amine functional groups, while the proteins will be dominated by negative charge. This situation can lead to an increase in

electrostatic interaction of the negatively charged proteins to the positively charged surface, resulting in increased binding sensitivity and overall saturation of the amine surface.

The least amount of adsorption monitored was predominately on the $-OH$ terminated thiol surface. This observation is consistent with literature reports of the anti-fouling nature of $-OH$ alkyl thiol SAMs⁴ and is consistent with the observation that electrically neutral hydrophilic surfaces that contain hydrogen bond receptors adsorb the least amount of protein.⁹ IgM and IgA adsorption isotherms exhibited behavior where $-OH$ terminated SAM layer allowed for adsorption greater than or equal to other functionalized SAMs. This situation will be discussed below.

Silin et al.³⁰ looked at hIgG adsorption to $-CH_3$, $-COOH$, $-NH_2$ and $-OH$ surface chemistries individually using thiol SAMs on Au and found adsorption decreased $CH_3 > COOH > NH_2 > OH$ at a single point concentration of 500 nM. These experiments utilized SPR spectroscopy detection and were performed under the same conditions of buffer and pH. While adsorption to NH_2 was weak, this is likely due to the use of 2-aminoethanethiol ($HS(CH_2)_2NH_2$) as the SAM. Thiols with alkyl chains less than 10 carbons long tend to form disordered heterogeneous surfaces with pin hole defects,⁴⁸ presenting a lower density of amine groups. This may ultimately limit the effectiveness of an $-NH_2$ surface to adsorb proteins when compared to a long chain amine SAM. Methyl and carboxyl terminated thiols were 15 carbons long while hydroxyl terminated thiol was 16 carbons long. These similar length SAMs exhibited the same order of hIgG adsorption as determined in this study.

The isotherm of human fibrinogen adsorption to SAMs presenting $-NH_2$, $-COOH$, $-CH_3$ and $-OH$ terminal groups is shown in Figure 3.5. The adsorption of fibrinogen on various surfaces has been studied extensively.⁴⁹⁻⁵¹ The adsorption order for fibrinogen in this study is $-NH_2 > -CH_3 > -COOH > -OH$. This trend is consistent with previous studies.³¹ Although fibrinogen is a large protein with regions of both positive and negative charge, the overall charge of the protein at pH = 7.4 is negative.⁴⁵ As stated previously, the largest amount of adsorption is observed at the $-NH_2$ terminated SAM due to the electrostatic interaction between the protein and surface. Fibrinogen is also known to adsorb very readily to hydrophobic surfaces ($-CH_3$) through its hydrophobic β

sheets.^{49, 52} This adsorption results in a denaturing of the protein and increase in its molecular area as compared to adsorption on hydrophilic surfaces ($-\text{COOH}$) which results in molecular reorientation rather than denaturation.⁵³ Since the hydrophobic interactions of the methyl terminated SAM and fibrinogen are largely irreversible, and the weaker electrostatic interactions between the carboxyl surface and fibrinogen are more reversible, a greater degree of adsorption would be expected after subsequent rinsing steps. This type of preferential adsorption to hydrophobic surfaces compared to hydrophilic surfaces has been reported extensively in the literature.^{33, 49}

The shape of the isotherm for fibrinogen is also unique when compared to the isotherm of the other human plasma proteins. There are two plateau regions for the adsorption to the SAM surfaces. Up to approximately 100 nM concentration of fibrinogen a lower plateau of adsorption is reached. Above 100 nM a clear transition occurs, and a second plateau is reached at approximately 600 nM concentration of fibrinogen. This behavior is observed for all four functionalized surfaces. While fibrinogen has been used as a model protein in a wide variety of studies investigating protein adsorption to various surfaces, these studies have focused on a single concentration analysis for investigation of suitable surface chemistries minimizing adsorption.^{9, 54} Few reports have been published recently examining the adsorption properties of proteins over a wide concentration range. Those reports that do cover adsorption at various concentrations tend to focus on large protein concentration ranges in the mg mL^{-1} range.⁴⁹ However, literature reports of fibrinogen adsorption over wide concentration ranges do exist for studies focusing on the structural nature of fibrinogen upon adsorption to surfaces. These studies have also reported plateau levels of the fibrinogen adsorption isotherm on various surfaces.^{51, 55}

One study by Ward et al.⁵⁵ has described plateau levels found at concentrations of $\sim 4 \text{ mg mL}^{-1}$ for the lower plateau and 8 mg mL^{-1} at the higher plateau. These are 20 to 40 times higher solution concentrations than reported here. These solution concentrations are much higher than is possible to measure with SPR imaging. However, our reported concentration ranges for the lower and higher plateau levels have been described previously by Nygren et al.⁵¹ They investigated the adsorption of fibrinogen, over a similar range as this study, 0.1 – 1000 nM, on hydrophilic SiO_2 and hydrophobic

hexamethyl treated Si surfaces. They reported similar low concentration and high concentration plateaus at ~ 100 nM and ~ 600 nM, respectively. They also reported greater adsorption of fibrinogen to the hydrophobic surface compared to the hydrophilic surface. By using SEM images of the patterned surfaces they concluded that during packing on the surface the proteins undergo a compression. The higher concentration plateau may be explained by the further packing of the molecules on the surface into aggregate structures that have been reported previously.^{45, 56} It has been shown that the structure of fibrinogen adsorbed to surfaces can alter at higher concentrations to supramolecular structures of large aggregates having various shapes and sizes greater than $1 \mu\text{m}$.⁵⁷

As has been shown in previous studies, examining the adsorption of fibrinogen over a wide concentration range rather than single concentration points, can lead to interesting findings about the behavior of protein adsorption onto surfaces. Here the plateau nature of the isotherm may be attributed to the supramolecular structures of the adsorbed fibrinogen layer. As mentioned, other studies have examined the adsorption of fibrinogen at much higher concentrations and noticed similar behavior. It may be that there exist multiple concentrations for fibrinogen at which various states of aggregate packing can occur.

Human serum albumin isotherm, Figure 3.4, shows an adsorption affinity to the different SAM surfaces in the following order, $-\text{NH}_2 > -\text{COOH} > -\text{CH}_3 > -\text{OH}$. HSA has a net negative charge of -10 at pH 7.4. This leads to a strong affinity for the positive charge of the protonated amine surface at pH 7.4. In contrast, as mentioned above, hydrophilic surfaces such as OH are associated with low levels of albumin adsorption. Despite the hydrophilicity and negative charge at pH 7.4 the $-\text{COOH}$ terminated SAM surface exhibits the second highest affinity for HSA adsorption. Tidwell et al.²⁴ observed the same adsorption behavior on similar surfaces for bovine serum albumin (BSA). However, Silin et al.³⁰ reported albumin adsorption in the order of $-\text{CH}_3 > -\text{COOH} > -\text{OH}$ terminated surfaces. They explain the adsorption of BSA to the hydrophobic surface as following the expected trend for hydrophobic surfaces. Hydrophobic surfaces are also usually associated with changes in albumin conformation during adsorption,⁵⁸ leading to denaturation of the protein. Dent et al.⁵⁹ have described the adsorption process of

albumin on hydrophobic surfaces as being a multistep process initiated by hydrophobic interactions of the surface and protein, followed by multipoint interactions due to the protein denaturation. This type of mechanism may ultimately limit the total amount of protein capable of binding to the surface.

Albumin can however, also bind to negatively charged surfaces ($-\text{COOH}$), via cationic counter ions acting as an electrostatic bridge⁵⁹ between the negative charged albumin and carboxyl surface. Since on hydrophilic surfaces adsorbed proteins can maintain their native structure³⁰ the adsorption to the surface can potentially be highly oriented, retaining its native form. Upon adsorption denaturation will be minimized because of the few points of attachment resulting in a greater total amount of protein binding to the surface.

To the author's knowledge, the adsorption isotherm of IgA and IgM (Figure 3.4) to various SAM surfaces are the first reported. Both IgA and IgM exhibit the greatest adsorption affinity and sensitivity to the $-\text{NH}_2$ terminated SAM surface. As stated previously this results from the electrostatic interaction of the net negative charge on IgA and IgM with the positive charge of the protonated amine terminated SAM surface at pH 7.4. Aside from sharing a similar strong affinity for the amine terminated surface, the surface adsorption pattern is quite different between the two immunoglobulins.

IgA shows an overall adsorption decreasing in the order $-\text{NH}_2 > -\text{COOH} > -\text{OH} > -\text{CH}_3$. It should be noticed that at low concentrations the differences between the adsorption on the $-\text{COOH}$, $-\text{OH}$ and $-\text{CH}_3$ surfaces are minor, with differences in adsorption increasing at higher concentrations. IgM exhibits an overall adsorption affinity decreasing in the order $-\text{NH}_2 > -\text{CH}_3 > -\text{COOH} \approx -\text{OH}$. Both immunoglobulins have reported pI values of 4.5-6.5⁴⁷ therefore they possess net negative charge at the experimental pH of 7.4. As was observed for all other plasma proteins investigated in this study, the strong affinity towards the amine terminated surface can be explained by the electrostatic interaction between the negatively charged protein and positively charged protonated amine surface.

Surface protein adsorption can be caused by electrostatic, van der Waals forces, hydrophobic and Lewis acid-base interactions. Also, portions of the protein structure are amphiphatic and consequently exhibit pronounced surface activity. Thus, it is important

to examine the structural nature of IgA and IgM when considering the nature of their adsorption affinities to various surfaces.

IgA is considered the most heterogeneous immunoglobulin possessing two isotypes, serum IgA and secretory IgA (S-IgA).^{60, 61} Serum IgA is mainly present (>80%) in the monomeric form with a 6 – 10% carbohydrate composition. The remaining IgA in serum and all S-IgA are mainly found in the dimeric form, with monomers connected by disulphide bonds and linked by an additional polypeptide called a J chain. The J chain has a molecular weight of ~ 16 kDa and its composition is 8% carbohydrates. The J chain is also present in IgM, which mainly exists in the pentameric form, and plays a role in the polymerization of the IgA and IgM isotypes.⁶² S-IgA also contains an additional unit over serum IgA, called the secretory component (SC). It is a highly glycosylated (22%) glycoprotein with molecular mass of ~ 70 kDa. Its function is to aid in the transport of the IgA protein through epithelial cells. For this study S-IgA was used from human colostrums (Sigma Aldrich #I1010).

The glycan moiety of IgA has been studied in detail.^{62, 63} It has been reported that there is considerable O- and N-glycosylation of the IgA protein. Interestingly, unlike the corresponding N-linked glycans in the IgG protein, which is confined to the space between the two heavy chains, the glycan units of IgA are directed away from the protein backbone and are highly sialylated.⁶³ With this configuration, the glycans are thought to confer a greater degree of hydrophilicity and net negative charge to the IgA molecule. Considering specifically S-IgA, the total carbohydrate content is considerably higher than that of serum IgA because both J chain and SC are rich in carbohydrates. It has also been reported that both the J chain and SC are sialylated.^{64, 65} This adds significantly to the hydrophilicity and negative charge of S-IgA.

The increased sialylated glycosylation of the J chain and SC help explain the low pI value, and net negative charge, of IgA and IgM. As stated previously this accounts for the selective affinity towards the positively charged amine surface at pH 7.4. The increased hydrophilicity resulting from the greater degree of glycosylation can reasonably explain the reduced affinity of IgA towards the hydrophobic -CH₃ terminated SAM surface compared to the increased binding to the hydrophilic -OH and -COOH terminated SAM surfaces. With increased surface hydrophilicity from the glycosylation

of the IgA J chain and SC, hydrogen bonding and dipole binding would dominate over hydrophobic surface interactions.

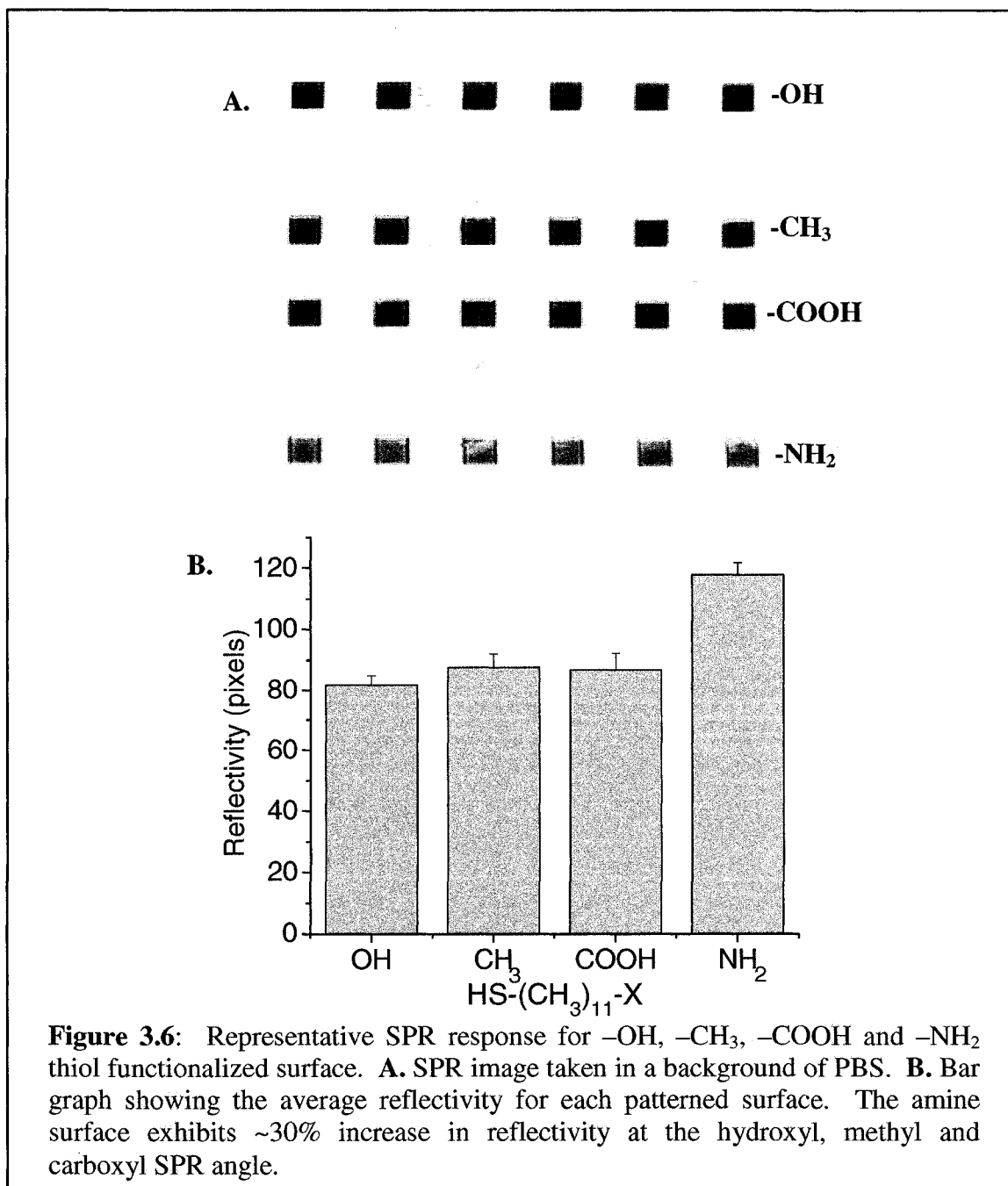
Unlike S-IgA, IgM is a pentameric protein only containing the J chain which aids in the polymerization of the polymeric molecule. This pentameric structure adds increased size and hydrophilicity to IgM potentially causing greater interaction of the hydrophobic residues with the $-CH_3$ terminated surface, thus leading to increased binding. Due to the increased hydrophilicity of the IgM structure the adsorption towards the polar $-COOH$ and $-OH$ terminated SAM surfaces is comparable.

3.3.2 THIOL REFRACTIVE INDEX CHANGES

SPR is a surface optical technique sensitive to changes in refractive index caused by surface binding events. In SPR imaging these changes in refractive index are measured between an initial state and a final experimental state due to surface binding. To achieve the largest linear range of response the initial baseline signal is set to the SPR angle, where reflectivity of the surface is minimal. By maintaining the angle constant during binding, reflectivity increases allowing for the determination of signal change from the initial to final state. For multi component analysis it is important to achieve a consistent baseline signal for each component, to ensure an equal dynamic signal range for each surface type being monitored.

To the author's knowledge these are the first studies to simultaneously observe binding events to $-NH_2$, $-OH$, $-COOH$, $-CH_3$ functionalized alkyl thiol SAM surfaces using SPR. While work has been done observing binding to these, or similar, surfaces, reports have focused on discrete experiments for each surface. Our experiments resulted in a direct comparison of not only the binding to these surfaces, but of the SAM surfaces themselves.

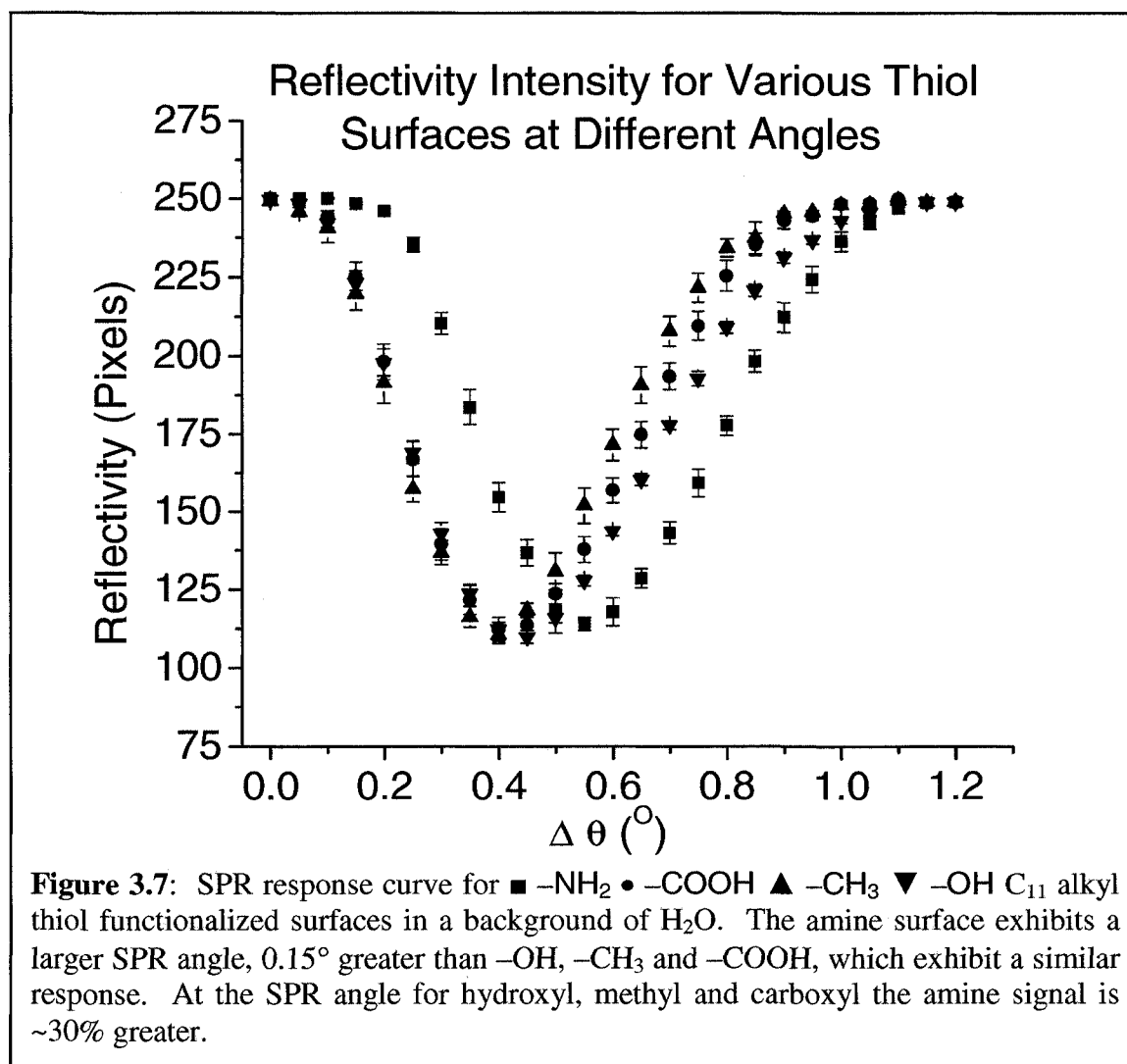
In examining the adsorption of proteins to various functionalized alkyl chain thiols it was consistently observed that the baseline signal for the various SAMs, prior to protein adsorption, was higher for the amine functionalized surface than $-CH_3$, $-COOH$, or $-OH$. Figure 3.6 shows the different SPR responses between the $-NH_2$ and $-CH_3$, $-COOH$, $-OH$ functionalized thiol SAMs in a background of phosphate buffer.



As shown in Figure 3.4 $-\text{NH}_2$ terminated alkyl thiols are the most sensitive to surface protein adsorption compared to $-\text{CH}_3$, $-\text{COOH}$ and $-\text{OH}$ SAMs. It was first considered that ambient adsorption to the amine surface during surface preparation may account for the angle differences as organic contaminants may have preferentially adsorbed to the more sensitive amine surface. To test this SAMs of $-\text{CH}_3$, $-\text{COOH}$ and $-\text{OH}$ were first formed on an SPR slide. The slide was mounted into the SPR flow cell

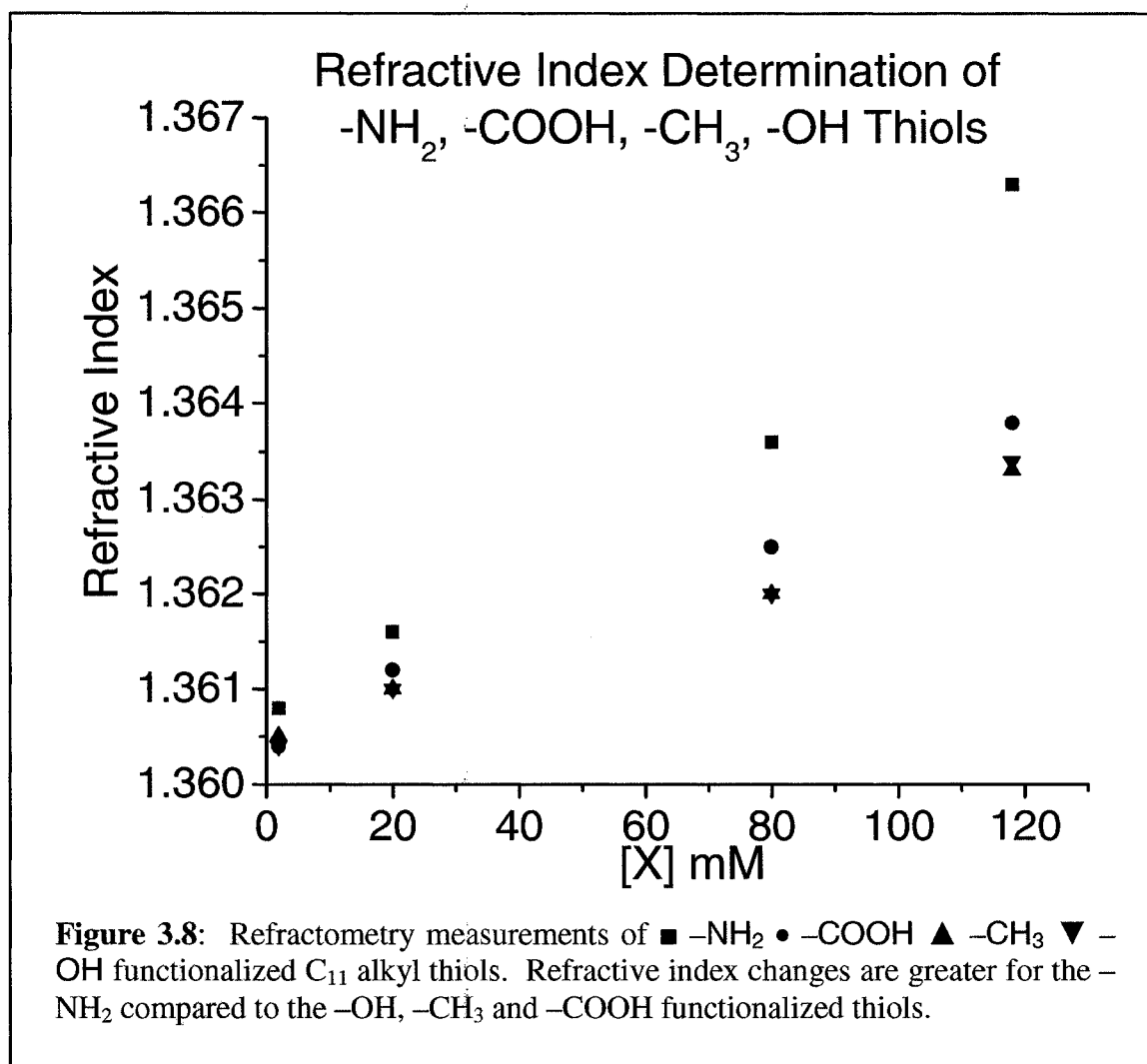
and amine thiol was introduced. After an incubation time of 2 hours the amine thiol was rinsed with ethanol, then water and finally PBS. This procedure would limit the exposure of the amine SAM to ambient conditions. This experimental procedure resulted in similar responses as shown in Figure 3.6. The patterned amine thiol consistently exhibited greater reflectivity, larger SPR angle, even with limited exposure to ambient laboratory conditions when compared to the $-\text{CH}_3$, $-\text{COOH}$ and $-\text{OH}$ surfaces.

By measuring the intensities of each line of patterned SAMs at various angles a characteristic SPR curve can be constructed.⁴⁰ The SPR angle is determined at the point of minimum reflectivity, and is an intrinsic property of the surface sample. Figure 3.7 is the reflectivity response at varying angles for patterned $-\text{NH}_2$, $-\text{CH}_3$, $-\text{COOH}$ and $-\text{OH}$ SAMs.



As the angle is adjusted the reflectivity of the patterned spots decreases until the SPR angle is reached. As the angle is adjusted past the SPR angle the reflectivity increases again. For the $-\text{CH}_3$, $-\text{COOH}$ and $-\text{OH}$ functionalized thiols the SPR curves are similar resulting in similar SPR angles. The $-\text{NH}_2$ functionalized thiol curve is shifted to the right and has a SPR angle $\sim 0.15^\circ$ greater than $-\text{CH}_3$, $-\text{COOH}$ and $-\text{OH}$ thiols. Therefore, when the angle is set to the minimum reflectivity of $-\text{CH}_3$, $-\text{COOH}$ and $-\text{OH}$ thiols the $-\text{NH}_2$ thiol reflectivity is greater due to its greater SPR angle. This situation of differing SPR angles among the $-\text{NH}_2$ and $-\text{CH}_3$, $-\text{COOH}$, and $-\text{OH}$ thiols results in the response observed in Figure 3.6.

The thiols used throughout this study are C_{11} alkyl thiols whose only differences are the functional end groups. For the four thiols studied, only 1-dodecanethiol ($-\text{CH}_3$) refractive index is known, $n^{20} = 1.458$. Due to the similar SPR curves of the $-\text{COOH}$ and $-\text{OH}$ thiols they must possess similar refractive indexes. To compare the affect that the various end groups have on refractive index a refractometer was used to measure each thiol's refractive index at increasing thiol concentration. Figure 3.8 is a graph of refractive index at various concentrations of $-\text{NH}_2$, $-\text{COOH}$, $-\text{CH}_3$ and $-\text{OH}$ thiols.



Each thiol was dissolved in 100% anhydrous ethanol to the appropriate concentration. Amine, carboxyl and hydroxyl thiols are solids while methyl thiol is a liquid. To eliminate potential interferences from un-dissolved solids, each concentration solution was centrifuged and filtered through a 0.2 μm filter. The refractive index response determined from refractometry shows that the amine terminated alkyl thiol diverges greatly from the refractive index response of -COOH, -CH₃ and -OH at increasing concentration. While refractometry measures the concentration dependence of refractive index of a liquid thiol and SPR measures the difference in reflectivity caused by refractive index on a surfaced immobilized SAM, both methods illustrate the affect that the -NH₂ functionalized end group has on refractive index compared to -CH₃, -COOH and -OH thiols. This type of observation was only elucidated because of the

ability to simultaneously pattern different functionalized alkyl thiols through microfluidic device developed through this study.

3.4 CONCLUSIONS

Investigated in this study is the non-specific binding of the human plasma proteins, IgG, IgA, IgM, fibrinogen and albumin to four model self assembled alkyl thiol monolayers with the following functional groups; $-\text{NH}_2$, $-\text{COOH}$, $-\text{CH}_3$ and $-\text{OH}$, representing polar, nonpolar and neutral groups. While many studies have investigated the binding of proteins at single concentrations, here isotherm binding curves were determined for each protein investigated. This allowed for the determination of the binding behavior of the investigated proteins over a range of concentrations. The isotherm binding curves were successfully constructed utilizing the SPR imaging technique and could be used to determine the relative binding strength of proteins on various surfaces.

By using a proof of concept PDMS microfluidic device and Au patterned substrate surface, various model alkanethiolates in organic solvent were immobilized on the surface of an SPR sensor. When coupled with the multi component detection system of an SPR imaging instrument, these patterned surfaces allowed for the simultaneous investigation of the binding behavior of various human proteins. This simultaneous detection of binding to various model surfaces increases throughput, provides for standardized and reproducible experimental conditions, and allows for easier unambiguous comparison of binding results.

From the binding curves constructed the $-\text{NH}_2$ surface exhibited the greatest sensitivity and degree of saturation for all proteins investigated. This is attributed to the electrostatic interaction of the positively charged amine surface to the negatively charged proteins at the investigated pH of 7.4. The fibrinogen isotherm confirms previous reports of various regimes of surface binding at low solution concentrations and further supports the proposition of supramolecular fibrinogen structures. Binding isotherms of IgA and IgM were also constructed, and are thought to be the first reports of binding to functionalized alkane thiols. They exhibited binding behavior markedly different

compared to other proteins investigated, and this was associated with their oligomeric structures resulting in greater hydrophilicity.

Also, due to the ability to monitor the simultaneous binding to various surfaces under the same experimental conditions, differences in the properties of the thiols used were noticed. Specifically, the $-NH_2$ terminated thiol exhibited a greater refractive index compared to the $-COOH$, $-CH_3$ and $-OH$ terminated thiols. This was confirmed by refractometry and SPR sensitivity curves. Since the only difference between the structures of the various thiols used was the end functional groups, the difference of refractive index is thought to result from the $-NH_2$ group.

3.5 REFERENCES

- (1) Andrade, J. D.; Hlady, V. *Advances in Polymer Science* **1986**, *79*, 1-63.
- (2) Deligianni, D. D.; Katsala, N.; Ladas, S.; Sotiropoulou, D.; Amedee, J.; Missirlis, Y. F. *Biomaterials* **2001**, *22*, 1241-1251.
- (3) Denis, F. A.; Hanarp, P.; Sutherland, D. S.; Gold, J.; Mustin, C.; Rouxhet, P. G.; Dufrene, Y. F. *Langmuir* **2002**, *18*, 819-828.
- (4) Prime, K. L.; Whitesides, G. M. *Science* **1991**, *252*, 1164-1167.
- (5) Shen, M. C.; Horbett, T. A. *Journal of Biomedical Materials Research* **2001**, *57*, 336-345.
- (6) Tengvall, P.; Lundstrom, I.; Liedberg, B. *Biomaterials* **1998**, *19*, 407-422.
- (7) Michael, K. E.; Vernekar, V. N.; Keselowsky, B. G.; Meredith, J. C.; Latour, R. A.; Garcia, A. J. *Langmuir* **2003**, *19*, 8033-8040.
- (8) Frutos, A. G.; Brockman, J. M.; Corn, R. M. *Langmuir* **2000**, *16*, 2192-2197.
- (9) Holmlin, R. E.; Chen, X. X.; Chapman, R. G.; Takayama, S.; Whitesides, G. M. *Langmuir* **2001**, *17*, 2841-2850.
- (10) Sigal, G. B.; Bamdad, C.; Barberis, A.; Strominger, J.; Whitesides, G. M. *Analytical Chemistry* **1996**, *68*, 490-497.
- (11) Lahiri, J.; Isaacs, L.; Tien, J.; Whitesides, G. M. *Analytical Chemistry* **1999**, *71*, 777-790.

- (12) Martins, M. C. L.; Fonseca, C.; Barbosa, M. A.; Ratner, B. D. *Biomaterials* **2003**, *24*, 3697-3706.
- (13) Bain, C. D.; Troughton, E. B.; Tao, Y. T.; Evall, J.; Whitesides, G. M.; Nuzzo, R. G. *Journal of the American Chemical Society* **1989**, *111*, 321-335.
- (14) Ulman, A. *Chemical Reviews* **1996**, *96*, 1533-1554.
- (15) Ostuni, E.; Yan, L.; Whitesides, G. M. *Colloids and Surfaces B-Biointerfaces* **1999**, *15*, 3-30.
- (16) McClary, K. B.; Ugarova, T.; Grainger, D. W. *Journal of Biomedical Materials Research* **2000**, *50*, 428-439.
- (17) Scotchford, C. A.; Gilmore, C. P.; Cooper, E.; Leggett, G. J.; Downes, S. *Journal of Biomedical Materials Research* **2002**, *59*, 84-99.
- (18) Hlady, V.; Andrade, J. D. *Colloids and Surfaces* **1988**, *32*, 359-369.
- (19) Shen, D.; Huang, M.; Chow, L.-M.; Yang, M. *Sensors and Actuators B: Chemical* **2001**, *77*, 664-670.
- (20) Taborelli, M.; Eng, L.; Descouts, P.; Ranieri, J. P.; Bellamkonda, R.; Aebischer, P. *Journal of Biomedical Materials Research* **1995**, *29*, 707-714.
- (21) Wadu-Mesthrige, K.; Amro, N. A.; Liu, G. Y. *Scanning* **2000**, *22*, 380-388.
- (22) Takahara, A.; Hara, Y.; Kojio, K.; Kajiyama, T. *Colloids and Surfaces B-Biointerfaces* **2002**, *23*, 141-152.
- (23) Margel, S.; Vogler, E. A.; Firment, L.; Watt, T.; Haynie, S.; Sogah, D. Y. *Journal of Biomedical Materials Research* **1993**, *27*, 1463-1476.
- (24) Tidwell, C. D.; Ertel, S. I.; Ratner, B. D.; Tarasevich, B. J.; Atre, S.; Allara, D. L. *Langmuir* **1997**, *13*, 3404-3413.
- (25) Kyo, M.; Usui-Aoki, K.; Koga, H. *Analytical Chemistry* **2005**, *77*, 7115-7121.
- (26) Singh, B. K.; Hillier, A. C. *Analytical Chemistry* **2006**, *78*, 2009-2018.
- (27) Dutra, R. F.; Kubota, L. T. *Clinica Chimica Acta* **2007**, *376*, 114-120.
- (28) Dong, Y.; Wilkop, T.; Xu, D. K.; Wang, Z. Z.; Cheng, Q. *Analytical and Bioanalytical Chemistry* **2008**, *390*, 1575-1583.

- (29) Sigal, G. B.; Mrksich, M.; Whitesides, G. M. *Journal of the American Chemical Society* **1998**, *120*, 3464-3473.
- (30) Silin, V.; Weetall, H.; Vanderah, D. J. *Journal of Colloid and Interface Science* **1997**, *185*, 94-103.
- (31) Evans-Nguyen, K. M.; Tolles, L. R.; Gorkun, O. V.; Lord, S. T.; Schoenfish, M. H. *Biochemistry* **2005**, *44*, 15561-15568.
- (32) Sjoelander, S.; Urbaniczky, C. *Anal. Chem.* **1991**, *63*, 2338-2345.
- (33) Evans-Nguyen, K. M.; Schoenfish, M. H. *Langmuir* **2005**, *21*, 1691-1694.
- (34) Kanda, V.; Kariuki, J. K.; Harrison, D. J.; McDermott, M. T. *Analytical Chemistry* **2004**, *76*, 7257-7262.
- (35) Wegner, G. J.; Lee, N. J.; Marriott, G.; Corn, R. M. *Analytical Chemistry* **2003**, *75*, 4740-4746.
- (36) Mrksich, M.; Sigal, G. B.; Whitesides, G. M. *Langmuir* **1995**, *11*, 4383-4385.
- (37) Chapman, R. G.; Ostuni, E.; Yan, L.; Whitesides, G. M. *Langmuir* **2000**, *16*, 6927-6936.
- (38) Krishnan, A.; Cha, P.; Liu, Y. H.; Allara, D.; Vogler, E. A. *Biomaterials* **2006**, *27*, 3187-3194.
- (39) Krishnan, A.; Siedlecki, C. A.; Vogler, E. A. *Langmuir* **2004**, *20*, 5071-5078.
- (40) Brockman, J. M.; Nelson, B. P.; Corn, R. M. *Annual Review of Physical Chemistry* **2000**, *51*, 41-63.
- (41) Knoll, W. *Annual Review of Physical Chemistry* **1998**, *49*, 569-638.
- (42) Chen, S. F.; Liu, L. Y.; Zhou, J.; Jiang, S. Y. *Langmuir* **2003**, *19*, 2859-2864.
- (43) Jenney, C. R.; Anderson, J. M. *Journal of Biomedical Materials Research* **2000**, *50*, 281-290.
- (44) Kusnezow, W.; Hoheisel, J. D. *Journal of Molecular Recognition* **2003**, *16*, 165-176.
- (45) Lin, Y.; Wang, J.; Wan, L. J.; Fang, X. H. *Ultramicroscopy* **2005**, *105*, 129-136.
- (46) Jin, Y.; Luo, G. A.; Oka, T.; Manabe, T. *Electrophoresis* **2002**, *23*, 3385-3391.

- (47) Francesca Chiodi, Å. S. E. Ö. *Electrophoresis* **1985**, 6, 124-128.
- (48) Porter, M. D.; Bright, T. B.; Allara, D. L.; Chidsey, C. E. D. *Journal of the American Chemical Society* **1987**, 109, 3559-3568.
- (49) Tunc, S.; Maitz, M. F.; Steiner, G.; Vazquez, L.; Pham, M. T.; Salzer, R. *Colloids and Surfaces B-Biointerfaces* **2005**, 42, 219-225.
- (50) Cacciafesta, P.; Humphris, A. D. L.; Jandt, K. D.; Miles, M. J. *Langmuir* **2000**, 16, 8167-8175.
- (51) Nygren, H.; Stenberg, M. *Journal of Biomedical Materials Research* **1988**, 22, 1-11.
- (52) Lu, D. R.; Park, K. *Journal of Colloid and Interface Science* **1991**, 144, 271-281.
- (53) Feng, L.; Andrade, J. D. *Journal of Biomedical Materials Research* **1994**, 28, 735-743.
- (54) Chapman, R. G.; Ostuni, E.; Takayama, S.; Holmlin, R. E.; Yan, L.; Whitesides, G. M. *Journal of the American Chemical Society* **2000**, 122, 8303-8304.
- (55) Ward, C. A.; Stanga, D. *Journal of Colloid and Interface Science* **1986**, 114, 323-329.
- (56) Brynda, E.; Houska, M.; Lednický, F. *Journal of Colloid and Interface Science* **1986**, 113, 164-171.
- (57) Eberhart, R. C.; Prokop, L. D.; Wissenger, J.; Wilkov, M. A. *Transactions American Society for Artificial Internal Organs* **1977**, 23, 134-140.
- (58) Norde, W.; Giacomelli, C. E. *Journal of Biotechnology* **2000**, 79, 259-268.
- (59) Dent AH; M., A. *Bioconjugation, protein coupling techniques for the biomedical sciences*; Macmillan: London, 1998.
- (60) Hanson, L. A. *International Archives of Allergy and Applied Immunology* **1961**, 18, 241-&.
- (61) Tomasi, T. B.; Tan, E. M.; Solomon, A.; Prendergast, R. *Journal of Experimental Medicine* **1965**, 121, 101-&.
- (62) Mestecky, J.; Moro, I.; Underdown, B. J. In *Mucosal Immunology*; Ogra, P. L., Ed.; Academic Press, 1999, pp 133-552.

- (63) Mattu, T. S.; Pleass, R. J.; Willis, A. C.; Kilian, M.; Wormald, M. R.; Lellouch, A. C.; Rudd, P. M.; Woof, J. M.; Dwek, R. A. *Journal of Biological Chemistry* **1998**, *273*, 2260-2272.
- (64) Niederme.W; Mestecky, J.; Tomana, M. *Biochimica Et Biophysica Acta* **1972**, *257*, 527-&.
- (65) Mizoguchi, A.; Mizuochi, T.; Kobata, A. *Journal of Biological Chemistry* **1982**, *257*, 9612-9621.

CHAPTER 4

MICROFLUIDIC DEVICES FOR PROTEIN MICROARRAYS

4.1 INTRODUCTION	114
4.2 EXPERIMENTAL	116
4.2.1 REAGENTS AND SOLUTION	117
4.2.2 CHIP DESIGN AND FABRICATION.....	118
4.2.3 SPR IMAGING	119
4.2.4 PROCEDURES	122
4.3 RESULTS	124
4.4 IgE ASSAY DEVELOPMENT	139
4.5 CONCLUSIONS.....	144
4.5 REFERENCES	145

4.1 INTRODUCTION

Protein microarrays have the potential to become even more useful in clinical diagnostics than DNA arrays. In recent years, considerable effort has been directed at research for the development of rapid and convenient methods for the fabrication of protein microarrays. Much of this work in the development of protein microarrays has focused on the transfer of technologies and techniques from DNA microarrays, however, a number of barriers remain along the road to successful development. Detection by fluorescence is much less convenient than for DNA, due to the challenges of protein labeling leading to multiple labels and the potential of those labels interfering with binding sites. Non-specific adsorption of proteins is much more significant than for DNA, due to the aliphatic nature of proteins. Also, the complexity of immobilizing proteins in a preferred orientation and conformation can be challenging compared to homogeneous DNA molecules and their associated immobilization techniques. These difficulties along with the demands for high throughput and massively parallel analyses for proteomics, have lead to a variety of fabrication and reading methods of protein microarrays.¹⁻³

The most common and extensively used format to perform binding assays for diagnostic purposes is the enzyme linked immunosorbent assay (ELISA). This method involves the coating of plastic wells with ligands and then blocking the wells with bovine serum albumin (BSA) to prevent non-specific adsorption in subsequent steps. Typically, the volumes used for each rinse and exposure step of ligand or analyte are ~ 100 μ L and requires 1 hour to overnight incubation times. The binding between the ligand and analyte is detected by either fluorescence labeled or enzyme conjugated antibodies. Delamarche et al.⁴ examined the use of microfluidic devices as an alternative format for immunoassays. By creating rows of microfluidic channels cast in polydimethylsiloxane and bonding the polydimethylsiloxane to a glass slide they were able to pattern ligands through microfabricated channels. These patterned surfaces could then be exposed to analyte solutions through another set of polydimethylsiloxane channels. Using fluorescence detection, they showed the advantages for using microfluidics to consume nanoliter quantities of potentially precious reagents and decrease incubation times. This methodology of patterning and fabricating protein microarrays has been successfully used

by others.^{5, 6} However, limits exist to the number of usable channels for patterning and detection that can be fabricated on one device, as well as being limited in the number of binding events detected per exposure. These drawbacks exist as potential hurdles to the widespread application of this technique.

In the area of biosensor technology a label free technique, surface plasmon resonance (SPR) imaging has been found to be compatible for immunodiagnostic and other protein assays.⁷⁻⁹ By immobilizing one component of a bio-specific pair to Au coated glass slides, detection of its counterpart can be monitored in real time by changes in optical properties that occur during binding. This results in a label free method of detecting spatially resolved binding events on a 2 dimensional surface. This has made SPR imaging a very attractive alternative for the detection of the protein and biomolecular arrays. Improving the contrast and precision of SPR imaging read protein microarrays, and developing convenient fabrication methods for protein microarrays are two of the challenges of this methodology addressed in this work.

A widely used method for microarray fabrication is robotic pin printing which can allow for increased surface density of ligands and throughput.^{3, 10-12} These advantages are complementary with the use of SPR imaging. Corn et al.¹³ have shown the potential in using pin printing with SPR imaging. However, drawbacks include the relative expense of pin printing systems, the surface evaporation of printed small volume droplets and the difficulty in printing organic solutions. The use of microfluidics for immobilization onto discrete regions can potentially overcome drawbacks associated with pin printing. Microfluidics can provide an environment of low surface area to volume ratio per channel, thus limiting evaporation, while simultaneously allowing immobilization to occur in the bulk solution. Channels can be formed which allow for the manipulation of solution streams to discrete areas localizing immobilization of ligands to specific areas.

To expand on the work of miniaturized bio-diagnostics for small laboratories and point of care instrumentation, we have investigated the use of microfluidics with label free SPR imaging detection. The method explored here employs polydimethylsiloxane microfluidic networks for both the immobilization of discrete spots of proteins and as a flow cell for multicomponent analysis of surface binding events. The label free binding

of the fabricated protein arrays was monitored by SPR imaging. Since SPR is a nonspecific detection method, discrete detection elements were fabricated by Au patterning. Thus, signal is only observed at these sensing regions. This limits the number of surface treatments required for blocking, since non-patterned Au regions produce no signal. Demonstrated here is the use of microfluidic networks and SPR imaging for the facile fabrication of antigen arrays capable of yielding qualitative and quantitative binding information. Methods outlined in this work can be applied to various other types of proteomic and genomic arrays. As an example, initial work is presented on the development of IgE immunoassay arrays using SPR detection for allergy testing.

Current methods of testing for allergy sensitivities include the skin prick method and radioallergosorbent test (RAST). These methods are used for testing of low levels of specific IgE, since radiological assay tests are extremely sensitive and skin prick tests assess patients inherent allergy sensitivity.

The skin prick is performed by pricking the skin of a patient with a needle tip containing small amounts of allergen and observing that local area's physiological response. The severity of the response is associated with a standardized scale and interpreted by the tester. While inexpensive and fast it suffers from interpretation errors of the tester and the possibility of severe side effects such as anaphylactic shock in patients with unknown sensitivities.

Due to the high sensitivities of radiologic labels, RAST is used for specific quantification of IgE levels in atopic patients. While suitable for determining low levels of IgE, radiological labels possess short shelf lives and require special equipment and handling. With these considerations, work was initiated in assessing the applicability of using label free SPR detection for IgE determination in human plasma.

4.2 EXPERIMENTAL

Arrays were imaged using GWC Instruments SPRImager II (GWC Instruments; Madison, WI) and has been described in detail elsewhere.¹⁴ The array sensor was constructed from the thermal evaporation of a 45 nm gold (Au) film deposited on SF-10 glass (Schott; Toronto, ON, Canada) with a 1 nm adhesive chromium layer through

polydimethylsiloxane shadow mask, as described in Chapter 2.2.2.2. Alignment to a PDMS microfluidic manifold was achieved through the use of a homebuilt alignment microscope, described in Chapter 2.2.4. Upon activation of the Au sensor regions two methods of mounting the sensor to the SPRImager II were employed, depending on the experimental setup: 1. the sensor was mounted within a two port (inlet and outlet) flow cell to which solutions were introduced to the entire surface via a peristaltic pump. 2. the sensor bound to the polydimethylsiloxane microfluidic manifold was mounted directly into the SPRImager II holder, thus using the microfluidic channels as the flow cell. In both methods the sensor surface would be incubated with running buffer for the determination of the SPR angle. A reference image was taken in the running buffer from the averaging of 30 individual images. Difference images were determined by subtracting the image taken after a binding event from the reference image taken prior to the binding event. Since the SPR angle was maintained, any differences between the images, as a result of binding from the incubation solution, appear as illuminated areas of higher reflectivity.

4.2.1 REAGENTS AND SOLUTIONS

All proteins used were purchased in the highest available purity from Sigma Aldrich and used as received. IgE was purchased from Athens Research (Athens, GA). Lyophilized proteins (human IgG, sheep IgG and BSA) were dissolved in HEPES buffered saline (HBS; 10 mM HEPES, 150 mM NaCl) pH = 7.4 from which they were aliquoted to their appropriate concentrations determined from the measured weight and accurate molecular mass. HBS buffer was prepared as a stock solution from 4-(2-hydroxyethyl)piperazine-1-ethanesulfonic acid $\geq 99.5\%$ (Sigma Aldrich) using ultra pure, 0.2 μm filtered Milli Q de-ionized water and refrigerated until needed. Working buffer was prepared by 10x dilution with ultra pure water as needed. Concentrations for liquid anti serum proteins were determined by the dilution, with HBS, of the received commercial antisera.

11-mercaptoundecanoic acid, 1-ethyl-3-[3-dimethylaminopropyl]carbodiimide hydrochloride (EDC) and N-hydroxysuccinimide (NHS) were all purchased from Sigma Aldrich and stored in a freezer between use. 11-mercaptoundecanoic acid was prepared

as 100 mM stock solutions using anhydrous ethanol and stored in a freezer at -4°C . Working solutions of 5 mM were prepared as needed by dilution of the stock solution with anhydrous ethanol. EDC/NHS were prepared as fresh solutions prior to their use. Solutions were formed by dissolving the solids in 0.2 μm filtered ultra pure Milli Q de-ionized water. Polydimethylsiloxane (PDMS) was purchased from Dow Corning under the formulation Sylgard 184. It is packaged in a two component kit with an elastomer and a hardener to be mixed in the ratio of 10:1, respectively.

4.2.2 CHIP DESIGN AND FABRICATION

Two chip designs (discussed previously in Chapter 2) were used during this study; the 20 spot and 4 channel microfluidic arrays. Their design and fabrication was detailed in Chapter 2.4. Briefly, the Au patterned sensor regions for both the spotting and channel devices were formed on pre-cut 1.8 x 1.8 cm SF-10 glass using a thin membrane of PDMS as the shadow mask layer during metal deposition. Deposition of 45 nm of Au on a 1 nm Cr adhesion layer was carried out using a thermal evaporator (Torr International Inc., NY, USA) operating at a pressure of 10^{-7} torr. Upon metal patterning of the substrate glass the PDMS shadow masks were removed and the sensors stored in a vacuum desiccator until needed. When needed the Au patterned glass substrates were removed from the desiccator and washed with ultra pure 0.2 μm filtered Milli Q water, $\text{N}_{2(\text{g})}$ dried, washed with 100% anhydrous ethanol, N_2 dried and placed in a ozone cleaner for 10 mins.

PDMS fabrication of the microfluidic devices used during this study follow the description given in Chapter 2.2.2. Briefly, PDMS devices were formed from the thermal curing of a 10:1, elastomer to hardner, mixture of PDMS over a positive relief photoresist master. The photoresist master was formed on a Si wafer as previously described in Chapter 2.2.1. Upon curing of the PDMS a scalpel was used to cut the microfluidic devices from the bulk material. Each device was cut to a size of 1.8 x 1.8 cm matching the dimensions of the SPR glass sensor substrate. Access holes were formed by using a 16 gauge needle whose tip had been flattened and sharpened in a lathe, resulting in inlet and outlet reservoirs of approximately 1 mm diameter. Organic extraction with refluxed

hexane was performed on each cured device using a Soxhlet setup to eliminate uncured low molecular weight monomers.

Assembly of the microfluidic spotting and channel arrays was achieved through the use of a homebuilt alignment microscope, described previously in Chapter 2.2.4. Briefly, the SPR sensor substrate is mounted on a translation stage capable of moving in the x, y, z and θ directions. The PDMS manifold is held stationary above the substrate. A single objective microscope is used to position the SPR sensor substrate relative to the PDMS manifold. Upon alignment the glass sensor substrate is raised in the z direction for reversible or irreversible bonding to the PDMS. Reversible bonding is achieved through the native conformal contact between PDMS and glass. Irreversible bonding is achieved through plasma oxidation of the PDMS manifold prior to contact with the SPR glass sensor.

4.2.3 SPR IMAGING

Surface plasmon resonance imaging is an optical technique that can monitor differences in reflectivity of incident light from changes in refractive index due to adsorption to a noble metal thin film, silver or Au. In this study a SPRImager II (GWC Instruments; Madison, WI) is employed for all SPR imaging measurements. It is shown schematically in Figure 4.1 and has been described extensively previously.¹⁵

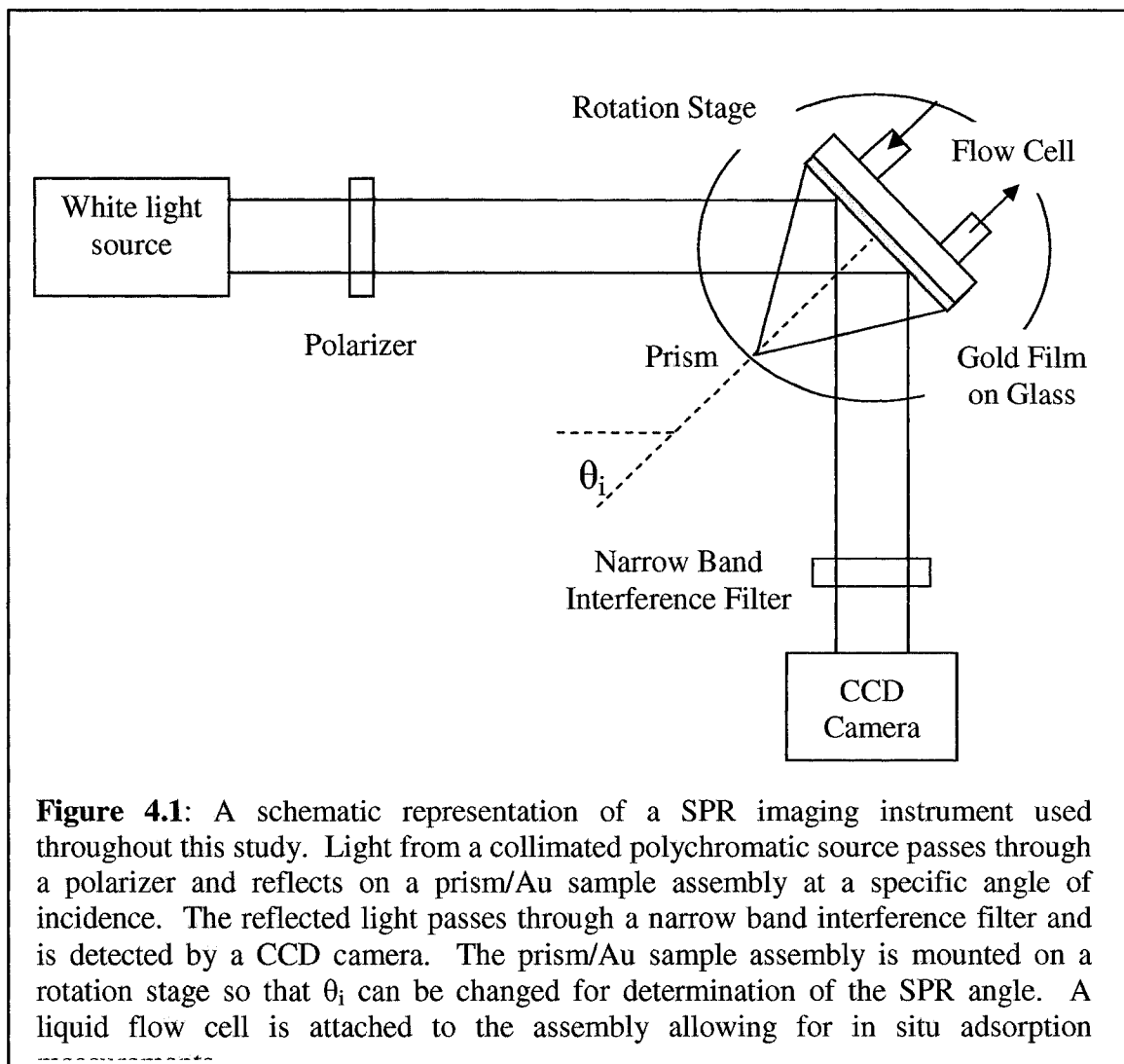


Figure 4.1: A schematic representation of a SPR imaging instrument used throughout this study. Light from a collimated polychromatic source passes through a polarizer and reflects on a prism/Au sample assembly at a specific angle of incidence. The reflected light passes through a narrow band interference filter and is detected by a CCD camera. The prism/Au sample assembly is mounted on a rotation stage so that θ_i can be changed for determination of the SPR angle. A liquid flow cell is attached to the assembly allowing for in situ adsorption

Briefly, light from a collimated polychromatic source passes through a polarizer and impinges on a sample cell at a specific angle near the SPR angle. A rotation stage holds sample cell in the path of the polarized light and allows for manipulation of the incident angle. The light interacts with the glass prism-Au sensor substrate interface, generating surface plasmons on the metal interface, which attenuate the light reflected from the surface. The light reflected from the Au substrate then passes through a narrow band interference filter propagating towards the detector. The detector in the SPRImager II is a CCD camera, which captures an image of the entire optical field of the chip surface. Image capturing from the CCD camera and subsequent analysis are done with the provided software from GWC Technologies.

The glass prism–Au sensor substrate–flow cell assembly is arranged in the Kretschmann geometry,¹⁶ as described previously in Chapter 3.2.2. Briefly, to achieve this type of configuration a glass prism is placed on top of the backside of the Au patterned sensor glass slide. To ensure no attenuation of photons through the prism/slide assembly the same type of glass, SF-10, is used for both pieces. This ensures a consistent refractive index. To compensate for the air glass boundary between the sensor slide and prism a refractive index matching fluid is used to ensure a consistent index of refraction through the completed assembly. A single drop of matching fluid (~ 5 μL) is placed on the leading edge of the glass slide. The prism is then positioned at this edge and slowly lowered causing the matching fluid to spread evenly between the slide and prism. This ensures no trapped air bubbles. The index of refraction of the SF-10 glass and matching fluid is 1.720. The two flow cells used during this study were the manufacturer's provided two port (inlet/outlet) flow cell and the developed PDMS microfluidic channel flow cell (Chapter 2.4).

The two port flow cell allowed for complete coverage of the sensor surface with one analyte solution. The flow cell consisted of a 1.2 cm diameter 0.1 cm deep reservoir defined by a rubber o-ring. This o-ring ensures a tight seal with the SPR slide and results in an approximate flow cell volume of 100 μL . The flow cell is held in place with four mounting screws to the SPR holder. Solutions are passed through the flow cell through 1/16'' tubing screwed into an inlet and outlet port on the fluid cell. The inlet port tubing is connected to peristaltic pump tubing (ID = 1/32'') whose inlet is placed inside a vial of solution. The peristaltic pump drives solution flow through the fluid cell. The total volume of solution required to fill the pump tubing, fluid cell tubing and fluid cell is ~ 225 μL . This arrangement is useful for single analyte investigations over the whole sensor surface. However, the two port flow cell requires a large volume of sample solution, for filling the tubing and subsequent rinse steps. It also suffers from the disadvantage of allowing only one analysis per experiment. By using the PDMS microfluidic channel manifold, reversibly and conformally bonded to the glass sensor surface, 4 analyte solutions can be investigated simultaneously. Also, the maximum volume of each channel is 250 nL.

4.2.4 PROCEDURES

Proteins used during this study were covalently attached to the SPR Au sensor regions through amine coupling, using the well characterized EDC/NHS attachment chemistry.¹⁷ The basic reaction scheme is given in Figure 4.2. Briefly, EDC reacts with carboxyl groups forming an amine reactive intermediate. This intermediate can react with amine functional groups on the surface of proteins forming a stable covalent amide bond.

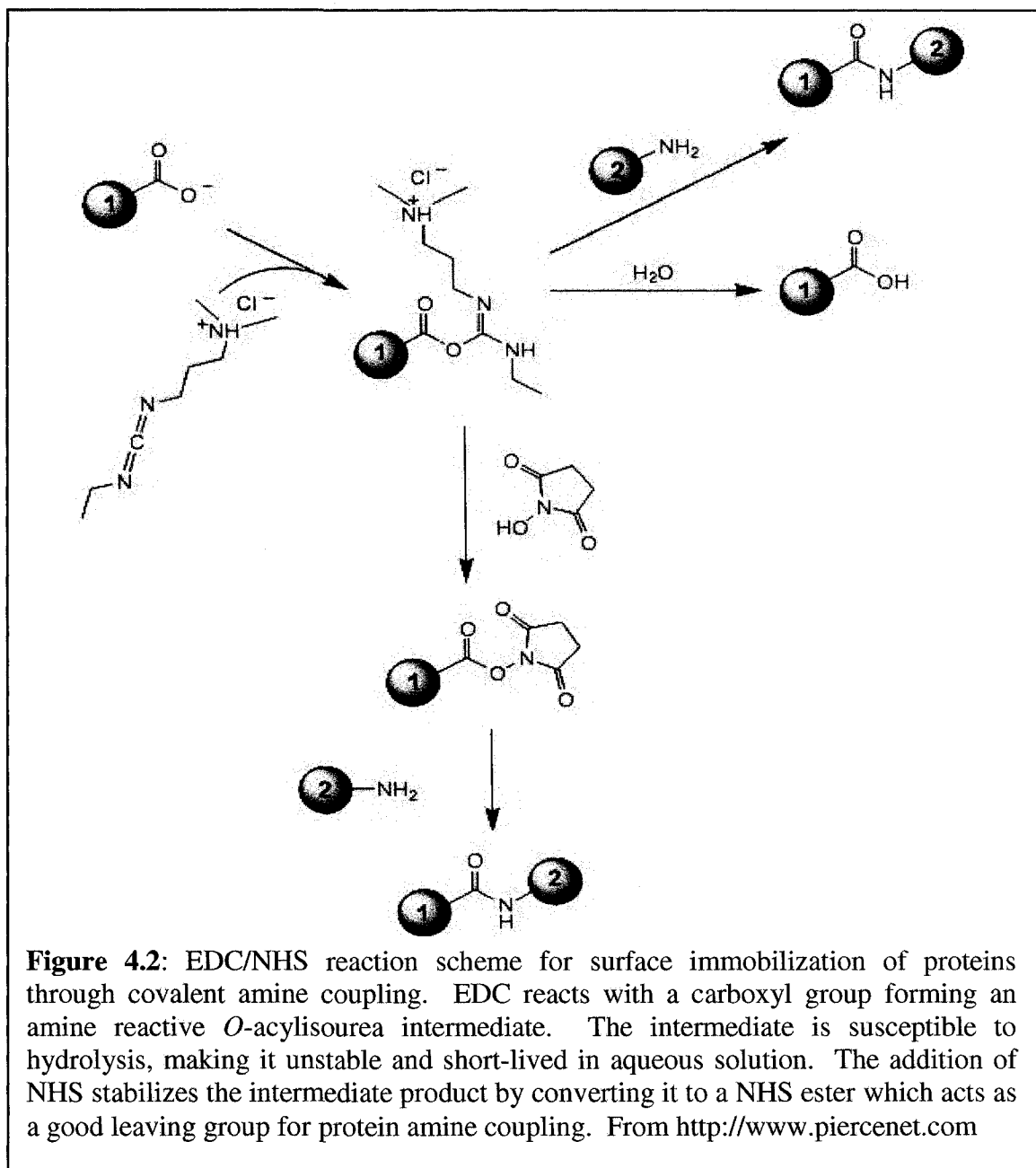


Figure 4.2: EDC/NHS reaction scheme for surface immobilization of proteins through covalent amine coupling. EDC reacts with a carboxyl group forming an amine reactive *O*-acylisourea intermediate. The intermediate is susceptible to hydrolysis, making it unstable and short-lived in aqueous solution. The addition of NHS stabilizes the intermediate product by converting it to a NHS ester which acts as a good leaving group for protein amine coupling. From <http://www.piercenet.com>

Formation of a carboxyl terminated SAM layer, to act as the seeding layer for the covalent surface attachment of proteins, was achieved through the complete immersion of the SPR Au patterned substrate in a 1 mL solution of 5 mM 11-mercaptopundecanoic acid (HS-CH₁₁-COOH) in anhydrous ethanol. The SPR slide was allowed to incubate in this solution for 2 hours to overnight to allow for the complete formation of a SAM terminated in -COOH. Upon activation of the Au sensor regions with a -COOH terminated SAM, the slide was removed and rinsed with copious amounts of ethanol to remove any unbound thiols, and dried under a stream of N_{2(g)}. The sensor slide was then ready for alignment and attachment to the microfluidic manifold, as described in Chapter 2.2.4.

The formation of a succinimide layer results in a very sensitive surface chemistry and was used immediately for amine coupling. Therefore, EDC/NHS activation of the carboxyl terminated SAM was performed within the microfluidic channels after bonding between the glass sensor substrate (coated with -COOH SAM) and the PDMS microfluidic manifold. This limited the exposure of the succinimide layer, after formation, to ambient room conditions. EDC/NHS was prepared at concentrations of 0.4 mM and 0.1 mM, respectively. Reagents were dissolved in degassed 0.2 μm filtered ultra pure Milli Q water. A co-solution, used for reaction with the carboxyl SAM surface, was formed through 1:1 mixing of each individual solution.

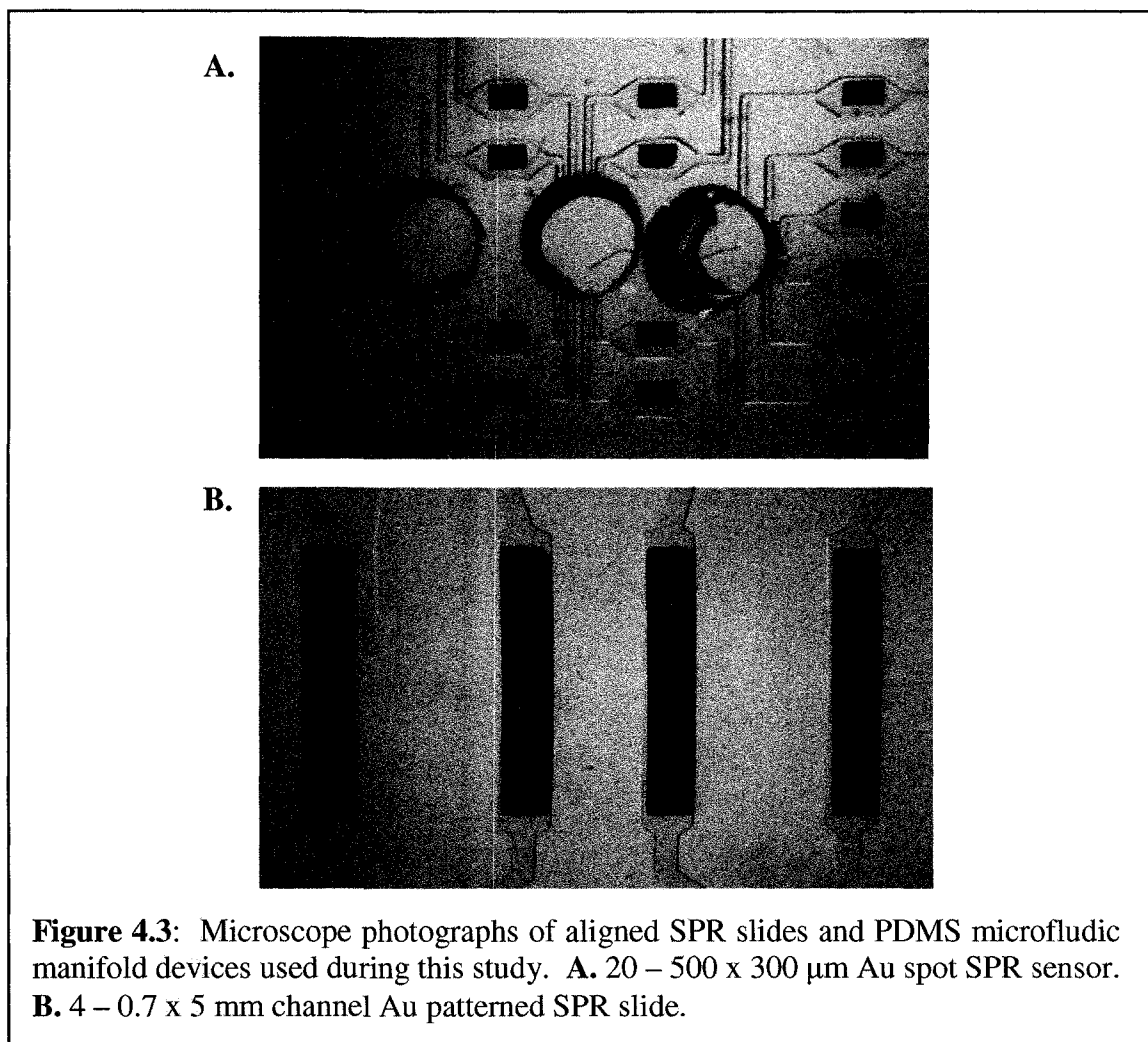
EDC/NHS was introduced to the microfluidic channels by pipetting 7 μL of solution into each inlet and applying vacuum at the outlet. Vacuum was removed once the solution covered the entire Au sensors. After activation of the -COOH SAM by EDC/NHS the solution was removed by vacuum. Immediately following the drying of the channels by vacuum, 7 μL of protein solution of interest was pipetted to the inlets and vacuum applied to the outlet to transport the protein solution to the Au sensor regions for amine coupling to the freshly formed succinimide surface. Once incubation of the protein solution was completed each channel was rinsed with 100 μL of HBS, to remove excess and unbound protein. A blocking step to deactivate un-reacted succinimide groups on the surface was achieved by addition of 0.01% BSA to each channel. A final rinse with 100 μL HBS per channel was used to remove excess and unbound BSA.

The activated SPR glass slides with covalently coupled proteins on the Au sensor regions were used in two configurations with the SPRImager II. If the sensor was to be used for a single analysis over the whole surface the PDMS microfluidic manifold was removed and the glass SPR slide was mounted with the 2 port flow cell provided by the manufacturer. For multi sample analyses, the PDMS manifold was left on the glass SPR slide in the case of the 4 channel device. In the case of the 20 spot device, it was replaced with the 4 channel PDMS device. The replacement was achieved by alignment and conformal bonding using a homebuilt alignment microscope.

4.3 RESULTS

Two devices were utilized for this study of coupling microfluidics and SPR imaging detection for protein microarrays. A 20 spot and 4 channel device were fabricated in PDMS as outlined previously in Chapter 2.4. These microfluidic devices were designed to align to Au patterned SPR sensor slides and are pictured in Figure 4.3.

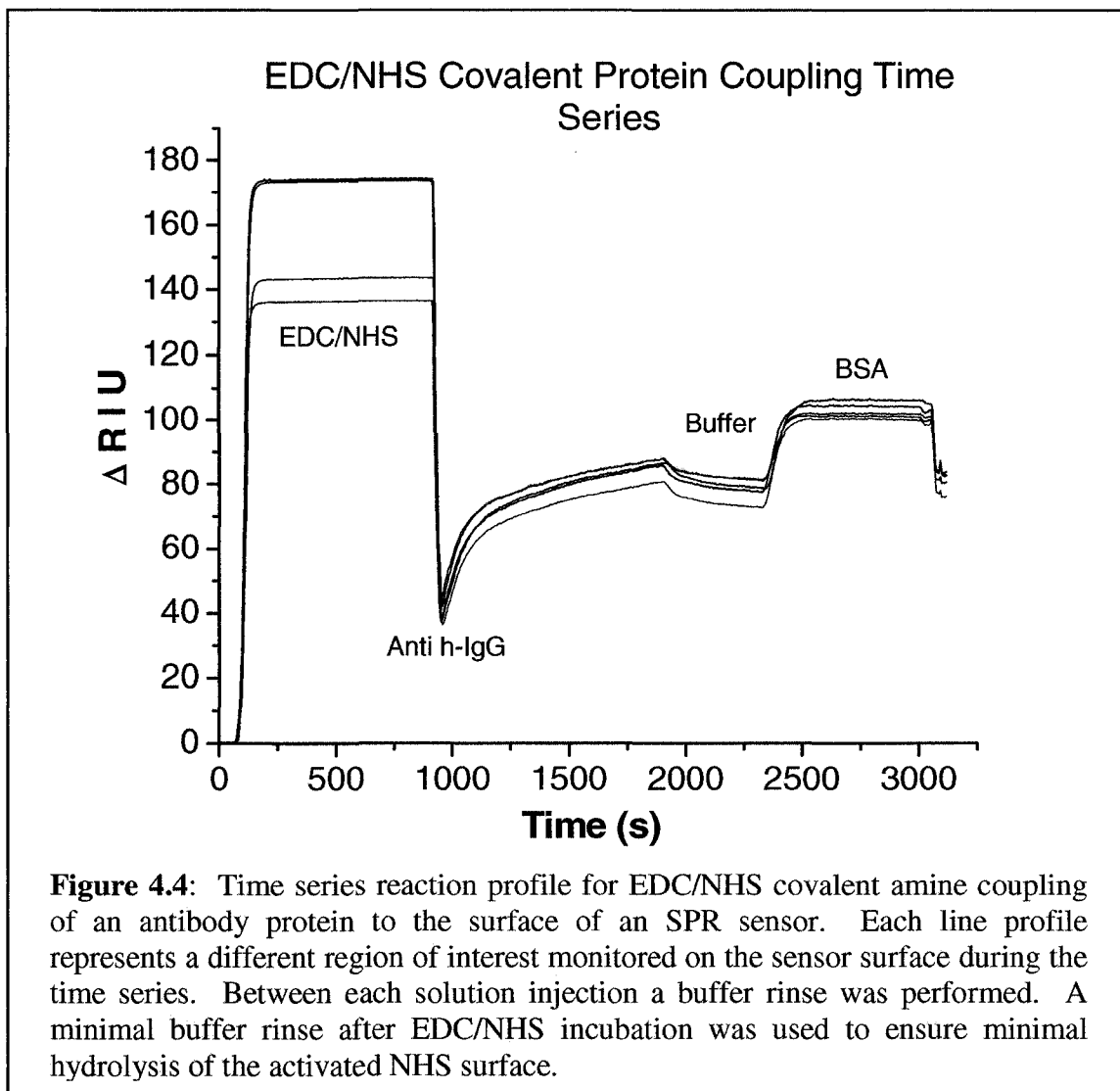
The Au patterned sensor areas provide the discrete active surfaces for protein immobilization and SPR detection. The dimensions of the Au patterned pads were determined from a combination of ease of visualization with the SPR imager and coupling with the PDMS microfluidic manifolds. For the 20 spot device the Au pads are 500 x 300 μm and for the 4 channel device the Au pads are 700 μm wide by approximately 5 mm long.



Previous reports for SPR detection for protein arrays have utilized simple physical adsorption of binding pairs to the metal surface prior to measurement.^{9, 18-20} While demonstrable of the technique there are drawbacks to direct surface adsorption of ligands. Direct adsorption is not suitable for proteins which can undergo denaturation when in contact with surfaces. Also, protein films formed by direct adsorption do not give well defined and stable adsorption layers as they can be susceptible to desorption by changing solution environments or exchange processes occurring between the adsorbed film and other solutes in solution. These exchange processes can lead to undefined films of mixed solutes difficult to characterize due to their changing composition based on changing reagent solutions. The ideal situation is a stable covalent bond of the ligand to the surface for the repeatable analyses to its binding partner. This can be achieved by a variety of covalent binding protocols involving either direct coupling of proteins to a

surface through amide linkages, various attachment chemistries, such as amine, carboxyl or thiol binding, or through the use of other binding intermediaries such as biotin/avidin. In this work amine coupling through the use of EDC/NHS is utilized to achieve a covalent bond for protein surface immobilization. The basic reaction mechanism by which the covalent attachment occurs have been explored and utilized extensively and shown schematically in Section 4.2.4.

The amine coupling immobilization procedure used was adapted from Johnsson et al.¹⁷ Examination of the subsequent incubation times necessary for the effective amine coupling of proteins was achieved by monitoring the immobilization sequence in real time. The time dependent change of the SPR response to the covalent coupling of proteins to the surface is measured in relative intensity units (RIU). Figure 4.4 is the response curve for the covalent attachment scheme employed.

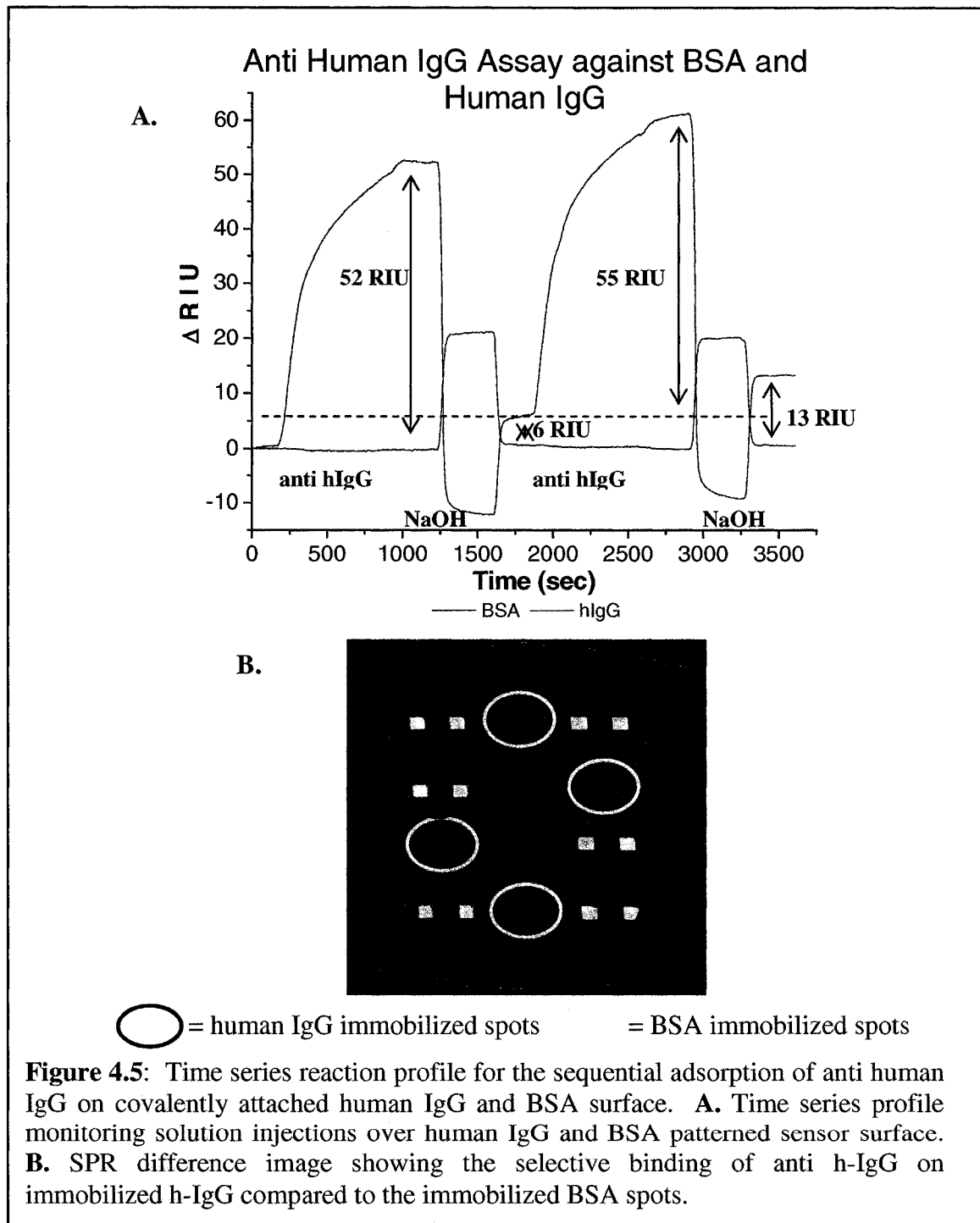


Prior to covalent protein immobilization, the Au patterned SPR slides are activated by the self assembled monolayer created by adsorption of 11-mercaptopundecaonic acid. This results in a SAM surface terminated in carboxyl groups. Activation was achieved by immersion of the SPR Au patterned slide in a 1 mL 5 mM thiol solution in ethanol for 2 hours. Contact angle measurements on a Au coated SPR slide were used to confirm the formation of a carboxyl terminated surface. The contact angle for a clean bare Au surface was $81 \pm 3^\circ$. The $-\text{COOH}$ SAM layer exhibited a pH-dependent contact angle ranging from 11 to 35° . This conforms well with reported contact angles and their pH sensitivities for aqueous droplets on carboxyl terminated surfaces.^{21, 22}

Once mounted into the SPR, signal changes were monitored upon exposure of the SAM surface to the various reagents. EDC/NHS was first introduced and the characteristic large increase in signal was observed. This sudden and dramatic increase is due to the bulk refractive index change associated with changing the solution from running HBS buffer to EDC/NHS. Incubation of the solution over the sensor surface was maintained for 15 minutes followed by removal of EDC/NHS by buffer solution and incubation with 667 nM anti human IgG antibody protein. This results in a dramatic decrease in signal intensity followed by a steady rise in signal, as protein covalently binds to the succinimide surface formed during EDC/NHS activation. To allow for maximum protein coverage, incubation is maintained for 20 minutes, followed by a 5 minute buffer rinse to remove excess and unbound protein. A subsequent dip in signal is monitored. A blocking step is used to deactivate any remaining succinimide groups through incubation with 0.01% BSA for 10 minutes. Finally, a rinsing step with buffer was performed resulting in a stable response. The signal difference is associated with the amount of anti human IgG bound to the sensor surface through covalent attachment. There is a minimal difference between the signal after antibody attachment and BSA blocking, indicating that most attachment points on the surface were occupied by antibody protein rather than BSA. This binding approach leads to a stable and reusable surface that requires no modification of the protein sample for attachment. It should be noted that this attachment protocol does result in proteins bound in a random orientation (binding occurs at any free surface amine group) and does require extra steps when compared to physical adsorption. This surface activation protocol for covalent bonding of proteins is utilized throughout this study to fabricate protein microarrays on SPR sensors using microfluidic devices formed in PDMS..

The 20 spot microfluidic spotting device allows for the selective patterning of predefined Au spots. By being able to selectively pattern to certain spots, activation of each spot with various samples is possible; potentially allowing for increased sample density and sample variety per unit of area. To initially test single spot addressability with this device two different proteins were patterned, human IgG and BSA, followed by monitoring of their antibody binding response. To adequately fill the channels, reservoirs and cover the Au spots, 5 μ L of solution was required. Figure 4.5 shows an

SPR difference image and accompanying sensorgram for the immunoassay response of a hIgG and BSA patterned sensor slide to anti hIgG.



Covalent attachment of hIgG was performed on 12 spots while BSA was covalently attached to 8 spots. Upon amine coupling of the proteins to the surface the PDMS microfluidic manifold is removed and the patterned slide is mounted into the SPR

imager for exposure to 130 nM anti hIgG. The recorded sensorgram shows the average response for each immobilized protein towards anti hIgG. The response to anti hIgG is 52 ± 6 RIU for the hIgG patterned spots. The BSA patterned spots record no signal response to anti hIgG. This is consistent with BSA serving as an effective blocking agent in many biochemical protocols. Since the glass slide is Au patterned, signal is only recorded for those regions. Thus, there is no bulk background effect and visualization of individual spots is made easier. The protein patterned surface was then regenerated through the exposure of the surface to 10 mM NaOH for 5 minutes. This regeneration step disrupts the non-covalent binding between the antibody and antigen and removes the bound antibody. Buffer is introduced to remove NaOH and recondition the protein surface. The BSA surface is regenerated back to its initial signal and the hIgG patterned spots exhibit a regenerated signal response of 6 ± 2 RIU. While effectively removing most bound anti hIgG the signal does not return to the pre-exposure conditions. This shows that some remaining anti hIgG is still bound to the surface. A second exposure to 130 nM anti hIgG is run exhibiting similar response from the hIgG and BSA patterned surfaces. The measurements of the second exposure are taken against the new baseline created after the first regeneration step. Regeneration is achieved again with exposure to 10 mM NaOH and again the BSA patterned surface returns to its pre-exposure condition while the hIgG surface retains residual antibody binding. More effective regeneration of the surface may possibly be achieved by using higher concentration NaOH or increasing the exposure time. However, care must be taken in choosing regeneration conditions that are not harsh enough to disturb the integrity of the covalently attached protein layer.

For sensitive and accurate quantitative binding analysis it is crucial to ensure, that the background signal remains low following antibody exposure. Since detection will only occur at the Au surface the bulk background retains a 0 RIU signal response. The SPR difference image with zero signal background shows the effectiveness in using patterned Au sensor regions for increasing sensitivity and ease of visualization while eliminating patterning steps to reduce non-specific adsorption. As described this method has allowed for the microfluidic enabling of addressable protein spotting and required no background surface modifications for blocking non-specific adsorption.

The fabrication of a two protein microarray utilizing a 20 spot microfluidic manifold is overkill, as the 20 spot device is more cumbersome than it needs to be for the application: 1. filling of multiple inlet reservoirs, 2. using three separate outlets per 6 or 8 inlets and 3. monitoring small detection areas. While research into large protein libraries is vast, it is also necessary to evaluate protein characteristics individually or against fewer comparative samples. To this end, a lower sample density channel array was developed that maintained the benefits of limited drying and fewer bulk surface modifications necessary to minimize non-specific adsorption while easing microarray fabrication, patterning and ease of detection visualization. A channel array device was fabricated as outlined previously, Chapter 2.4, which comprises 4 Au patterned sensing regions coupled to an aligned four channel microfluidic manifold cast in PDMS with one inlet per channel and a bifurcated outlet design to one waste reservoir (Figure 4.3). This design and protein patterning procedure differs from that described by Delamarche et al.⁴ in that vacuum pressure is applied at only one outlet due to the bifurcated design to drive fluid flow. This type of design allows for the incorporation of rinsing steps directly within each channel. This design also differs from work by Kanda et al.¹⁸ since protein immobilization is achieved through covalent attachment chemistry with immobilization only occurring at localized Au patterned regions. This eliminates the need for bulk background blocking with BSA or ethylene glycol. This design also provides increased Au sensing regions, allowing for easier quantification of signal. Finally, due to the Au patterning, strong adhesion between the PDMS microfluidic manifold and SPR glass substrate can be achieved either by conformal contact or O₂ plasma treatment for irreversible bonding. This allows for the introduction of solutions with high organic content without leakage.

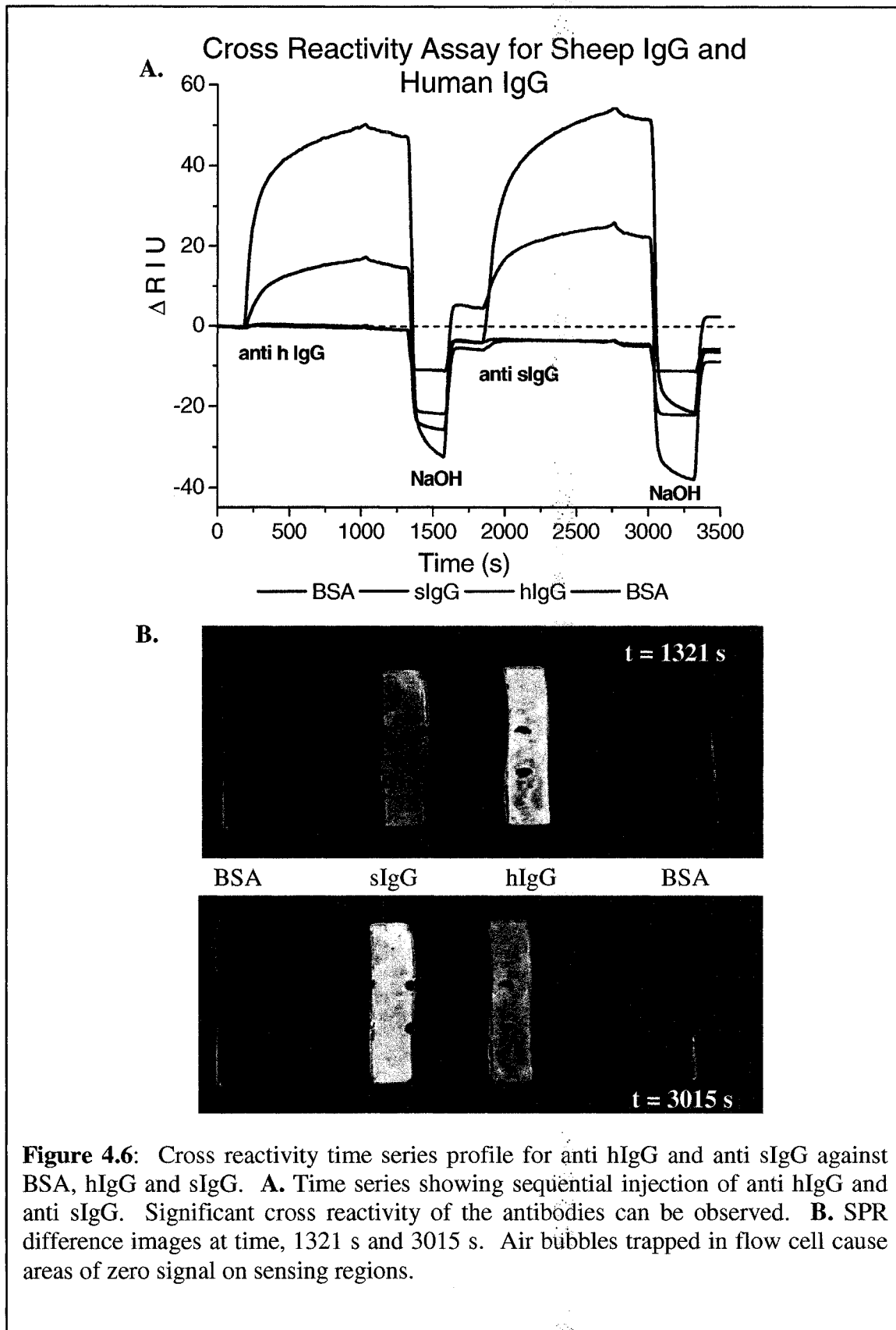
Patterning of the four channel array involved pipetting approximately 5 μ L of solution per channel at the inlet reservoirs. This volume was sufficient to fill the channels and reservoirs and cover the Au sensor regions. BSA, sheep IgG (sIgG) and hIgG were covalently immobilized to the surface using amine coupling and the previously described immobilization protocol. Upon fabrication of the protein microarray on the Au sensors, the PDMS channel manifold was removed and the slide was mounted into the SPR using the single inlet/outlet flow cell. Figure 4.6 shows the

SPR difference images and sensorgrams for the sequential exposure of the four channel microarray to 130 nM anti hIgG and anti sIgG.

Upon injection of anti hIgG the largest signal increase occurs on the hIgG immobilized surface (47 ± 4 RIU). A significant signal (15 ± 5 RIU) is also observed for the sIgG patterned surface due to cross reactivity with the anti hIgG. Minimal signal change is observed for the binding of anti hIgG to the BSA patterned surface. A rinsing step with buffer to remove excess and unbound binding antibody, is performed, resulting in the slight decrease in signal prior to the dramatic drop in signal upon regeneration of the surface with 10 mM NaOH. After buffer stabilization of the surfaces it is observed that the NaOH regeneration was very effective for the BSA and sIgG surfaces however resulted in an increase in the new baseline signal of the hIgG surface. As noted previously, regeneration after significant binding may require higher concentration NaOH or longer incubation times. Injection of 130 nM anti sIgG results in an increase in the sIgG patterned surface (55 ± 6 RIU) as well as substantial cross reactivity to the hIgG surface (17 ± 5 RIU). Again BSA results in limited signal change.

The antibodies used here are polyclonal immunoglobulins directed against whole IgG and will bind light chain sites common among immunoglobulins. This leads to the observed cross reactivity between various antibodies and antigens. Since the hIgG and sIgG covalently bonded to the surface were absorbed from identical solution concentrations of $200 \mu\text{g mL}^{-1}$, the surface density of antigens will be similar. Therefore, the observed difference in antibody binding to the various surfaces accounts for the specificity difference each antibody has to different IgGs.

While based on similar design features, Au patterning, aligned PDMS microfluidic manifolds and shared outlets, the spotting and channel array devices each prove useful for different purposes. However, when combined in conjunction with each other a powerful array assembly emerges. Figure 4.7 outlines the combination of the two devices.



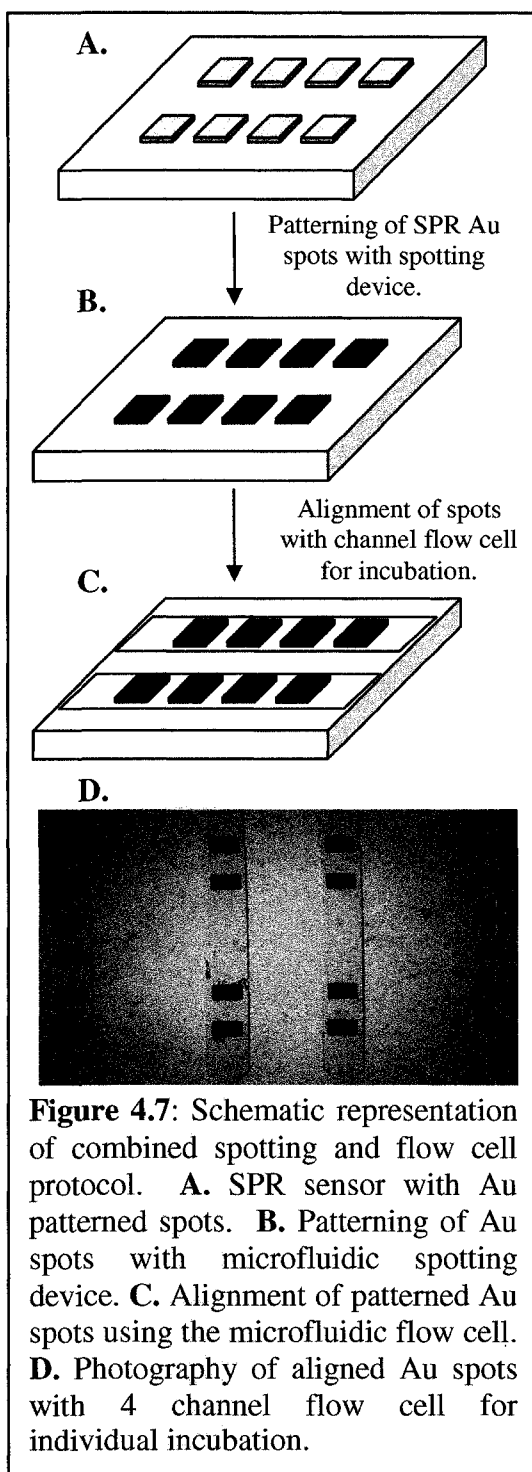
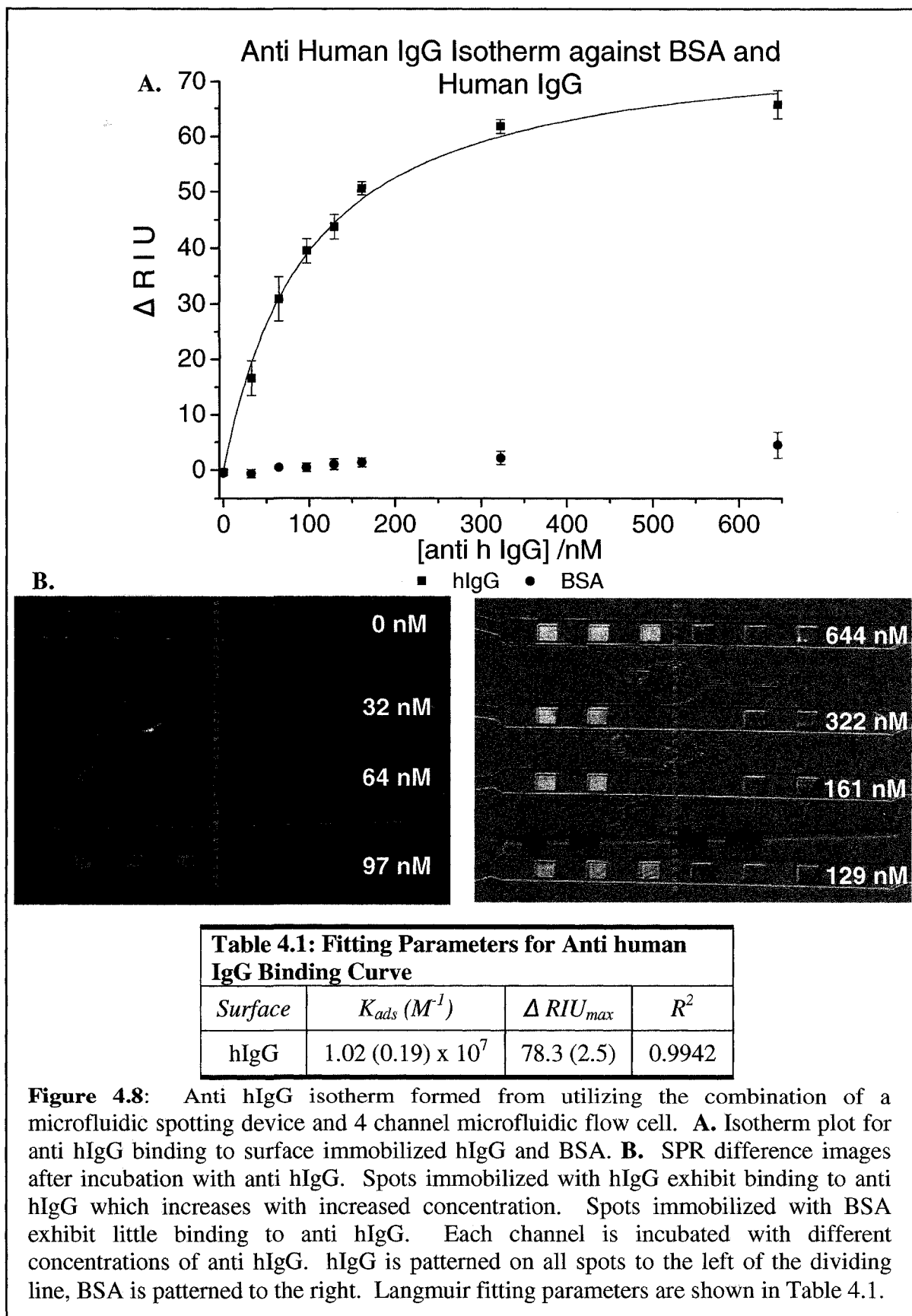


Figure 4.7: Schematic representation of combined spotting and flow cell protocol. **A.** SPR sensor with Au patterned spots. **B.** Patterning of Au spots with microfluidic spotting device. **C.** Alignment of patterned Au spots using the microfluidic flow cell. **D.** Photography of aligned Au spots with 4 channel flow cell for individual incubation.

The spot array provides for the patterning of multiple targets on the Au spots. Upon immobilization of the targets the spot array is replaced with the channel array, which allows for the alignment of the spots to the center of the cast PDMS channels. The combined device, Au spot patterned SPR slide with aligned PDMS channel manifold, is then mounted into the SPR imager for detection. In this configuration the channel array is used as a four channel flow cell providing simultaneous investigation of multiple samples against multiple immobilized targets. Compared to the single port flow cell used in Figure 4.5 and 4.6, this results in fewer individual experiments and chips for the same number of samples.

A widely determined and important protein characteristic is the binding strength of protein interactions.²³ SPR imaging has been demonstrated as a means to measure binding isotherms and determine adsorption coefficients (K_{ads}) which can be related to binding constants.²⁴ As an illustration of the benefit of this combined approach for reducing the total number of experiments necessary to collect experimentally important

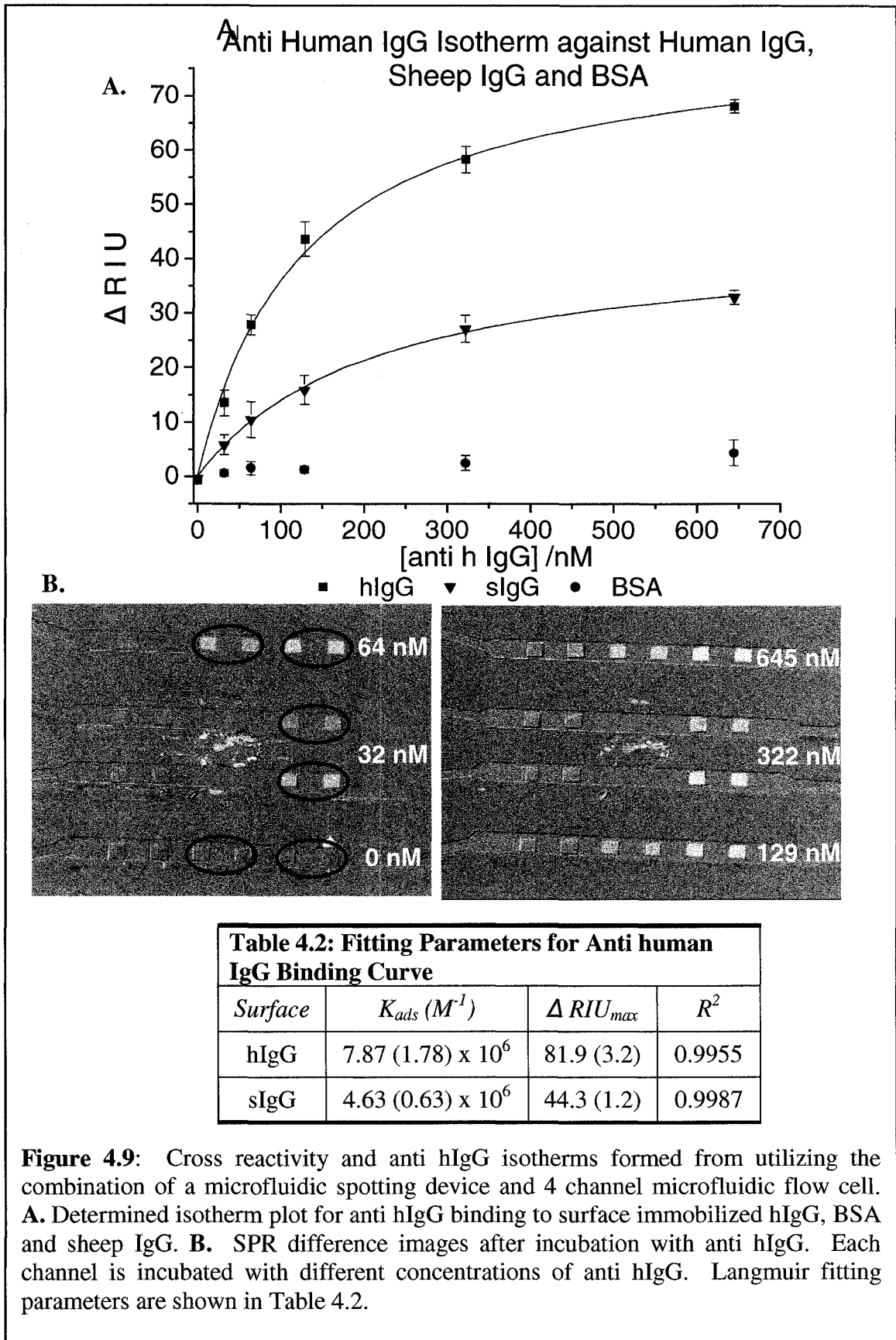


Using the spotting device each row was covalently patterned with BSA (0.01%) and hIgG (200 $\mu\text{g mL}^{-1}$). Three spots were patterned with BSA and hIgG for the outside rows and two spots were patterned with each for the inner rows. Replacement of the spotting device with the four channel array device allowed for the incubation of the surface with four different concentrations of anti hIgG simultaneously. The concentrations investigated were 0, 32, 64, 97, 129, 161, 322 and 645 nM. Sets of four concentrations were incubated twice for a total of 16 data point, 8 for each type of surface, hIgG and BSA. The SPR signal due to anti human IgG binding reached a steady state value in approximately 10 minutes. Each point in Figure 4.8 was collected after an incubation time of 20 minutes. Average signal and standard deviation, reported in reflected intensity units (RIU) was determined from regions of interest (ROI) selected around the boundary of each spot. The general shape of the isotherm is consistent with literature reports of antibody binding¹⁸ and fits a Langmuir description which is commonly used for the description of protein binding.^{18, 25, 26} The curve through the data points of the graph is the Langmuir fit and results in a K_{ads} for anti hIgG binding to hIgG of $1.02(0.19) \times 10^7 \text{ M}^{-1}$ with a R^2 of 0.9985. Our K_{ads} value compared well to that determined by Kanda et al.¹⁸ ($1.1(0.1) \times 10^7 \text{ M}^{-1}$) for bovine IgG binding to adsorbed anti bovine IgG on mercaptoundecylamine hydrochloride SAM. However, experimentally our value was determined from eight measurements taken over two incubations, while Kanda et al. used six measurements taken over six incubations. Minimal adsorption, over the concentration range studied, was observed for immobilized BSA. Immobilized BSA was used as a reference background for determination of non-specific adsorption.

Along with specific isotherm binding information for an immunogenic pair, a cross reactive comparison of antibody binding, illustrating the antibody's relative binding strengths to various antigen patterned surfaces, can be determined. This type of multi component analysis procedure benefits from the ability of the spot and channel array devices to reduce the total number of experiments performed. It has been shown²⁷ that K_{ads} values can be used to rank binding strengths in similar systems, even though K_{ads} values determined from Langmuir fits are not equivalent to binding association constants. Cross reactivity is investigated for polyclonal anti human IgG against hIgG and sheep IgG. Figure 4.9 shows the binding curves collected in two incubation steps for binding

between anti human IgG and three pre-patterned proteins, hIgG, sIgG and BSA. Six data points are collected over the concentration range of 0 to 645 nM of anti hIgG. Sets of three concentrations were incubated twice for 6 data points for each patterned surface. Antibody solutions were incubated for 20 minutes and ROIs of each spot provided signal average and stand deviation.

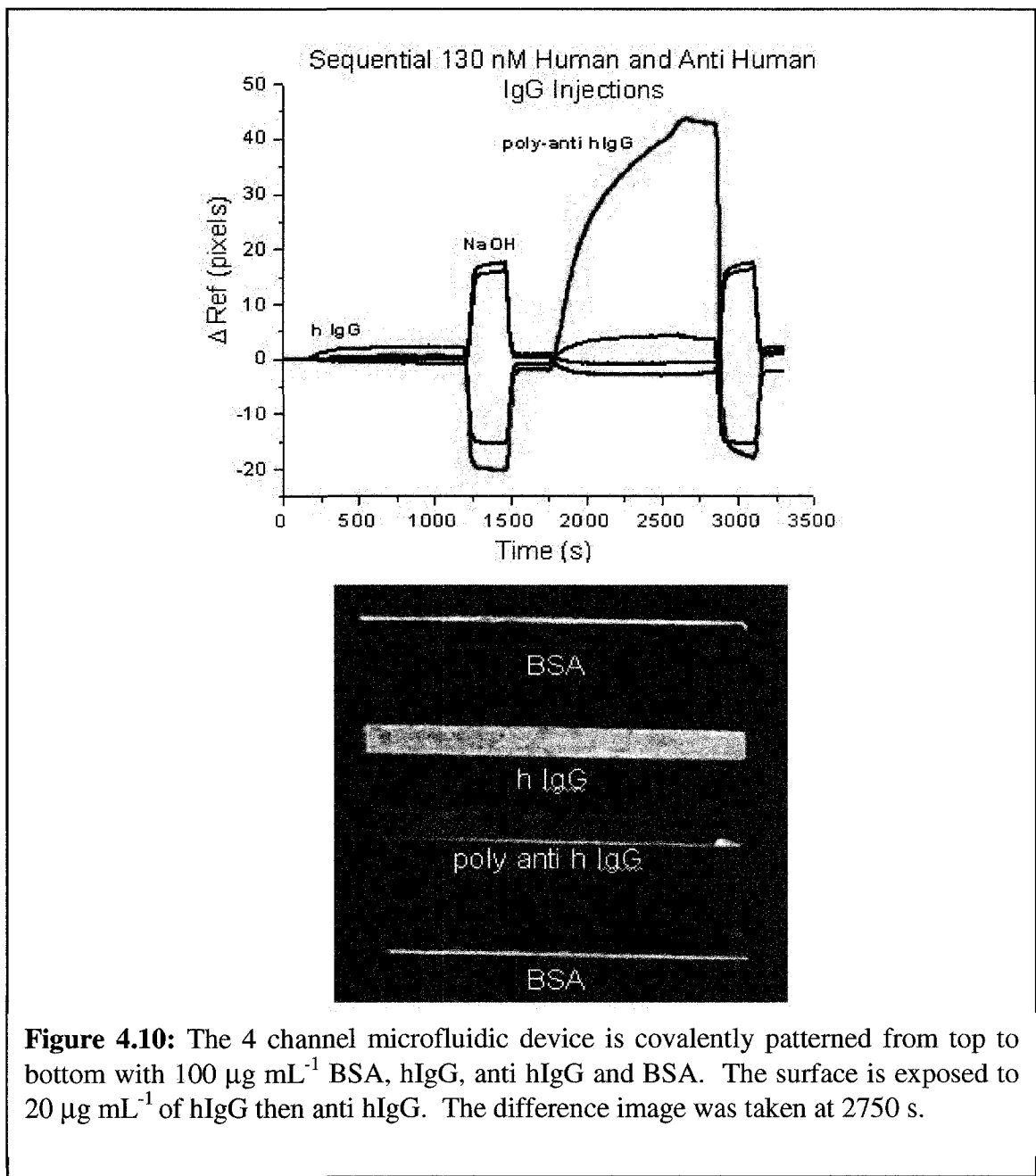
Using the spotting microfluidic manifold, three different proteins were covalently patterned at $200 \mu\text{g mL}^{-1}$; BSA, sIgG and hIgG. Since the two inner rows only contained spots of BSA, and only one of the IgG antigens, these rows were exposed to the same concentration of antibody solutions. The data collected fit a Langmuir isotherm description and the curve through the data points is the Langmuir fit. The determined fitting parameters are shown for hIgG and sIgG. It is observed that sIgG significantly binds anti human IgG. sIgG has a determined maximum saturation of approximately 50% that of hIgG. BSA again is used as a reference for non-specific adsorption and is relatively inert towards binding of anti human IgG. As was seen in Figure 4.6 for the single concentration binding of anti human IgG to sIgG, this isotherm over a large concentration range shows the full extent of sIgG cross reactivity towards anti hIgG in two incubation experiments. The determined K_{ads} for hIgG are slightly lower compared to that of Figure 4.8, however, they are within experimental error of each other. This difference may be attributed to differences arising due to the random nature of the covalent attachment protocol used for protein immobilization.

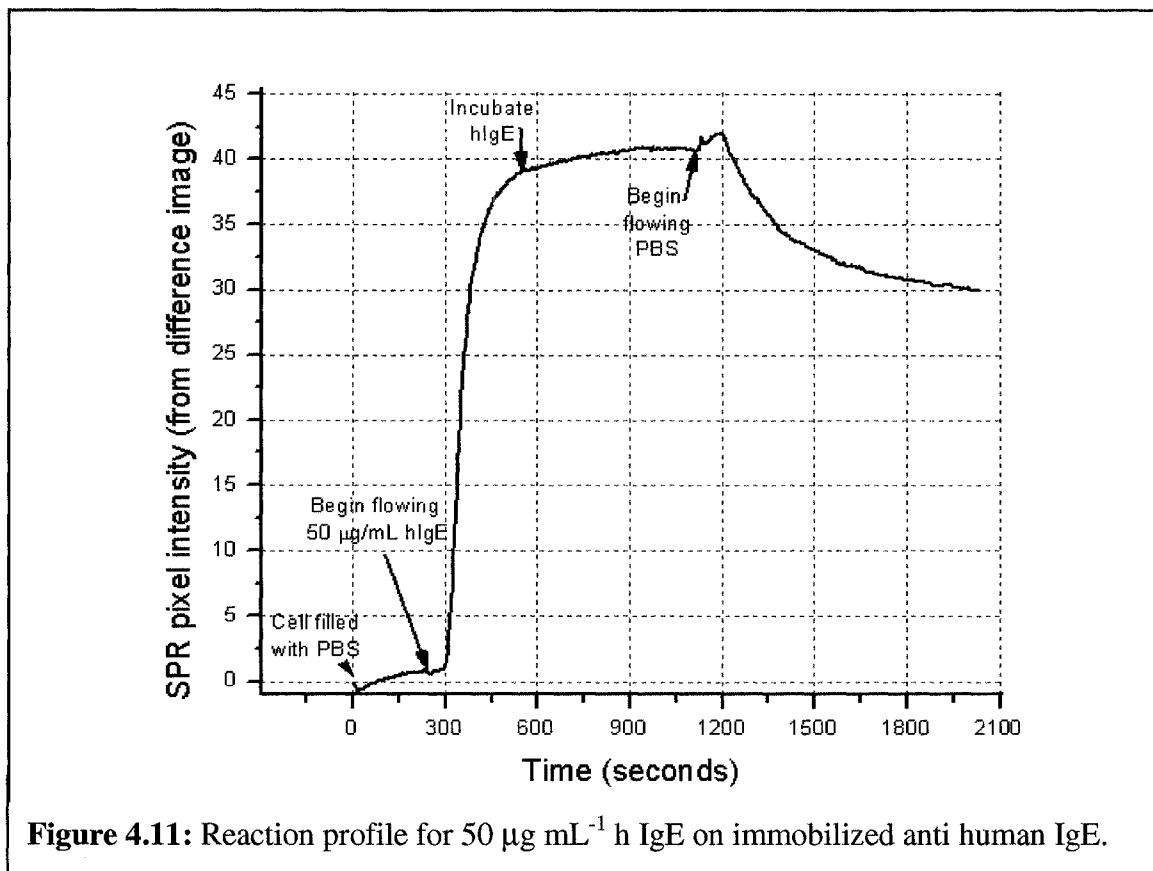


4.4 IgE ASSAY DEVELOPMENT

The easiest method of detecting an analyte of interest in a sample is direct capture of that analyte by a complementary binding partner and measuring the binding event. In SPR the binding event is measured as changes in the refractive index of the surface. Figure 4.10 is an SPR time series for the binding of human IgG antibody and antigen to surface immobilized human IgG antigen and antibody, respectively. It illustrates the importance of protein orientation in immunoassays for SPR imaging.

As in other work,¹⁸ immobilizing the antibody on the surface for analyte capture results in less binding compared to surface immobilizing the analyte. This may be due to the random orientation of the covalent attachment resulting in fewer exposed F_{ab} binding sites of the antibody. Since polyclonal antibodies were used the orientation of surface bound antigens was less critical. Thus, detection of IgE by surface bound anti IgE would prove to be difficult. A straightforward IgE capture experiment with surface immobilized anti-human IgE resulted in relatively low signal for a comparably large concentration ($50 \mu\text{g mL}^{-1}$) (Figure 4.11).





Considering the high cost of human IgG, further direct binding experiments of IgE immunoassays was conducted using a Biacore 3000 SPR from the University of Alberta Institute for Bimolecular Design. This instrument allows for minimum analyte injections of $30 \mu\text{L}$, thus significantly reducing the amount of sample used per analysis compared to the large volumes necessary to fill the GWC-SPR imager flow cell. Also, the Biacore 3000 SPR possesses greater measurement sensitivity. Increased measurement sensitivities are achieved within the Biacore instrument partly through the use of a novel proprietary carboxymethyl dextran matrix for antibody immobilization. This surface treatment results in a 3 dimensional polymer structure which allows for a higher density of surface immobilizations compared to the 2 dimensional immobilization of the SPR imager sensor.

Immobilization of anti human IgE followed by exposures with varying concentrations of human IgE resulted in a calibration curve with a limit of detection (LOD) of 34 ng mL^{-1} (Figure 4.12).

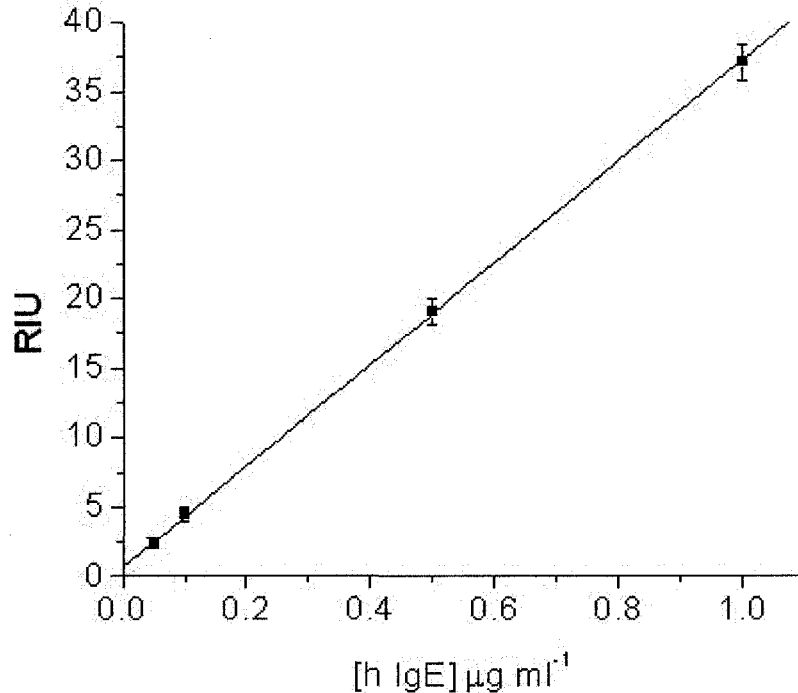
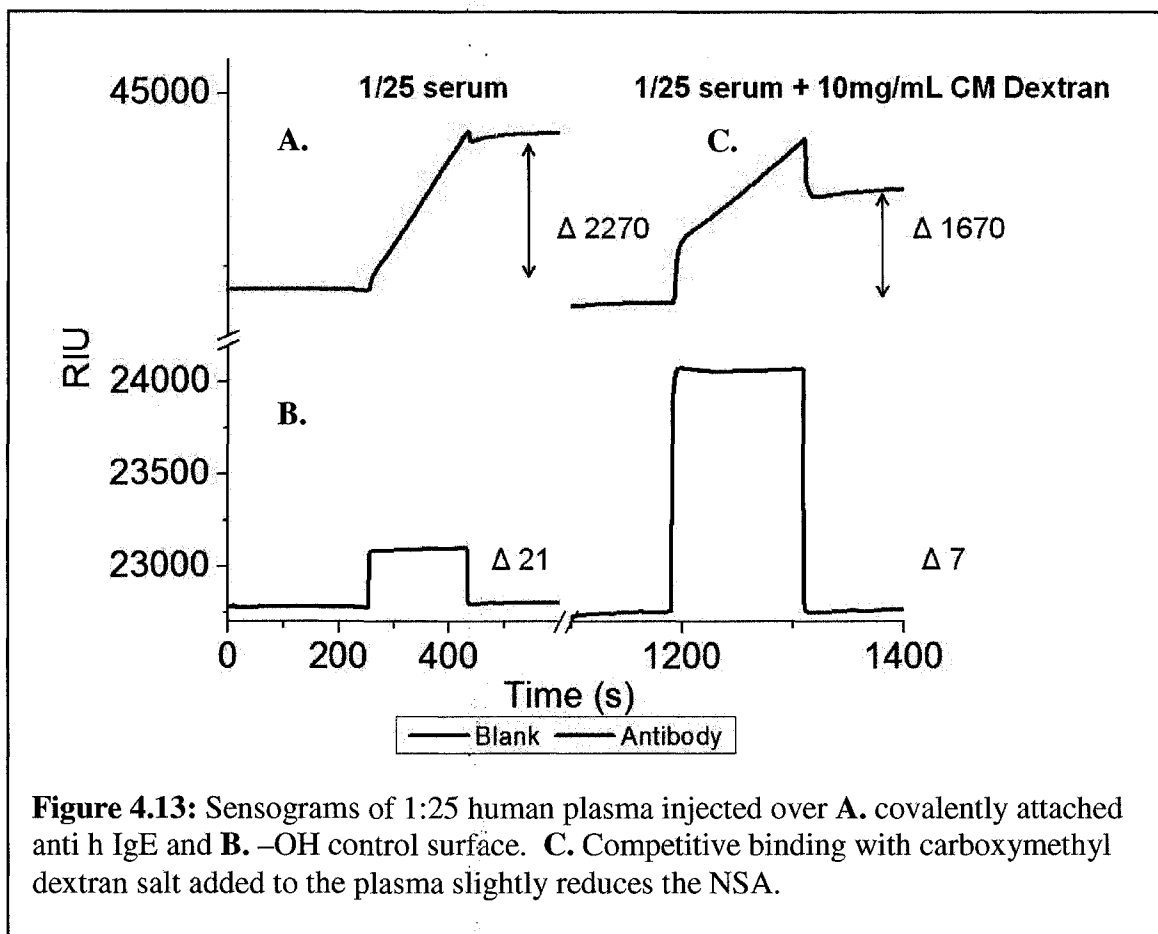


Figure 4.12: Calibration curve generated using the Biacore 3000. Each data point is composed of 3 separate measurements. LOD is determined from 3 times the signal of a blank injection.

While the observed LOD is within the clinically relevant range of detection, rarely are samples tested as pure analytes. Consideration must be made to the sample matrix of the collected sample. Thus, the degree of non-specific adsorption (NSA) of human blood plasma was investigated.

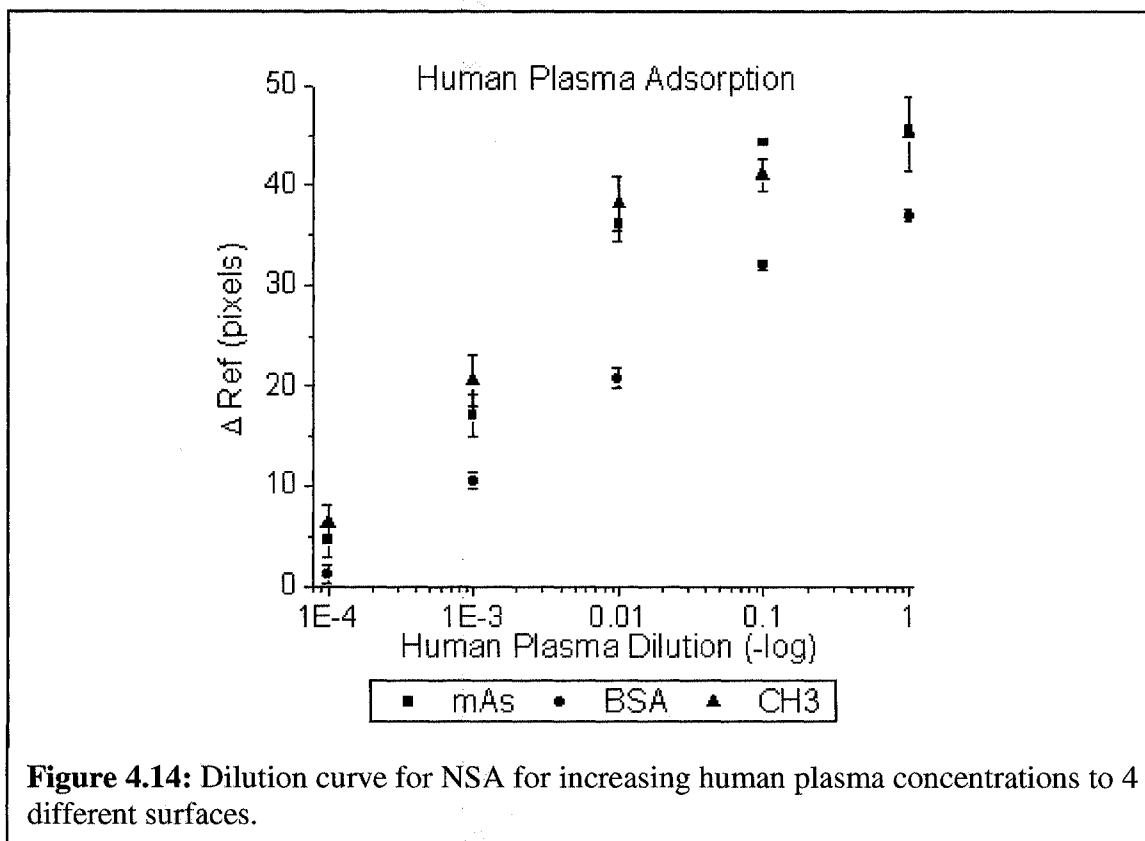
As discussed previously (Chapter 1.5) blood plasma is a complicated mixture composed of many proteins in a variety of concentrations. Because of the large amounts of proteins found in blood plasma, dilutions are often performed to reduce the quantity of background elements. This also has the effect of reducing the concentration of the species being tested for.

Considering the NSA of blood plasma, injections of diluted plasma were monitored in both the Biacore and SPR imager. The Biacore showed significant NSA at 1:25 dilution over a surface of covalently immobilized anti human IgE.



The signal for IgE binding at $1 \mu\text{g mL}^{-1}$ was ~ 37 RIU (Figure 4.12) compared to ~ 2000 RIU for non-specific adsorption with a 1:25 plasma dilution. The control channel of -OH terminated surface showed little NSA. To see the affects of adding a competing binding agent to the plasma sample, carboxymethyldextran salt was added at a concentration of 10 mg mL^{-1} . While this reduced the NSA by a third, signal intensity was still high.

Similarly, the NSA behavior of human plasma was investigated in SPR imaging using the 4 channel PDMS microfluidic flow cell. Here 3 different surfaces were patterned for exposure to different dilutions of human plasma. Covalently immobilized BSA, anti sheep IgG, and $-\text{CH}_3$ terminated thiol surfaces were prepared on the sensor surface. Figure 4.14 is the dilution curve collected for NSA of human plasma to different surfaces.



Considering the low signal of IgE binding shown in Figure 4.11 and the maximum signal observed for ideal binding patterns such as hIgG and anti hIgG (Figure 4.10) further work is needed to minimize the NSA of human plasma to achieve detection of real world samples.

Future work of developing SPR IgE assays can focus on increasing the specificity of IgE capture by changing binding pairs from antibodies to aptamers or specific allergens. Methods of reducing non-specific adsorption should be investigated such as pre-cleaning of the plasma sample to remove excess HSA and fibrinogen the highest concentrated proteins. Also, allowing for pre-concentration of IgE in plasma may increase its relative concentration after plasma dilution.

4.5 CONCLUSIONS

This work has demonstrated a straightforward method for the preparing and detection of antigen microarrays, allowing for the determination of antigen isotherm binding and cross reactivity. From this the development of facile and convenient

customizable protein arrays can be envisioned through a combination of microfluidic platform and label free detection schemes. It has been demonstrated that a microfluidic network coupled with SPR imaging detection can be a viable method in reducing sample consumption of analytes while minimizing total number of experiments in an easy to setup detection scheme for protein microarrays. Binding isotherms for hIgG and cross reactivity isotherms for sIgG against anti human IgG were developed in two experiments on the same antigen array. Having a plurality of array elements and analyte binding channels allows for a greater number of binding interactions leading to fewer experiments. Covalent patterning of proteins onto Au with PDMS microfluidic networks provides an easy and effective means of fabricating protein arrays for SPR imaging detection. These microfluidic networks have been demonstrated in 20 spot and 4 channel configurations for the easy covalent patterning of protein arrays. The 4 channel configuration allowed for the simultaneous detection of 4 different analyte samples and provided a means by which to increase the total number of detectable surface binding events. Although a low density of array elements was demonstrated in this work, this methodology easily lends its self to scaling. Fabrication of higher density arrays, with greater number of addressable spots, and increased analyte channels for measuring many more simultaneous interactions would be possible.²⁸ Through the use of patterned Au sensor surfaces and microfluidic networks, controlling solution flow, customizable surface patterns and densities can be created. Coupled with the use of label free SPR imaging detection, these fabricated substrates create a background of zero signal intensity, increasing image contrast and ease of detection.

4.5 REFERENCES

- (1) Angenendt, P.; Glokler, J.; Sobek, J.; Lehrach, H.; Cahill, D. J. *Journal of Chromatography A* **2003**, *1009*, 97-104.
- (2) David S. Wilson, S. N. *Angewandte Chemie International Edition* **2003**, *42*, 494-500.
- (3) MacBeath, G.; Schreiber, S. L. *Science* **2000**, *289*, 1760-1763.
- (4) Bernard, A.; Michel, B.; Delamarche, E. *Analytical Chemistry* **2001**, *73*, 8-12.

- (5) Furuki, M.; Kameoka, J.; Craighead, H. G.; Isaacson, M. S. *Sensors and Actuators B-Chemical* **2001**, *79*, 63-69.
- (6) Kurita, R.; Yokota, Y.; Sato, Y.; Mizutani, F.; Niwa, O. *Analytical Chemistry* **2006**, *78*, 5525-5531.
- (7) Shumaker-Parry, J. S.; Campbell, C. T. *Analytical Chemistry* **2004**, *76*, 907-917.
- (8) Jung, S. O.; Ro, H. S.; Kho, B. H.; Shin, Y. B.; Kim, M. G.; Chung, B. H. *Proteomics* **2005**, *5*, 4427-4431.
- (9) Huang, H. W.; Chen, Y. *Biosensors & Bioelectronics* **2006**, *22*, 644-648.
- (10) Delehanty, J. B.; Ligler, F. S. *Analytical Chemistry* **2002**, *74*, 5681-5687.
- (11) Bassil, N.; Maillart, E.; Canya, M.; Levy, Y.; Millot, M. C.; Pissard, S.; Narwa, W.; Goossens, M. *Sensors and Actuators B-Chemical* **2003**, *94*, 313-323.
- (12) Endo, T.; Kerman, K.; Nagatani, N.; Hiepa, H. M.; Kim, D. K.; Yonezawa, Y.; Nakano, K.; Tamiya, E. *Analytical Chemistry* **2006**, *78*, 6465-6475.
- (13) Lee, H. J.; Nedelkov, D.; Corn, R. M. *Analytical Chemistry* **2006**, *78*, 6504-6510.
- (14) Nelson, B. P.; Frutos, A. G.; Brockman, J. M.; Corn, R. M. *Analytical Chemistry* **1999**, *71*, 3928-3934.
- (15) Brockman, J. M.; Nelson, B. P.; Corn, R. M. *Annual Review of Physical Chemistry* **2000**, *51*, 41-63.
- (16) Knoll, W. *Annual Review of Physical Chemistry* **1998**, *49*, 569-638.
- (17) Johnsson, B.; Löfås, S.; Lindquist, G. *Analytical Biochemistry* **1991**, *198*, 268-277.
- (18) Kanda, V.; Kariuki, J. K.; Harrison, D. J.; McDermott, M. T. *Analytical Chemistry* **2004**, *76*, 7257-7262.
- (19) Kanda, V.; Kitov, P.; Bundle, D. R.; McDermott, M. T. *Analytical Chemistry* **2005**, *77*, 7497-7504.
- (20) Chen, S. F.; Liu, L. Y.; Zhou, J.; Jiang, S. Y. *Langmuir* **2003**, *19*, 2859-2864.
- (21) Bain, C. D.; Whitesides, G. M. *Langmuir* **1989**, *5*, 1370-1378.
- (22) Evans-Nguyen, K. M.; Schoenfish, M. H. *Langmuir* **2005**, *21*, 1691-1694.

- (23) Rich, R. L.; Myszka, D. G. *Journal of Molecular Recognition* **2002**, *15*, 352-376.
- (24) Wegner, G. J.; Lee, N. J.; Marriott, G.; Corn, R. M. *Analytical Chemistry* **2003**, *75*, 4740-4746.
- (25) Jackson, D. R.; Omanovic, S.; Roscoe, S. G. *Langmuir* **2000**, *16*, 5449-5457.
- (26) Almalah, K.; Mcguire, J.; Sproull, R. *Journal of Colloid and Interface Science* **1995**, *170*, 261-268.
- (27) Smith, E. A.; Thomas, W. D.; Kiessling, L. L.; Corn, R. M. *Journal of the American Chemical Society* **2003**, *125*, 6140-6148.
- (28) Luo, Y.; Yu, F.; Zare, R. N. *Lab on a Chip* **2008**, *8*, 694-700.

CHAPTER 5	CONCLUSIONS AND FUTURE WORK
5.1 INTRODUCTION	149
5.2 CONCLUSIONS.....	149
5.3 ON-GOING WORK	150
5.3.1 CHIP DESIGN	150
5.3.2 PROTEIN ADSORPTION STUDIES	153
5.4 REFERENCES	155

5.1 INTRODUCTION

The following summarizes the research presented in this thesis and proposes improvements and considerations required for the further development of the presented work.

5.2 CONCLUSIONS

Functioning, proof of concept, microfluidic devices for SPR imaging have been designed, fabricated and experimentally tested. These devices are fabricated in PDMS, formed from casting against a thick positive photoresist masters. PDMS was selected because of its biocompatibility, inexpensive cost, and ease of fabrication and prototyping. Two distinct microfluidic flow manifolds were fabricated: 1. a spotting device capable of immobilizing samples to defined locations and 2. a channel device capable of low density arrays and use as an integrated flow cell for SPR imaging detection. Various considerations were made in the design of these devices to allow for easy usability and compatibility with the detection system. Considering the increasing interconnectivity of future higher density devices, modeling of the channel resistances to flow through the use of PSpice will prove to be of more importance in order to minimize production costs and time. While marginally used during this study, future work should more readily rely on modeling software, as an indication of the possible performance of designed devices.

For the minimization of protein array steps, a method of Au patterning using thin film PDMS shadow masks was developed. This method proved a versatile and easy, once developed, micron-scale surface patterning procedure for metals. Here it was utilized to form arrays of Au spots, on glass substrates, used as sensing regions for SPR. This gold patterning technique was shown to be effective in limiting the use of blocking chemistries in microarray fabrication, increasing image contrast by providing zero background signal and allowing for a more secure glass PDMS bond between the microfluidic manifold and SPR sensor.

By utilizing Au patterning and a microfluidic channel manifold studies of surface protein adsorption and novel protein array experiments were achieved. In considering the protein adsorption studies, simultaneous patterning of the gold surface with different thiol SAMs was achieved. This allowed for the simultaneous investigation of the affect of various surface chemistries on the adsorption of proteins. Furthermore, novel protein

arrays were demonstrated combining the various devices designed here. These experiments illustrate the potential for increased throughput and decrease in the number of experiments necessary to perform certain analyses. These demonstrable results allow for further progression and consideration of the possibility and potential of easy, customizable and robust biochemical analysis platforms for point of care and diagnostic use.

5.3 ON-GOING WORK

While shown as a proof of concept, the approach of fabricating protein arrays using microfluidic devices, outlined in this work, faces several hurdles which need to be further developed for this method to be fully viable. Outlined here is where further effort should be concentrated.

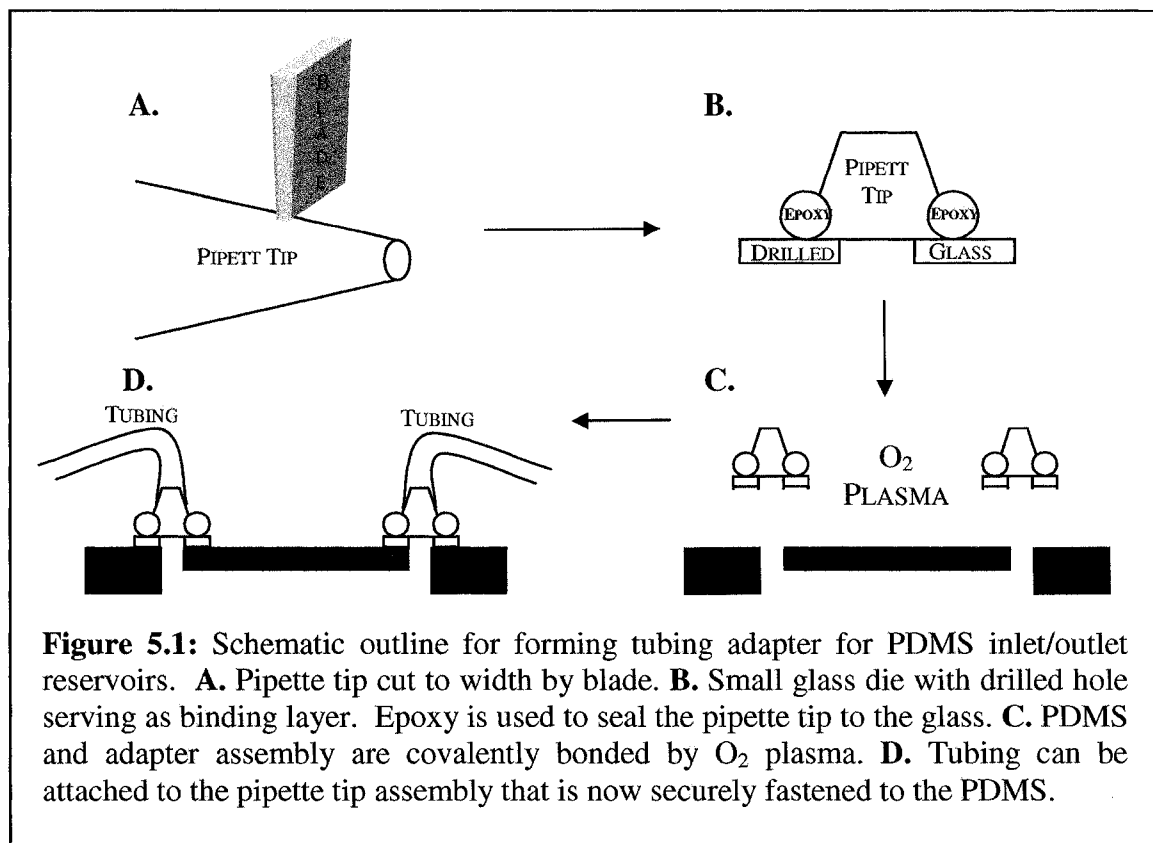
5.3.1 CHIP DESIGN

Currently all solution flow through the various devices is achieved by the application of negative pressure at the outlet, drawing predefined volumes of solution through the channels pipetted at the inlet. Two factors make this method impractical. First, the vacuum application is achieved by hand and second the maximum amount of solution that can be loaded in the channels is limited by the size of the punched reservoir well. This results in an unreliable method of flow control and is impractical, for easy, well defined or possibly automated use of the device. More significantly it limits the use of the various devices to a stop flow method for protein immobilization and incubation. Here solution is drawn to the Au sensor regions and stopped by the removal of the applied vacuum. Incubation is allowed to occur in stagnate solution, where adsorption is diffusion limited. After sometime, the solution is removed and the surface rinsed. This method does not allow for the investigation of the affect of flow rate on protein adsorption, which has been shown to result in increased surface adsorption of proteins.¹ Furthermore, the lack of inlet and outlet ports does not allow for time series experiments to be conducted when the device is used as a flow cell integrated into the SPR. Time series experiments can potentially be important in monitoring surface protein adsorption behavior over time with changing incubation solutions.

To alleviate these problems it becomes necessary to develop a port system capable of allowing for the easy connecting of flexible tubing to be attached to the inlets

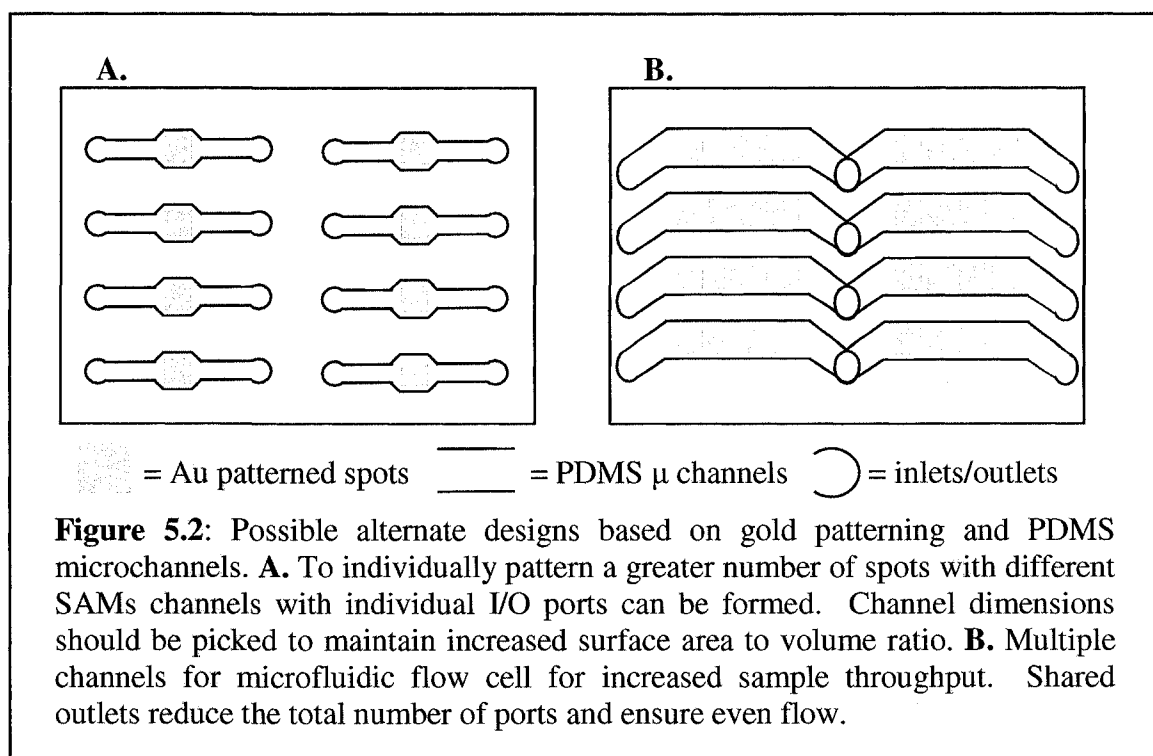
and outlets. This would result in reliable seals for the application of vacuum or pressure, allowing for movement of solution streams by connecting to external tubing providing continuous supply of samples to the inlet from solution vials. Since inlet tubing would be continuously switched from various solutions (samples and running buffers), and flow control would be achieved by either applying negative or positive pressure, there would be a need for a versatile port capable of handling the strain on the tubing.

There exist multiple methods for coupling tubing connections to microfluidic devices. Nanoports (Upchurch Scientific) are used commonly for connection to glass microfluidic devices, and are commercially available. Unfortunately, both cost and large size limit their use in the work presented here. Capillary coupling is a facile inexpensive method of coupling microfluidic channels to external sources.² However, considering the cross sectional size of the current device's channels, appropriate matching would be necessary. Also, alignment of the PDMS channel manifolds and sensor substrates would not be possible with capillary tubing protruding from the device. Using a form of tubing adapter at the inlet and outlet would be ideal. Figure 5.1 is a schematic outline for the fabrication of such a device.



The tubing adapter could be formed from the tips of various size plastic pipette tips. This allows for the formation of virtually any sized tubing connection. Upon punching of access holes in the PDMS these tips could be fastened to the reservoirs, via glass, and serve as connections for plastic tubing. By selecting the right size of tip and tubing, self sealing would be possible. To achieve a strong fit between the tips and PDMS a glass connecting layer would be necessary. Epoxy glues have been tried for sealing against PDMS however this method results in weak adhesion. PDMS glass bonding has been extensively studied and characterized.³ This type of bond is very strong and versatile. Also, epoxy bonding between plastic tips and glass is very strong. This combination of PDMS-glass-epoxy should prove to be a strong connection method of fastening tubing adaptors and has been demonstrated previously in the literature.⁴ Ultimately, this type of connection, coupled with a sensitive flow controller, such as a syringe pump, would allow for easier and more precise control of flow through these devices, for both surface protein immobilization and solution incubation when using the device as a microfluidic flow cell.

Devices designed in this work do not need to be used as templates for future devices and applications. Illustrated in this work, of importance, is the design features that these devices incorporate and which could be used for any future devices. Designs could be customized to the desired application but retain the same basic features, of Au patterned sensor regions aligning to a microfluidic manifold. A situation which might better benefit from a different microfluidic design is an increased number of discrete channels for investigation of multiple surface chemistries or immobilized surface proteins. These channels would align to Au patterned areas and provide for a greater number of solutions to be exposed to the Au sensors. Furthermore, the pre-patterned Au sensor areas could be further aligned with a microfluidic channel system incorporating a greater number of channels for use as a flow cell. Ultimately, the only limit to the design of subsequent devices is the optical system of the SPR imaging detection instrument. Figure 5.2 shows a schematic outline of such designs.



The design of all devices presented in this work has been in PDMS which has been used for a variety of bio-analytical applications. However, it is known to avidly adsorb proteins.^{5, 6} Within the context of the work presented here no consideration was given to the possibility of protein adsorption to the PDMS walls or the possibility of protein bleeding from subsequent washing steps. For sensitive applications, or low concentration samples, these considerations may need to be explored for their affect when using SPR imaging detection. As an initial step, investigating the compatibility of biopassivation coatings⁷ on PDMS devices for integrated SPR imaging detection should be undertaken.

5.3.2 PROTEIN ADSORPTION STUDIES

As was explored in Chapter 3 that many fields are concerned with, and many researchers have investigated, the behavior of protein adsorption to various types of surfaces. This work presented here has shown the ability for the first time to effectively monitor the simultaneous adsorption of proteins to different thiol SAM surfaces without the need for blocking steps and utilizing a label free detection method. By utilizing the

design features developed in this work it is possible to increase the number of different surface coatings investigated simultaneously. Here only four patterned surfaces were investigated at once. By designing a device with increased array elements investigation of many various surface chemistries is possible. By ensuring discrete channels per spotting region or group of spotting regions (Figure 5.2) mixing of various surface treatments is not a consideration. This could allow for in situ reactions for the formation of various types of surface chemistries, such as the EDC/NHS reaction scheme. By allowing for single component surfaces and multi component reaction schemes in the channels, surfaces for both physical and covalent adsorption studies could be developed on the same chip and investigated. Also, various types of covalent adsorption schemes could be investigated. This would allow for the simultaneous monitoring of adsorption behavior. The only consideration necessary, would be to ensure matching SPR responses to the various types of chemistries immobilized on the surface. This would allow for easy comparison (Chapter 3.3.2).

Another area of protein adsorption that is of interest and could be investigated using the methods outlined in this work, is the protein properties of conformation and orientation upon adsorption to surfaces. Monoclonal antibodies have been used to investigate the conformation of proteins on surfaces upon adsorption. While conceivably possible within this outlined method, work would need to be done to interpret results obtained from these types of experiments. Physical adsorption proved to be vastly different on different types of surfaces. This type of result would make it difficult to achieve a consistent background for antibody binding to the surface. Antibody investigation of adsorbed protein layers may only be easily performed, and the results properly interpreted, if the surfaces exhibit approximately the same initial response.

Also, surfactant elution studies of adsorbed proteins have been used to investigate conformation and orientation changes of surface adsorbed proteins.⁸ This method could easily be incorporated into investigating and characterizing the surface induced changes of proteins adsorbed to various surface chemistries.

5.4 REFERENCES

- (1) Ortega-Vinuesa, J. L.; Tengvall, P.; Walivaara, B.; Lundstrom, I. *Biomaterials* **1998**, *19*, 251-262.
- (2) Saarela, V.; Franssila, S.; Tuomikoski, S.; Marttila, S.; Ostman, P.; Sikanen, T.; Kotiaho, T.; Kostianen, R. *Sensors and Actuators B-Chemical* **2006**, *114*, 552-557.
- (3) Bhattacharya, S.; Bhattacharya, S.; Datta, A.; Berg, J. M.; Gangopadhyay, S. A. G. S. *Microelectromechanical Systems, Journal of* **2005**, *14*, 590-597.
- (4) Legendre, L. A.; Bienvenue, J. M.; Roper, M. G.; Ferrance, J. P.; Landers, J. P. *Analytical Chemistry* **2006**, *78*, 1444-1451.
- (5) Butler, J. E.; Lu, E. P.; Navarro, P.; Christiansen, B. *Journal of Molecular Recognition* **1997**, *10*, 36-51.
- (6) Butler, J. E.; Navarro, P.; Lu, E. P. *Journal of Molecular Recognition* **1997**, *10*, 52-62.
- (7) Linder, V.; Verpoorte, E.; Thormann, W.; de Rooij, N. F.; Sigrist, M. *Analytical Chemistry* **2001**, *73*, 4181-4189.
- (8) Arnebrant, T., Wahlgren M. C. In *Proteins at Interfaces II: Fundamentals and Applications*; Horbett, T. A., Brash, J. L., Ed.; American Chemical Society: Washington DC, 1995; Vol. 602, pp 239.